Order Number 9301997

Quantum action variable description of bound and scattering states

Balasubramanya, Mirley K., Ph.D.

Iowa State University, 1992

U·M·I
300 N. Zeeb Rd.
Ann Arbor, MI 48106

Quantum action variable description of bound and scattering states

by

Mirley K. Balasubramanya

A Dissertation Submitted to the

Graduate Faculty in Partial Fulfillment of the

Requirements for the Degree of

DOCTOR OF PHILOSOPHY

Department: Physics and Astronomy
Major: Physics

Approved:

Signature was redacted for privacy.

In Charge of Major Work

Signature was redacted for privacy.

For the Major Department

Signature was redacted for privacy.

For the Graduate College

Iowa State University
Ames, Iowa
1992

TABLE OF CONTENTS

LIST OF TABLES

LIST OF FIGURES

CHAPTER 1. INTRODUCTION

Classical periodic systems can be described elegantly in terms of their action and angle variables which constitute a set of canonically conjugate momenta and coordinates. The Hamiltonian of such systems is a function of the action variables only. These action variables, like angular momentum and energy, are a measure of the total motion of periodic systems. The angle variables evolve linearly in time, advancing by one unit every cycle. The period of such systems can be found using the functional relationship between the action variable and the other constants of the motion without requiring a complete solution of the dynamical equations. Delaunay invented action and angle variables in classical mechanics. This canonical set of coordinates and momenta arise in the Hamilton-Jacobi form of classical mechanics. They also assumed importance in early quantum mechanics; the Wilson-Sommerfeld quantization rules involved the quantization of action variables to explain the bound state spectra. These rules, however, suffered from the same inadequacy as the Bohr quantization conditions; they were ad hoc. With the establishment of the wave and matrix forms of quantum mechanics the construction of action variables in the quantum context were essentially dropped. Leacock and Padgett [1] built a form of quantum mechanics, equivalent to the Schrödinger theory, that involved the formulation of a quantum version of the action variable. The bound states of a system were characterized by

the quantization of the action variable which, in turn, led to the quantization of the system's energy.

Systems that admit both bound and scattering states may display the phenomenon of resonant scattering. Quantum resonance is characterized by a maximum in the delay time of the scattering process. Their resemblance to bound states, which have an infinite delay time, is striking. Leacock and Nanayakkara [2] have explored the unified description of bound and scattering states of two particles interacting via the Coulomb potential, using the action variable. It required the extension of the notion of the action variable to scattering states (which are aperiodic). The classical definition of the action variable as $1/2\pi \oint pdq$ over an orbit in phase space is unsatisfactory; it cannot be extended to scattering states. Neither can it provide leads to define action variables for the corresponding quantum scattering states. An action variable was successfully defined for the Coulomb potential that had the same form for all states of the system, bound and scattering. In this thesis we show that one can define an action variable for particles that interact through the Yukawa potential, both classically and quantum mechanically. This potential, unlike the Coulomb one, admits resonant scattering states. It will also be shown that the method is general and can be employed for all long range central potentials that cut off sufficiently smoothly. This work is a prelude to the construction of particle resonances in terms of the radial action variable.

CHAPTER 2. ACTION VARIABLE IN CLASSICAL MECHANICS

In this chapter we review the role of *action(J)-angle(w)* variables in classical mechanics. Their definitions and utility are illustrated using the one dimensional harmonic oscillator.

Hamiltonian mechanics and the Hamilton-Jacobi equation

The time evolution of a mechanical system is governed by its *Hamiltonian* H which is a function of the n *coordinates* x_i, the n *conjugate momenta* p_i and the time t. The dynamics of such a system is determined by *Hamilton's equations of motion*

$$\dot{x}_i = \partial H(x_i, p_i, t)/\partial p_i, \quad \dot{p}_i = -\partial H(x_i, p_i, t)/\partial x_i. \tag{2.1}$$

The Hamiltonian of a particle moving in one dimension under the influence of a potential $V(x)$ is given by

$$H = p^2 + V(x). \tag{2.2}$$

The units of mass have been so chosen that $2m = 1$. We maintain these units throughout for convenience. It can be shown [3] that such a Hamiltonian is a constant of the motion and is the total energy E of the system. Thus,

$$p^2 + V(x) = E. \tag{2.3}$$

Transformations $(x,p) \rightarrow (X,P)$ that preserve the form of Hamilton's equations are termed *canonical transformations.* One such transformation is generated by the generating function $W(x,P)$:

$$p = \partial W(x,P)/\partial x, \quad X = \partial W(x,P)/\partial P. \tag{2.4}$$

If this transformation transforms the Hamiltonian into a function of P only, then, using (2.1),

$$\dot{X} = \partial H(P)/\partial P = \text{constant} \Rightarrow X(t) = [\partial H(P)/\partial P]\, t + X_0 \tag{2.5}$$

$$\dot{P} = -\partial H(P)/\partial X = 0 \Rightarrow P(t) = P = \text{constant}. \tag{2.6}$$

Thus X and P evolve very simply in time, the former linearly and the latter a constant. $W(x,P)$, which generates a canonical transformation in which the new coordinate X is cyclic, is called *Hamilton's characteristic function.* It satisfies the *Hamilton-Jacobi equation* which is obtained by using (2.4) in (2.3):

$$W_x{}^2(x,P) + V(x) = E(P) \tag{2.7}$$

where the subscript x denotes partial differentiation with respect to x.

The use of this method to solve the dynamical problem then involves the following steps:

(*i*) Define the new constant momentum P,

(*ii*) Integrate (2.7) to obtain $W(x,E(P))$,

(*iii*) Obtain $x(X,P)$ and $p(X,P)$ using (2.4),

(*iv*) Express X_0 and P in terms of the initial values x_0 and p_0.

Action-angle variables and periodic motion

The method of Hamilton-Jacobi is particularly suited to the study of periodic or bound motion. By a particular choice of the new momentum P one obtains the period of the motion without requiring a complete solution of the dynamical problem. The new coordinate and momentum are chosen to be

$$X = w, \quad P = J_c, \tag{2.8}$$

with

$$J_c = \frac{1}{2\pi} \oint p(x, E) dx, \tag{2.9}$$

where $p(x, E)$ is obtained by solving for p from (2.3) and the integral is done over one cycle of the periodic motion. The subscript c refers to the classical problem. A similar momentum is defined in the corresponding quantum problem and it will be referred to as J. Since $J_c = J_c(E)$ we can invert it to obtain $H = E = E(J_c)$. Using (2.1) we get,

$$\dot{w} = \partial H(J_c)/\partial J_c \Rightarrow w(t) = [\partial H(J_c)/\partial J_c]\, t + w_0 \tag{2.10}$$

It can be shown [3] that the angular frequency of the periodic motion is

$$\omega = \dot{w} = \partial H(J_c)/\partial J_c. \tag{2.11}$$

Thus the problem of finding the frequency of periodic motion is reduced to that of doing the integral (2.9).

An equivalent definition of J_c, which can be generalized to nonperiodic motion as well as quantum motions, is

$$J_c = \frac{1}{2\pi} \oint_C p_c(x, E) dx, \tag{2.12}$$

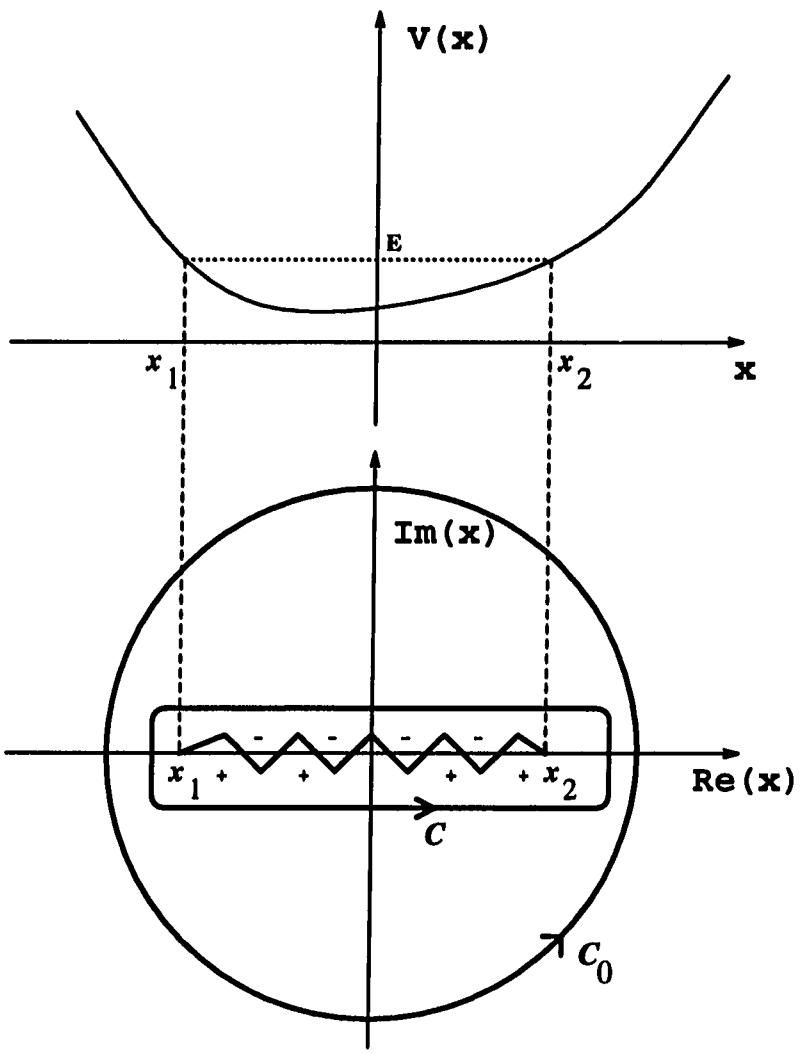

Figure 2.1: The potential and the turning points

where $p_C(x,E)$ is an analytic function of x (considered complex) defined by

$$p_C(x,E) \;=\; [E-V(x)]^{\frac{1}{2}}. \tag{2.13}$$

The classical turning points x_1 and x_2 are defined by $p_C(x_1,E) = p_C(x_2,E) = 0$. These two real turning points are the branch points of $p_C(x,E)$. There is a branch cut connecting x_1 and x_2. $p_C(x,E)$ is chosen as that branch of the square root which is positive along the bottom of the cut. The contour C encloses counterclockwise the two turning points x_1 and x_2. A graph of the potential and the branch cut are shown in Figure 2.1.

The contour integral definition of J_C is more than a mathematical trick. It will be shown in later chapters that such a definition is necessary in order to analytically continue the definition of J_C to positive energy states. It is also essential for defining the quantum counterpart of J_C.

The frequency of a simple harmonic oscillator using $w - J_C$

We now illustrate the use of action-angle variables by obtaining the frequency of a particle moving in one dimension in the simple harmonic potential $V(x) = x^2$. The contour C can be deformed continuously into a circle C_0 centered at $x = 0$ in the region external to the turning points. Here $x_1 = -x_2$ and, in the region $|x| > |x_1|$, $p_C(x,E)$ has the form

$$p_C \;=\; [E-x^2]^{\frac{1}{2}} \;=\; ix - iE/2x + ..., \tag{2.14}$$

and by residue theorem and definition (2.12)

$$J_C \;=\; \frac{E}{2}. \tag{2.15}$$

Inverting this, we get

$$E = E(J_c) = 2J_c \quad \Rightarrow \quad \omega = \partial E/\partial J_c = 2, \tag{2.16}$$

which is indeed the angular frequency of a simple harmonic oscillator of mass 1/2 and spring constant 2.

CHAPTER 3. QUANTUM ACTION VARIABLE

In this chapter we review quantum Hamilton-Jacobi theory. We show that the exact bound state energies of the quantum harmonic oscillator can be obtained using a quantum action variable J whose definition closely resembles that of J_C.

Quantum Hamilton-Jacobi equation

Leacock et al. [1] have constructed a version of quantum mechanics which parallels the classical Hamilton-Jacobi theory. We consider systems whose Hamiltonian is of the form

$$\hat{H} = \hat{p}^2 + \hat{V}(\hat{x}). \tag{3.1}$$

Here, a hat denotes a linear operator. The measurable values of the observables $\hat{H}$, $\hat{p}$, $\hat{x}$, etc. are their eigenvalues. We write the equations of a *quantum canonical transformation* in terms of the eigenvalues and functions of eigenvalues. Using the *quantum characteristic function* $W(x, P)$ these transformation equations are

$$p = \partial W(x, P)/\partial x, \qquad X = \partial W(x, P)/\partial P \tag{3.2}$$

The *quantum Hamilton-Jacobi equation* is postulated as

$$-i\hbar W_{xx}(x, E(P)) + {W_x}^2 = E(P) - V(x), \tag{3.3}$$

where subscript refers to partial differentiation. Physical boundary conditions have to be imposed on $W(x, E(P))$ to complete its definition. We note that this equation resembles the classical Hamilton-Jacobi equation (2.7) but for the first term involving $\hbar$.

A new function $p(x, E)$, called the *quantum momentum function*, is defined as below:

$$p(x, E) = \partial W(x, E)/\partial x. \tag{3.4}$$

$p(x, E)$ is the quantum analogue of the classical momentum function $p_C(x, E)$ defined in Chapter 1. Using this in (3.3) we obtain an equation for $p(x, E)$:

$$-i\hbar\partial p(x, E)/\partial x + p^2(x, E) = E - V(x) = {p_C}^2(x, E). \tag{3.5}$$

We note that this quantum momentum function reduces to $\pm p_C$ defined by (2.13) in the limit of $\hbar \rightarrow 0$. The physical boundary condition on $p(x, E)$ is

$$\lim_{\hbar \rightarrow 0} p(x, E) = p_C(x, E). \tag{3.6}$$

Equation (3.5), along with (3.6), can be viewed as the defining equation for $p(x, E)$ which we will use in the definition of quantum action variable J. The relation between eq. (3.5) and the Schrödinger equation is shown in [1] ; we utilize it in Chapter 6.

Definition of quantum action variable

Further development of the quantum theory of action-angle variables requires the definition of a new momentum P which we call the quantum action variable J. It is defined as a contour integral in the complex x plane,

$$J = \frac{1}{2\pi} \oint_C p(x, E)dx, \tag{3.7}$$

with the counterclockwise contour C enclosing the two turning points, as shown in Figure (2.1). (3.5) and (3.6) imply $p(x, E)$ has poles of residue $-i\hbar$ (see Appendix A) between the two turning points. The number of these poles is $0, 1, 2, \ldots$ for the ground state, first excited state, second excited state, ... etc. respectively. Since the contour C encloses these poles, the residue theorem leads to the quantization of J:

$$J = J(E) = n\hbar. \tag{3.8}$$

Inverting this, we obtain the system's energy eigenvalues:

$$E = E(n\hbar). \tag{3.9}$$

As will be shown in the next section the integral (3.7) can be done without obtaining a solution of (3.5) all over the complex x plane. The energy eigenvalues can thus be obtained without solving any dynamical equation.

Energy levels of the harmonic oscillator

We now illustrate the use of the quantum action variable by obtaining the energy levels of a particle moving in one dimension in the harmonic potential $V(x) = x^2$. To evaluate J from (3.7) we deform the contour C into C_0, which is a circular contour centered at $x = 0$ enclosing the turning points x_1 and x_2, and evaluate the integral along C_0. Writing $p(x, E)$ and $p_c(x, E)$ on C_0 as

$$\begin{aligned} p(x, E) &= a_1 x + a_0 - a_{-1}/x + \ldots \quad \text{and} \\ p_c(x, E) &= b_1 x + b_0 - b_{-1}/x + \ldots \end{aligned}$$

where $b_1 = i, \quad b_0 = 0, \quad b_{-1} = -iE/2, \ldots$ from (2.14).

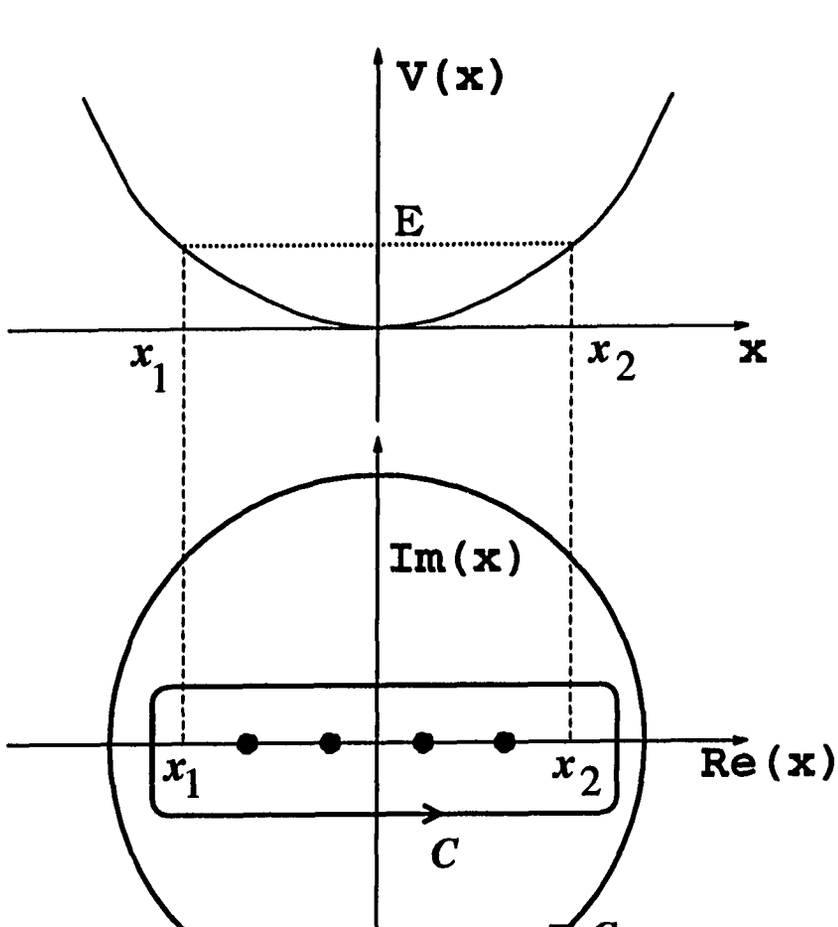

Figure 3.1: Harmonic oscillator potential and the poles of $p(x)$

Substituting these in (3.5) we get

$$a_1^2 = b_1^2, \quad a_0 = 0, \quad a_{-1} = (1/2a_1)[2b_1 b_{-1} + i\hbar a_1], \ \ldots. \tag{3.10}$$

The boundary condition (3.6) requires a_1 to be $+b_1$ and not $-b_1$. Thus, from (3.10),

$$a_1 = i, \quad a_0 = 0, \quad a_{-1} = -i/2(E - \hbar), \ \ldots \tag{3.11}$$

Using (3.11) in (3.7) we get, via the residue theorem,

$$J \ = \ ia_{-1} \ = \ (E - \hbar)/2,$$

and from (3.8) we have

$$J(E) \ = \ (E - \hbar)/2 \ = \ n\hbar, \tag{3.12}$$

and so $E = 2\hbar(n + 1/2)$ which are the energy eigenvalues of a quantum harmonic oscillator with angular frequency $\omega = 2$.

This method is general and can be used to find the energies of any bound system. For those potentials for which the integral (3.7) cannot be obtained in the closed form we can use asymptotic methods developed by Leacock [4].

CHAPTER 4. SPHERICALLY SYMMETRIC POTENTIALS

The motion of a particle moving in a spherically symmetric potential $V(r)$ is considered in this chapter. The first part examines the classical motion and the second part the quantum motion. The classical Hamiltonian of the particle is expressed in terms of spherical polar coordinates (r, θ, ϕ) and their conjugate momenta (p_r, p_θ, p_ϕ) as

$$H = {p_r}^2 + \frac{1}{r^2}\left({p_\theta}^2 + \frac{{p_\phi}^2}{\sin^2\theta}\right) + V(r). \tag{4.1}$$

The quantum Hamiltonian for this system is obtained by replacing the classical coordinates and momenta by the corresponding Hermitian operators. It is shown in this chapter that such a three dimensional problem, both classical and quantum, can be transformed into three one dimensional problems.

Classical motion

We show, first, that the motion can be separated into r, θ and ϕ motions. We define, for a particle with total energy E, total angular momentum L and azimuthal angular momentum L_ϕ, classical momentum functions $p_r(r, E, L)$, $p_\theta(\theta, L, L_\phi)$ and $p_\phi(\phi, L_\phi)$ with complex arguments r, θ and ϕ respectively. These definitions are analogous to the definition of momentum function in the one dimensional case. These complex momentum functions are then used to construct the action variables J_r, J_θ

and J_ϕ.

Separable solution of the Hamilton-Jacobi equation

A canonical transformation is made to a new set of coordinates and momenta $(X_r, X_\theta, X_\phi, P_r, P_\theta, P_\phi)$ such that the Hamiltonian is cyclic in the new coordinates X_r, X_θ and X_ϕ. The generator of this transformation is Hamilton's characteristic function $W_c(r, \theta, \phi, P_r, P_\theta, P_\phi)$. The equations of canonical transformation are

$$\begin{aligned} p_r &= \frac{\partial W_c}{\partial r}, \qquad p_\theta = \frac{\partial W_c}{\partial \theta}, \qquad p_\phi = \frac{\partial W_c}{\partial \phi}, \\ X_r &= \frac{\partial W_c}{\partial P_r}, \qquad X_\theta = \frac{\partial W_c}{\partial P_\theta}, \qquad X_\phi = \frac{\partial W_c}{\partial P_\phi}. \end{aligned} \tag{4.2}$$

The Hamilton-Jacobi equation for W_c, given (4.1) and (4.2), is

$$\left(\frac{\partial W_c}{\partial r}\right)^2 + \frac{1}{r^2}\left[\left(\frac{\partial W_c}{\partial \theta}\right)^2 + \frac{1}{\sin^2\theta}\left(\frac{\partial W_c}{\partial \phi}\right)^2\right] + V(r) = E, \tag{4.3}$$

where E is the particle's constant energy. This equation is separable if we let

$$W_c = W_{rc}(r, E, L) + W_{\theta c}(\theta, L, L_\phi) + W_{\phi c}(\phi, L_\phi),$$

L and L_ϕ being separation constants. These constants and E are functions of the new momenta, P_r, P_θ and P_ϕ, which will be defined later. Then, (4.3) can be separated, and becomes the three equations

$$\begin{aligned} \left(\frac{\partial W_{rc}}{\partial r}\right)^2 + \frac{L^2}{r^2} + V(r) &= E, \\ \left(\frac{\partial W_{\theta c}}{\partial \theta}\right)^2 + \frac{{L_\phi}^2}{\sin^2\theta} &= L^2, \\ \left(\frac{\partial W_{\phi c}}{\partial \phi}\right)^2 &= {L_\phi}^2. \end{aligned} \tag{4.4}$$

These three equations will be recast in terms of the classical momentum functions $p_{rc}(r, E, L)$, $p_{\theta c}(\theta, L, L_\phi)$ and $p_{\phi c}(\phi, L_\phi)$, where these functions and their coordinate arguments are considered complex. The momentum functions are defined thus:

$$p_{rc}(r, E, L) = \frac{\partial W_{rc}}{\partial r}(r, E, L),$$
$$p_{\theta c}(\theta, L, L_\phi) = \frac{\partial W_{\theta c}}{\partial \theta}(\theta, L, L_\phi),$$
$$p_{\phi c}(\phi, L_\phi) = \frac{\partial W_{\phi c}}{\partial \phi}(\phi, L_\phi).$$

Equations (4.4) then can be written as

$$p_{rc}{}^2(r, E, L) + L^2/r^2 + V(r) = E, \tag{4.5}$$
$$p_{\theta c}{}^2(\theta, L) + L_\phi{}^2/\sin^2\theta = L^2, \tag{4.6}$$
$$p_{\phi c}{}^2(\phi, L_\phi) = L_\phi{}^2. \tag{4.7}$$

Action variables $J_{\theta c}$ and $J_{\phi c}$

The above separation facilitates the definition of new momenta, P_r, P_θ and P_ϕ, which we choose as the action variables J_{rc}, $J_{\theta c}$ and $J_{\phi c}$ respectively. The latter two can be defined without reference to the central potential while the former requires further study of equation (4.5). We focus on defining $J_{\theta c}$ and $J_{\phi c}$ here. The definition of J_{rc} will be discussed in later chapters.

From (4.7) we have

$$p_{\theta c}(\theta, L, L_\phi) = [L^2 - L_\phi{}^2/\sin^2\theta]^{1/2}.$$

θ_1 and θ_2 are the two turning points of the θ–motion, i.e., $p_{\theta c}$ vanishes at θ_1 and θ_2. These two points are the branch points of $p_{\theta c}(\theta, L, L_\phi)$ and we connect them by

a branch cut through the real axis. $p_{\theta c}$ is positive just below the cut. We define J_θ by the contour integral in the complex θ plane by

$$J_{\theta c} = \frac{1}{2\pi} \oint_{C_\theta} p_\theta(\theta, L, L_\phi) d\theta, \tag{4.8}$$

where C_θ is a counterclockwise contour enclosing θ_1 and θ_2. On performing this integral by the method of residues we get [1]

$$J_{\theta c} = L - L_\phi. \tag{4.9}$$

The motion of the particle in the coordinate ϕ is unbounded and, unlike $p_{\theta c}$, $p_{\phi c}$ lacks any turning points, as is evident from eq. (4.7). We define the action variable $J_{\phi c}$ to be L_ϕ.

Our definition of J_{rc} will be a contour integral of $p_{rc}(r, E, L)$ in the complex r plane over a suitably chosen contour. Thus,

$$\begin{aligned} J_{rc} &= J_{rc}(E, L) \\ \text{Inverting this, } E &= E(J_{rc}, L) \quad = E(J_{rc}, J_{\theta c} + J_{\phi c}), \end{aligned}$$

from (4.9) and the definition of $J_{\phi c}$. Therefore $J_{\theta c}$ and $J_{\phi c}$ occur in E only in the combination $(J_{\theta c} + J_{\phi c})$ (see equation (4.9)). Hence the angular frequencies $\omega_\theta = \partial E/\partial J_\theta$ and $\omega_\phi = \partial E/\partial J_\phi$ are equal to each other for all central potentials.

Quantum motion

We now show, following the classical analysis, that the quantum Hamilton-Jacobi equation for a particle in a spherically symmetric potential can be separated into three one dimensional equations, one for each of r, θ and ϕ. The quantum action variables

J_r, J_θ and J_ϕ, will be introduced and will be shown to be quantized. The energy of the particle, being a function of these action variables, is therefore quantized.

Separation of the quantum Hamilton-Jacobi equation

The generalization of the quantum Hamilton-Jacobi equation to three dimensions [1] is

$$-i\hbar\nabla^2 W + (\nabla W)^2 = E - V \tag{4.10}$$

where $W = W(r, \theta, \phi, P_r, P_\theta, P_\phi)$ is the quantum characteristic function that generates a quantum canonical transformation between the "old" coordinates-momenta set $(r, \theta, \phi, p_r, p_\theta, p_\phi)$ and the "new" set $(X_r, X_\theta, X_\phi, P_r, P_\theta, P_\phi)$. We can separate (4.10) by letting

$$W(r, \theta, \phi, P_r, P_\theta, P_\phi) = W_r(r, E, L) + W_\theta(\theta, L, l_\phi) + W_\phi(\phi, l_\phi). \tag{4.11}$$

E and the separation constants L and l_ϕ are functions of the "new" momenta P_r, P_θ and P_ϕ which will be defined later. Equation (4.10) then separates into three equations:

$$\begin{aligned} -i\hbar\,\frac{1}{r^2}\frac{\partial}{\partial r}\left(r^2\frac{\partial W_r}{\partial r}\right) + \left(\frac{\partial W_r}{\partial r}\right)^2 + \frac{L^2}{r^2} + V(r) &= E, \\ -i\hbar\,\frac{1}{\sin\theta}\frac{\partial}{\partial\theta}\left(\sin\theta\,\frac{\partial W_\theta}{\partial\theta}\right) + \left(\frac{\partial W_\theta}{\partial\theta}\right)^2 + \frac{{l_\phi}^2}{\sin^2\theta} &= L^2, \\ -i\hbar\,\frac{\partial^2 W_\phi}{\partial\phi^2} + \left(\frac{\partial W_\phi}{\partial\phi}\right)^2 &= {l_\phi}^2. \end{aligned} \tag{4.12}$$

These are, as in the one dimensional case, recast in terms of the quantum momentum functions $\tilde{p}_r(r, E, L)$, $p_\theta(\theta, L, l_\phi)$ and $p_\phi(\phi, l_\phi)$ defined by

$$\tilde{p}_r(r, E, L) = \frac{\partial W_r}{\partial r}(r, E, L), \quad p_\theta(\theta, L, l_\phi) = \frac{\partial W_\theta}{\partial\phi}(\theta, L, l_\phi), \quad p_\phi(\phi, l_\phi) = \frac{\partial W_\phi}{\partial\phi}(\phi, l_\phi)$$

Equations (4.12) then become

$$-i\hbar\,\frac{1}{r^2}\,\frac{\partial}{\partial r}\left[r^2\,\tilde{p}_r(r,E,L)\right]+\tilde{p}_r^2(r,E,L)+\frac{L^2}{r^2}+V(r) \;=\; E, \tag{4.13}$$

$$-i\hbar\,\frac{1}{\sin\theta}\,\frac{\partial}{\partial\theta}\left[\sin\theta\,p_\theta(\theta,L,l_\phi)\right]\;+\;{p_\theta}^2+{L_\phi}^2/\sin^2\theta \;=\; L^2, \tag{4.14}$$

$$-i\hbar\frac{\partial p_\phi(\phi,l_\phi)}{\partial\phi}\;+\;{p_\phi}^2 \;=\; {L_\phi}^2. \tag{4.15}$$

The physical requirements on these momentum functions are

$$\lim_{\hbar\to 0}\tilde{p}_r(r,E,L) \;=\; p_{rc}(r,E,L), \tag{4.16}$$

$$\lim_{\hbar\to 0}p_\theta(\theta,L,l_\phi) \;=\; p_{\theta c}(\theta,L,l_\phi), \tag{4.17}$$

$$p_\phi(\phi+2\pi,l_\phi) \;=\; p_\phi(\phi,l_\phi). \tag{4.18}$$

(4.17) and (4.18) require the quantum momentum functions $\tilde{p}_r$ and $p_{\theta c}$ to approach their classical counterparts in the limit of $\hbar$ going to zero. This will be referred to as the classical limit. (4.18) requires $p_\phi(\phi,l_\phi)$ to be unchanged under a rotation of 2π around the azimuthal axis. Equations (4.13) - (4.15) and boundary conditions (4.16) - (4.18) define the three momentum functions uniquely for all complex values of their coordinate arguments.

Action variables J_θ and J_ϕ

Using the above p_r, p_θ and p_ϕ we can define the new momenta, the action variables J_r, J_θ and J_ϕ, as in the classical case. It will be shown that the the boundary conditions on the momentum functions quantize these action variables. The total energy of the system, being a function only of the the new momenta, is therefore quantized. J_r will be defined, in later chapters, as a contour integral of $\tilde{p}_r$ in the complex r plane over a suitably chosen contour C. We can define a related

momentum function $p_r(r, E, L)$ by

$$p_r(r, E, L) = \tilde{p}_r(r, E, L) - \frac{i\hbar}{r}.$$

It obeys the momentum function equation (see equation 4.14)

$$\begin{aligned} -i\hbar \frac{\partial p_r(r, E, L)}{\partial r} + {p_r}^2(r, E, L) &= E - V(r) - L^2/r^2 \\ &= {p_{rc}}^2(r, E, L), \end{aligned} \tag{4.19}$$

with p_r satisfying the same boundary condition as $\tilde{p}_r$. Equation (4.19) is a differential equation identical to the one dimensional equation (3.5). Also, one can define J_r as an integral over C in the complex r plane of p_r instead of $\tilde{p}_r$ provided the point $r = 0$ is not in the interior of C. Our later discussions of J_r will be based on p_r and eq. (4.19).

The action variable J_θ is defined as the contour integral in the complex θ plane

$$J_\theta = \frac{1}{2\pi} \oint_{C_\theta} p_\theta(\theta, L^2, l_\phi) d\theta, \tag{4.20}$$

where C_θ is a closed counterclockwise contour enclosing θ_1 and θ_2, the two turning points, and the part of the real axis in between them. From eq. (4.14) and the boundary condition (4.17) it can be shown that $p_\theta(\theta, L, l_\phi)$ has $0, 1, 2, \ldots$ poles of residue $-i\hbar$ between θ_1 and θ_2. Thus, by (4.20) and the residue theorem, $J_\theta = n_\theta \hbar$, with $n_\theta = 0, 1, 2, \ldots$ corresponding to $0, 1, 2, \ldots$ enclosed poles of p_θ. It is shown in [1] that

$$J_\theta = J_\theta(L, l_\phi) = [L^2 + (\hbar/2)^2]^{1/2} - \hbar/2 - l_\phi. \tag{4.21}$$

We next define the action variable J_ϕ as l_ϕ. The periodic boundary condition (4.18) restricts the allowed values of l_ϕ to integral multiples of $\hbar$ only. Thus,

$$J_\phi = n_\phi \hbar, \quad \text{with} \quad n_\phi = 0, \pm 1, \pm 2, \ldots. \tag{4.22}$$

Solving (4.21) for the separation constant L we get

$$\begin{aligned} L^2 &= [J_\theta + J_\phi + (\hbar/2)^2]^2 - (\hbar/2)^2 \\ &= (n_\theta + n_\phi)(n_\theta + n_\phi + 1)\hbar^2 \quad = \quad l(l+1)\hbar^2 \qquad (4.23) \\ &\qquad\qquad \text{where} \quad l \;=\; n_\theta + |n_\phi|. \end{aligned}$$

Thus the allowed values of L^2 are quantized; for a given value of l the allowed values of l_ϕ are $n_\phi\hbar$ with $-l \leq n_\phi \leq l$.

Using (4.24) in the momentum function equation (4.19) we obtain

$$\begin{aligned} -i\hbar \frac{\partial p_r(r,E,L)}{\partial r} + {p_r}^2(r,E,L) &= {p_r c}^2(r,E,L), \\ &= E - V(r) - l(l+1)\hbar^2/r^2. \qquad (4.24) \end{aligned}$$

This equation will be studied extensively for the locations of the the poles of $p_r(r,E,l)$ in the complex r plane with a view to defining the action variable J_r as a contour integral. Such a J_r should yield the bound state energies of the system when it is quantized in terms of $\hbar$. We will study the constructions of J_r for the two physically important spherical potentials, Coulomb and Yukawa.

CHAPTER 5. COULOMB POTENTIAL - CLASSICAL CASE

The Coulomb potential is of the form $-g/r$, where g, the coupling constant squared, is a measure of the attraction of the particle to the center of attraction. We study in this chapter the definition of the radial action variable J_{rc} for a particle moving in this potential. The bound state motion (negative energy) is first studied and the frequency of radial oscillations obtained using J_{rc}. We then review the work of Nanayakkara [2] in extending the definition of J_{rc} to the scattering states of the particle.

Bound states and radial periodic motion

From eq. (4.6) the classical momentum function $p_{rc}(r, E, L)$ is

$$p_{rc}(r, E, L) = [E + \frac{g}{r} - \frac{L^2}{r^2}]^{1/2}. \tag{5.1}$$

As shown in Figure 5.1 the particle has an energy $V_0 < E < 0$ where V_0 is the minimum of the effective potential energy. The particle's radial coordinate oscillates between the two turning points r_1 and r_2. There is a branch cut of p_{rc} connecting its two branch points r_1 and r_2. We define p_{rc} to be positive just below the cut. This is equivalent to the condition

$$p_{rc}(r, E, L) \simeq \frac{-iL}{r} \quad \text{around} \quad r = 0. \tag{5.2}$$

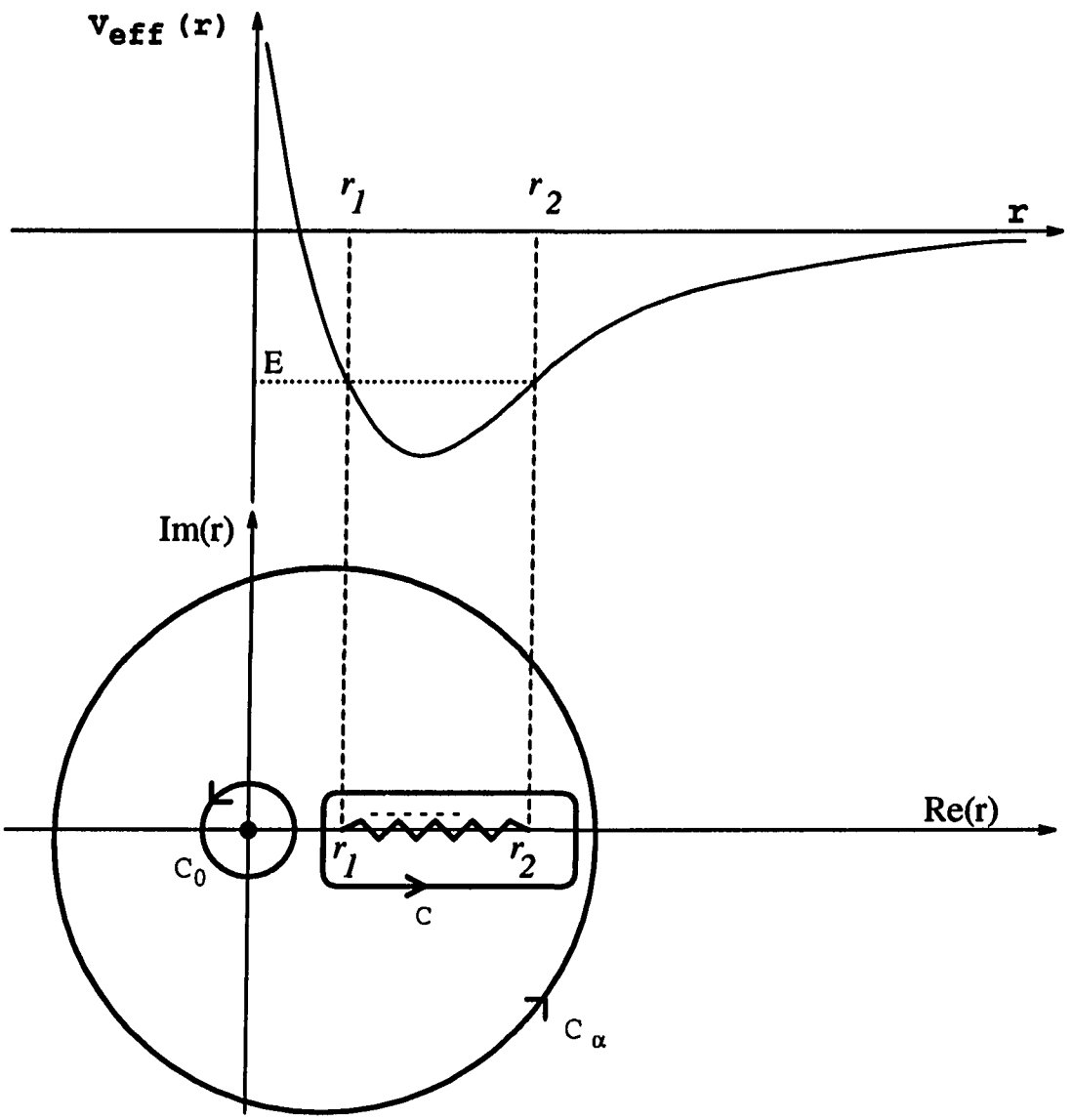

Figure 5.1: Bound state motion in Coulomb potential

The radial action variable is defined as

$$J_{rc} = \frac{1}{2\pi} \oint_C p_{rc}(r, E, L) dr, \tag{5.3}$$

where C encloses r_1 and r_2 and the branch cut between them. Condition (5.2) and the contour C make J_{rc} real and positive for physical bound motion; and furthermore, will be shown later to be consistent with the usual conventions of scattering theory. The integral (5.3) is evaluated by distorting C into C_0 and C_α and using the residue theorem. p_{rc}, given by (5.1), can be written in terms of the turning points as

$$p_{rc} = \frac{-iL}{\sqrt{r_1 r_2}} \frac{(r - r_1)^{1/2}(r - r_2)^{1/2}}{r}, \tag{5.4}$$

with

$$r_{1,2} = \frac{-g \mp \sqrt{g^2 + 4EL^2}}{2E}. \tag{5.5}$$

p_{rc} has a simple pole of residue $-iL$ at $r = 0$ (see eq. (5.2)). Thus, by the residue theorem,

$$\frac{1}{2\pi} \oint_{C_0} p_{rc}(r, E, L) dr = L. \tag{5.6}$$

The Laurent series for $p_{rc}(r, E, L)$ on C_α is obtained by binomial expansion:

$$p_{rc}(r, E, L) = \frac{-iL}{\sqrt{r_1 r_2}} [1 - \frac{1}{2}(r_1 + r_2) \frac{1}{r} + \ldots],$$

so,

$$\frac{1}{2\pi} \oint_{C_\alpha} p_{rc}(r, E, L) dr = \frac{-L}{2\sqrt{r_1 r_2}} (r_1 + r_2). \tag{5.7}$$

Using (5.6) and (5.7), we obtain

$$\begin{aligned} J_{rc} &= -L - \frac{L}{2\sqrt{r_1 r_2}} (r_1 + r_2) \\ &= -L + \frac{g}{2\sqrt{-E}}. \end{aligned} \tag{5.8}$$

Solving this for E in terms of J_{rc} we get

$$E = -\frac{(g/2)^2}{(J_{rc}+L)^2}. \tag{5.9}$$

The angular frequency ω_r is

$$\omega_r = \partial E/\partial J_{rc} = \frac{4(-E)^{3/2}}{g}.$$

As the semimajor axis of the particle's elliptic orbit is proportional to $1/(-E)$ we have derived Kepler's third law of planetary motion which states that the square of the planet's period is proportional to the cube of the semimajor axis.

Definition of J_{rc} as a contour integral for all energy

We seek to extend the definition of the radial action variable to positive energies. For these energies the particle's classical radial motion under the Coulomb potential is unbounded. If the initial condition is such that the particle approaches the attractive center then it is deflected by the center and it recedes from it continuously. Such a scattering state has only one physical radial turning point r_1, the other turning point r_2 being negative, and therefore unphysical. The traditional definition of J_{rc} for bound states as the integral $(1/2\pi)\oint p_{rc}\,dr$ over one cycle of the radial motion cannot be extended to scattering states; such an integral is singular for scattering states since the orbit is unbounded and the radial momentum p_r is non-zero even as the particle moves far away from the scattering center. The definition of J_{rc} as a contour integral in the complex r plane does not suffer from this deficiency; the definition used for bound states lends itself to a natural extension to scattering states.

The contour integral definition of J_{rc} requires a study of how r_1 and r_2, the branch points of $p_{rc}(r, E, L)$, move with energy. Also the nature of $p_{rc}(r, E, L)$ for all

complex r for both positive and negative energies is needed. The energy is considered complex with a positive imaginary part ϵ_E and is written as $\mathcal{E} = E + i\epsilon_E$. r_1 and r_2 are functions of $\mathcal{E}$ and L given by (5.5). We study the motion of these two turning points by varying $\mathcal{E}$, but keeping the total angular momentum L fixed at a positive value.

The motion of the turning points with respect to the energy is shown in Figure 5.2. Though the physically allowed energies of the particle are greater than V_0, the minimum of the effective potential energy, we study r_1, r_2 and p_{rc} as functions of $\mathcal{E}$ for all energy, to understand how their character transforms in a smooth way as $\mathcal{E}$ shifts from one region to the next. a_1 shows the location of r_1 for $E = E_a$, a_2 the location of r_2 for $E = E_a$, etc. The following is the variation of r_1 and r_2:

(i) For $E = E_a$, with $E_a < V_0$, r_1 is in the lower half plane and r_2 in the upper half plane and they are both near $r = 0$ (see Figure 5.3. The positive nature of ϵ_E makes r_1 lie wholly in the lower half plane and r_2 wholly in the upper half plane for the energies considered in Figure 5.3.

(ii) As E increases r_1 and r_2 loop and as $E \rightarrow V_0$ they approach each other. If $\mathcal{E} = V_0$ then $r_1 = r_2$. The non-zero ϵ_E thus avoids this situation.

(iii) As E increases to E_f, r_1 and r_2 are near the positive part of the real r axis, with r_1 a little below and r_2 a little above the real axis. r_1 remains close to the positive part of the real axis as E is increased further and approaches $r = 0_+$.

(iv) $Re(r_2)$ increases with increasing E and as E changes sign from negative to positive, r_2 moves along a counterclockwise curve in the upper half plane, approaching the negative real axis ($f_2 \rightarrow h_2$) in Figure 5.4. The radius of this curve is inversely proportional to $\sqrt{\epsilon_E}$.

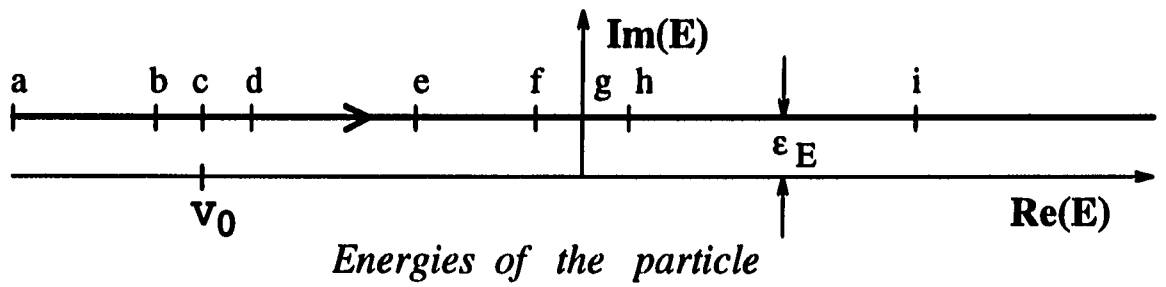

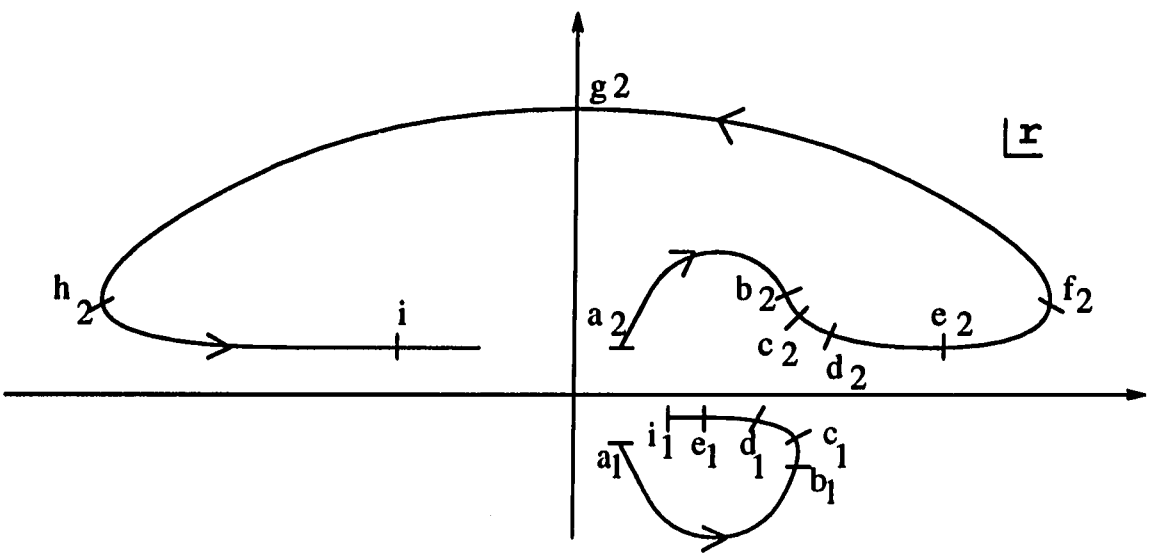

Figure 5.2: Variation of the turning points r_1 & r_2 with energy

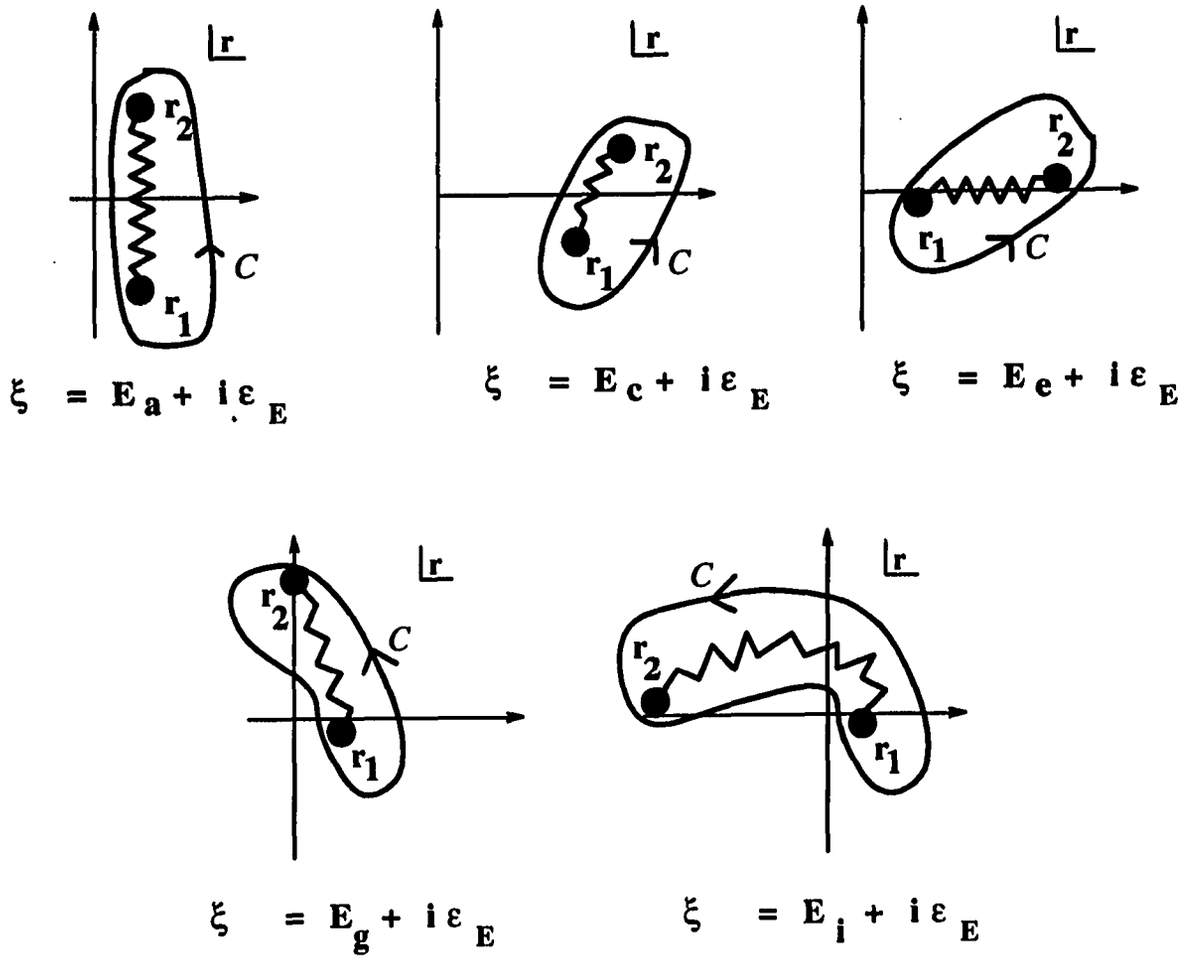

Figure 5.3: Contour C for evaluating J_{rc} for Coulomb potential

(v) With E positive and increasing, $Re(r_2)$ approaches $r = 0_-$.

The branch cut of $p_{rc}(r, \mathcal{E}, L)$ is drawn connecting r_1 and r_2 as shown in the Figure (5.3). It is a straight line for $E = E_a$ and is varied continuously as a simple curve connecting the moving turning points. The sense of the contour C, which encloses r_1 and r_2 and the cut, is counterclockwise for all $\mathcal{E}$. The condition (5.2) at the origin is maintained for all $\mathcal{E}$ so that when the particle is in the bound state region $V_0 < E < 0$, $Re(p_{rc})$ is negative just above the branch cut and positive just below the cut. As the particle's radial coordinate oscillates, its radial momentum is positive during the first half of the cycle and is negative during the second half. The nature of $p_{rc}(r, \mathcal{E}, L)$ just above and below the cut and the orientation of the contour C, over which the integral $\oint p_{rc} dr$ is performed in the definition of J_{rc}, reflects this. When the energy becomes positive $p_{rc}(r, \mathcal{E}, L)$ is positive in the physically allowed region of $r > Re(r_2)$, with r real. It represents the radial momentum of a particle going away from the attractive center.

We define J_{rc} for all $\mathcal{E}$ by

$$J_{rc} = \frac{1}{2\pi} \oint_C p_{rc}(r, \mathcal{E}, L) dr. \tag{5.10}$$

This definition of the radial action variable coincides with our previous definition (5.3) for the physical, bound state case of $V_0 < E < 0$. It analytically extends this definition to all other values of E. As in (5.3) the integral is evaluated in each case by distorting C into C_0 and C_α and using the residue theorem. As before, the integral over C_0 gives $-L$ and that over C_α gives $g/2\sqrt{-\mathcal{E}}$ yielding (5.8) again.

The variation of the radial action variable with energy is shown in Figure 5.4. With this definition of the radial action variable J_{rc} is a real monotonically increasing function of E for $E < 0$, correctly giving the frequency for the allowed periodic

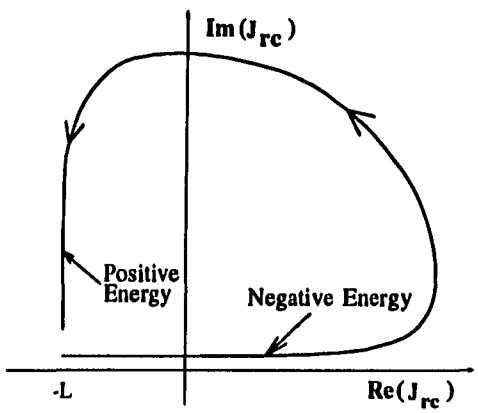

Figure 5.4: Dependence of J_{rc} on the particle's energy

motion. For positive energy J_{rc} is positive imaginary, with $Im(J_{rc})$ monotonically decreasing with E; the frequency becomes purely imaginary. These unbound orbits for positive energy have a periodicity in time if time were imaginary. J_{rc} for the bound state is a constant of the motion which is a measure of one complete cycle of the motion. This J_{rc} is a successful construction of such a measure of the entire motion for scattering states of positive energy.

Modified definition of J_{rc}

While definition (5.10) correctly serves as an analytic continuation of J_{rc} to all E a modified but equivalent definition of J_{rc} is presented in this section [2]. As will be seen in the next chapter this modified definition will be useful in the context of

quantum mechanics while (5.10) itself cannot be extended into quantum mechanics.

The integrand in (5.10) has two poles, one at $r = 0$ and the other at $r = \infty$ and they both make their contributions to J_{rc}, the former through the contour C_0 and the latter through C_α. If we changed this integrand in such a way that its pole at $r = \infty$ is "moved" to a point $r = 1/\epsilon_r$, with ϵ_r positive imaginary and, after the evaluation of J_{rc} as a contour integral, we take the limit of $\epsilon_r \to 0$, then we recover the definition of J_{rc} above. Such a modification is shown here.

The modified definition of J_{rc} is

$$\begin{aligned} \tilde{J}_{rc}(\epsilon_r) &= \frac{1}{2\pi} \oint_C p_{rc}(r, \mathcal{E}, L)\, dr/[1 - \epsilon_r r]^2, \\ J_{rc} &= \lim_{\epsilon_r \to 0} \tilde{J}_{rc}(\epsilon_r) \end{aligned} \tag{5.11}$$

with a positive imaginary ϵ_r, and the contour C defined as in Figure 5.5. The evaluation of this integral is done by distorting C into the contours C_0, C_ϵ and C_α (see Figure (5.5)). The denominator in the integrand makes the integral over C_α vanish. The denominator also produces a second order pole of the integrand at $r = 1/\epsilon_r$. The contribution from C_0 does not change. The integral over C_ϵ yields

$$\frac{g - 2L^2\epsilon_r}{2\sqrt{V_{\text{eff}}(r = 1/\epsilon_r) - \mathcal{E}}}, \tag{5.12}$$

where $V_{\text{eff}}(r) = -g/r + L^2/r^2$ is the effective potential. Thus,

$$\tilde{J}_{rc} = -L + \frac{g - 2L^2\epsilon_r}{2\sqrt{V_{\text{eff}}(r = 1/\epsilon_r) - \mathcal{E}}}.$$

In the limit of ϵ_r vanishing this becomes (5.10) again, showing thereby that this definition of J_{rc} which requires a modification of the integrand is equivalent to the one in the previous section.

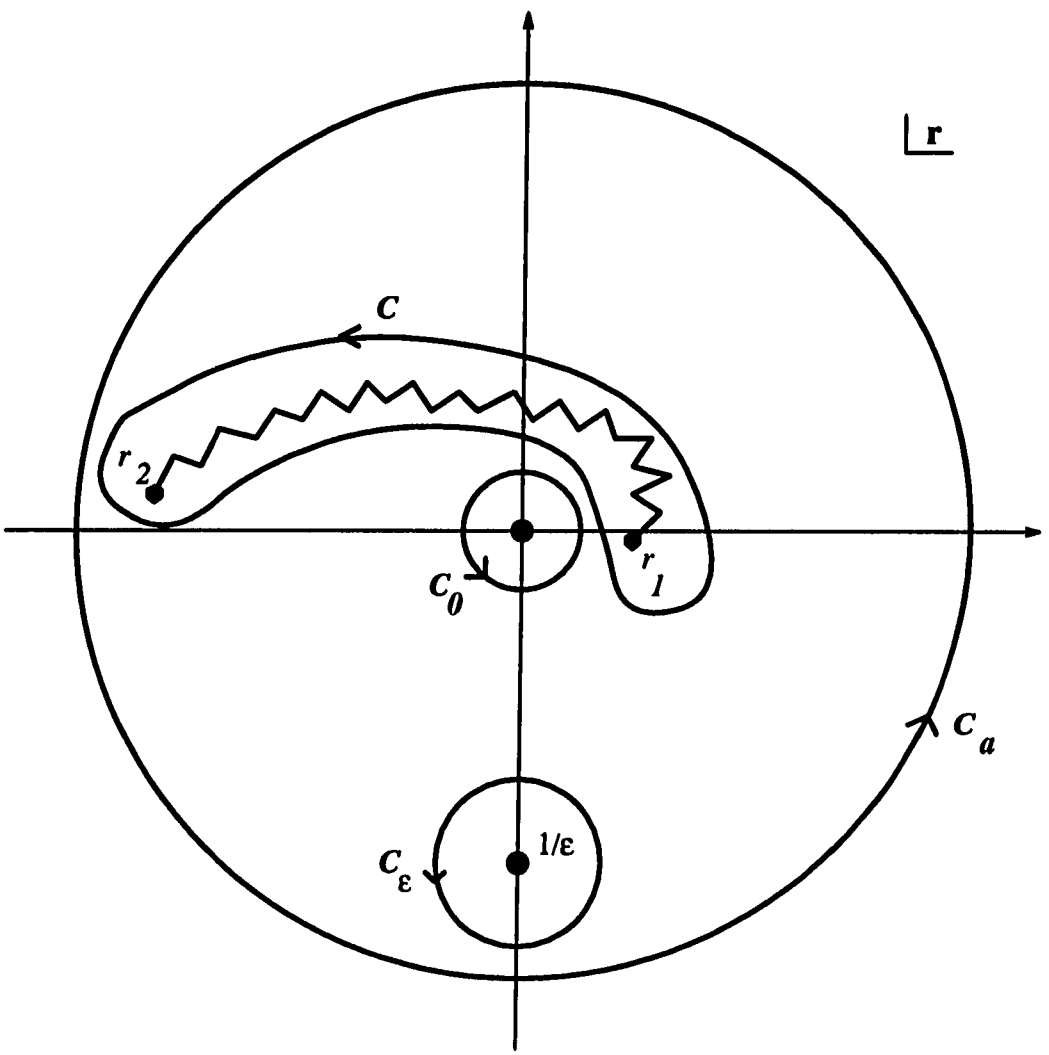

Figure 5.5: Contours for the modified J_{rc}

CHAPTER 6. SEMICLASSICAL STUDY - COULOMB POTENTIAL

The definition of the quantum radial action variable J_r requires a study of the locations of the poles of p_r in the complex r plane. This study is carried out here using a semiclassical method. Results of a numerical study based on the semiclassical method are presented.

J_r for bound states and energy eigenvalues

From eq. (4.19) the radial momentum function equation for a particle moving in the Coulomb potential is

$$\begin{aligned} -i\hbar \frac{\partial p_r(r,E,l)}{\partial r} + {p_r}^2(r,E,l) &= {p_{rc}}^2(r,E,l), \\ &= E + g/r - l(l+1)\hbar^2/r^2, \end{aligned} \tag{6.1}$$

with the boundary condition

$$\lim_{\hbar \to 0} \; p_r(r,E,l) = \; p_{rc}(r,E,l). \tag{6.2}$$

We define the quantum radial action variable J_r by

$$J_r = \frac{1}{2\pi} \oint_C p_r(r,E,l)dr, \tag{6.3}$$

where C is the same contour as the one used in evaluating J_{rc}, i.e., a counterclockwise contour in the complex r plane enclosing r_1 and r_2 and the region in between

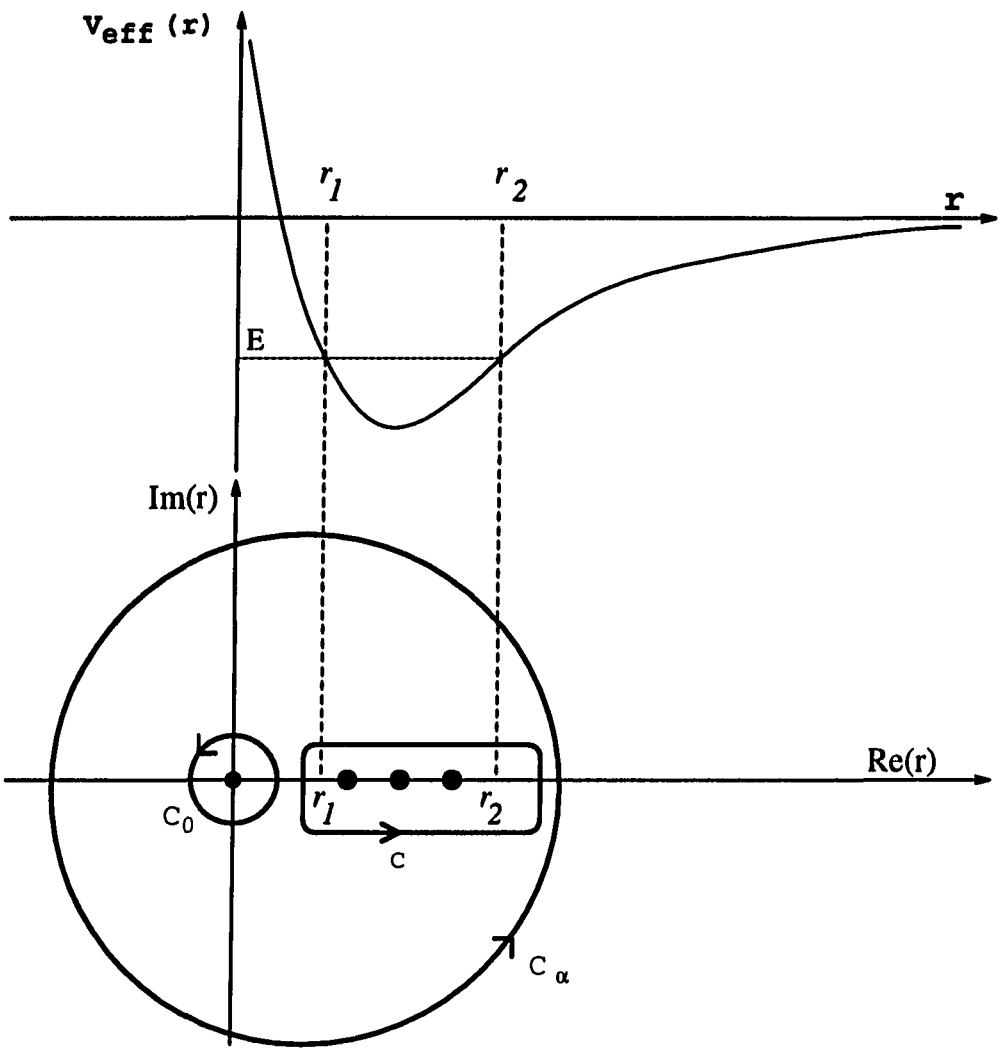

Figure 6.1: The poles of p_r in the complex r plane

them, as shown in Figure 6.1. This problem is identical to a one dimensional bound state problem studied in section 3.2. C encloses n_r poles of $p_r(r, E, l)$ of residue $-i\hbar$ on the real axis between r_1 and r_2, hence, by the residue theorem, $J_r = n_r\hbar$. The integral in (6.3) can be performed, as in the evaluation of J_{rc}, by distorting C into C_0 and C_∞. To obtain the series expansion for p_r on C_0, we note that it must have a simple pole at $r = 0$ since p_{rc}, its classical counterpart which it approaches in the classical limit, is of the form $-i\sqrt{l(l+1)\hbar^2}/r + \ldots$ there. Thus the momentum function equation (6.1)would be satisfied only if p_r is of the form

$$p_r = \frac{a_{-1}}{r} + a_0 + a_1 r + \ldots . \tag{6.4}$$

On the same contour C_0, the series form for p_{rc} is

$$p_{rc} = \frac{A_{-1}}{r} + A_0 + A_1 r + \ldots, \tag{6.5}$$

where

$$A_{-1} = -i\sqrt{l(l+1)\hbar^2}, \ldots .$$

Substituting (6.4) and (6.5) in (6.1), we get

$$a_{-1}^2 + i\hbar a_{-1} - A_{-1}^2 = 0,$$

thus $a_{-1} = -i(l+1)\hbar$ or $il\hbar$. The latter results in a series for p_r that does not satisfy the classical boundary condition (6.2) and, therefore, must be rejected. The contribution from C_0 to the integral (6.3) is therefore $l+1$. A similar method yields the contribution from C_∞ which is $g/2\sqrt{-E}$. The square root is positive for negative energy. Therefore,

$$J_r = -(l+1)\hbar + g/2\sqrt{-E} = n_r\hbar, \tag{6.6}$$

with $n_r = 0, 1, 2, \ldots$ Solving this for E we get the energy eigenvalues of the system:

$$E = -\frac{(g/2)^2}{(n_r + l + 1)^2 \hbar^2}. \tag{6.7}$$

Here n_r is the radial quantum number and $n = n_r + l + 1$ is the principal quantum number.

The boundary condition (6.2) was crucial in obtaining these eigenvalues. It is shown in [1] that this requirement is equivalent to the normalizability condition on the radial wave function of the particle. It is also shown there that for these discrete energies the only poles of the integrand in eq. (6.3) in the complex r plane are the ones on the real axis between r_1 and r_2 and the two fixed poles at $r = 0$ and $r = \infty$. The condition of normalizability is relaxed in the study of wave functions for positive energy states. Similarly, in the rest of this chapter, where we consider states of both negative and positive energy, the boundary condition (6.2) is relaxed. A study of the nature of p_r reveals that, for non-negative energy eigenvalues, in addition to the above poles there is a family of infinite poles. Before we can define J_r as a contour integral in the complex r plane for such energies we need to know the location and motion of these infinite poles of p_r; this will be the subject of the next part of this chapter.

Semiclassical method for the study of the poles of p_r

The quantum momentum function equation (6.1) is a Riccati equation which can be converted to the Schrödinger equation

$$\hbar^2 u'' + p_{rc}^2 u = 0, \tag{6.8}$$

by the transformation

$$p_r = -i\hbar u'/u, \tag{6.9}$$

where prime denotes differentiation with respect to r (see [1]). The poles of p_r in the complex r plane (to be referred to as 'poles') are then the zeroes of the radial wave function $u(r, E, l)$ (to be referred to as the 'zeroes').

Boundary condition on $u(r, E, l)$

The boundary condition (6.2) on the momentum function p_r is relaxed since we consider, besides energy eigenvalues, energies of the particle which are either unphysical or positive. This amounts to removing normalizability as a requirement on the wave function $u(r, E, l)$. Equation (6.8) is linear and has a regular singular point at $r = 0$, because ${p_r}^2$ around that point is of the form $-l(l+1)\hbar^2/r^2$. The two linearly independent solutions of u have the character of r^{l+1} and r^{-l}. The physical interpretation of u/r as the probability amplitude for the particle to be found between r and $r + dr$ rules out the solution of the second form, for energy eigenvalues. Thus $u \sim r^{l+1}$ around $r = 0$ for bound states. We continue to maintain this condition on u for all energies of the particle. Thus, for all energy E,

$$\begin{aligned} \lim_{r\to 0} \; u(r, E, l) &= 0 \text{ for } l \neq 0, \\ &= \text{a constant for } l = 0. \end{aligned} \tag{6.10}$$

If the energy is a negative eigenvalue then $u \to 0$ as $r \to +\infty$ and is normalizable, as we will see later. From eq. (6.9), the character of p_r at $r = 0$ on a negative energy eigenvalue, viz, a simple pole of residue $-i\hbar(l + 1)$, is maintained for all energies.

Approximate solution of Schrödinger equation - Stokes phenomenon

The WKB approximation for a solution of (6.8) is of the form

$$u \simeq (1/\sqrt{p_{rc}})[Ae^{iW_{rc}/\hbar} + Be^{-iW_{rc}/\hbar}], \tag{6.11}$$

where A and B are constants and

$$W_{rc}(r, E, l) = \int_{r_0}^{r} p_{rc}(r, E, l)dr, \tag{6.12}$$

r_0 being a turning point, viz, $p_{rc}(r_0, E, l) = 0$. Such a solution is good in regions which are far from the turning points and the singularities of p_{rc} (see [5]). The constants A and B have to be chosen differently in different regions of the complex plane for the following reason. u is single valued throughout the finite complex r plane but the right hand side of (6.11) is not, since W_{rc}, being the integral of p_{rc} (a discontinuous function) is discontinuous. It has a branch cut starting at the turning point r_0 and going to $r = \infty$. We describe here a method due to Furry [6] that selects A and B in the different regions such that the approximate solution is relatively smooth.

We need to know the nature of W_{rc} around the turning point r_0 before we can choose the appropriate constants A and B. Since ${p_{rc}}^2 = E - V(r) = V'(r_0)(r - r_0) + \ldots$, with $V(r)$ the effective potential, the functional form of p_{rc} very near r_0 is

$$p_{rc} \simeq [-V'(r_0)]^{1/2}(r - r_0)^{1/2}.$$

Thus, by (6.12), W_{rc} near r_0 is of the form

$$W_{rc} \simeq \frac{2}{3}[-V'(r_0)]^{1/2}(r - r_0)^{3/2}. \tag{6.13}$$

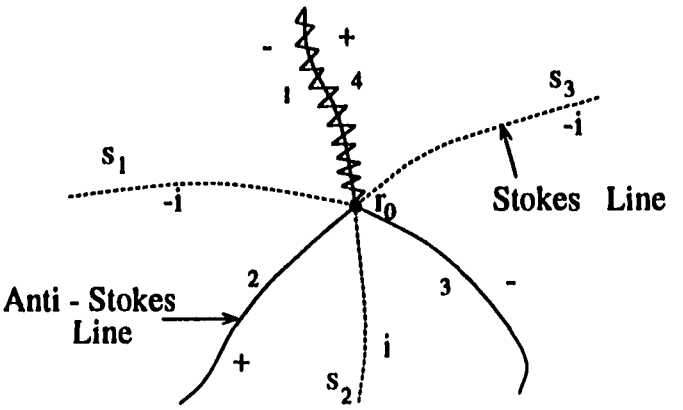

Figure 6.2: Stokes and anti-Stokes lines from turning point r_0

It follows from (6.13) that the phase of W_{rc} around $r = 0$ changes by 180^o as that of $\Delta r = r - r_0$ changes by 120^o. There are three directions, making angles of 120^o with each other, along which we can move from r_0 in the complex r plane in such way that the expression in (6.13) is purely imaginary. Once we have started out in any one of these directions we can choose the increments dr such that $p_{rc}dr$ is imaginary, and thus define a locus along which W_{rc} is purely imaginary. Such a locus is called a 'Stoke's line' and is, in general, a curved line (see Figure 6.2). One of the two exponentials in (6.11) dominates the other along a Stokes line. Complementing these Stokes lines are three 'anti-Stokes lines' which start out at angles of 60^o with respect to the Stokes lines and along which W_{rc} is purely real. In Figure 6.2 these anti-Stokes lines are marked 1, 2 and 3. The branch cut for W_{rc} is chosen along the anti-Stokes

line 1 and 4 represents the other side of the branch cut. W_{rc} is negative along 1 (the definition of p_{rc} fixes this character), negative imaginary along S_1, positive along 2, positive imaginary along S_2, negative along 3, negative imaginary along S_3 and positive along 4. In a solution of the form (6.11) both exp $(\pm iW_{rc})$ have unit magnitude along an anti-Stokes line. We represent the approximate solution along the anti-Stokes line 1 by $u_1 \simeq (1/\sqrt{p_{rc}})[A_1 e^{iW_{rc}/\hbar} + B_1 e^{-iW_{rc}/\hbar}]$. As we rotate from a point on 1 counterclockwise the magnitude of $\exp(iW_{rc})$ grows till we reach the Stokes line S_1 on which this exponential completely dominates in strength the other exponential $\exp(-iW_{rc})$. Now, if the approximate solution on the anti-Stokes line 2 were assumed to be $u_2 \simeq (1/\sqrt{p_{rc}})[A_2 e^{iW_{rc}/\hbar} + B_2 e^{-iW_{rc}/\hbar}]$, and extend this solution clockwise onto the Stokes line S_1, it must agree with the first solution u_1 within the limits of the approximation. This would force the two coefficients of the dominant exponential, viz, A_1 and A_2, to be identical while allowing for a discontinuity in the coefficients of the subdominant exponential B_1 and B_2. This is referred to as the Stokes phenomenon. Thus,

$$A_2 = A_1, \quad B_2 = B_1 + \gamma A_1,$$

where γ is called the 'Stokes constant'. That the constants $(A_2,\ B_2)$ are linear functions of $(A_1,\ B_1)$ follows from the linearity of the Schröedinger equation (6.8) whose solutions admit of superposition. A similar set of relations hold between $(A_2,\ B_2)$ and $(A_3,\ B_3)$ on the one hand and $(A_4,\ B_4)$ and $(A_3,\ B_3)$ on the other, with the subscripts on the constants denoting the respective anti-Stokes lines on which the constants are used in the representation of the approximate solution. Finally, we need to impose the continuity of the approximate solution on the branch cut. These requirements completely determine the four sets of constants $(A_j,\ B_j)$ if any one of

them is known. All the Stokes constants γ can be shown to be i [6] and the connection formulas relating the different $(A_j,\ B_j)$ are

$$A_2 = A_1 \qquad A_3 = A_2 + iB_2 \qquad A_4 = A_3,$$
$$B_2 = B_1 + iA_1 \qquad B_3 = B_2 \qquad B_4 = B_3 + iA_3. \tag{6.14}$$

In summary, there are, surrounding every turning point, three regions, with the Stokes lines separating adjacent regions and an anti-Stokes line in the middle of each region. Within each region we represent the wave function u by an expression of the form (6.11) with suitably chosen constants A and B to satisfy the boundary conditions on u in that region. The connection formulas (6.14) then provide the constants to be chosen in the other two regions. If in a region the solution has non-zero coefficients $(A_j,\ B_j)$, there is the possibility that the two exponentials cancel each other and that $u(r, E, l)$ has zeroes, and so p_r poles, in that region. Setting the right hand side of (6.11) to zero we obtain an equation for the zeroes r_n of u in the region where the solution is valid:

$$W_{rc}(r_n, E, l) \ = \ [\,(1/2i)\ln(-B/A) + n\pi\,]\,\hbar \tag{6.15}$$

This furnishes us with a means to search semiclassically for the poles in the complex r plane. We undertake such a search for the poles of p_r for a particle moving in the Coulomb potential; it is done analytically within the approximation of the semi-classical method above. In the last section of this chapter we examine the results of a numerical study based on the this method. A similar method is used to search for the poles in the case of the Yukawa potential.

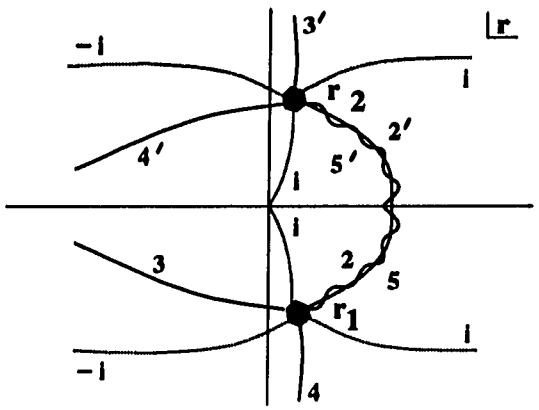

Figure 6.3: Stokes lines (broken lines) from turning points r_1 and r_2 for $E < V_0$

Poles for $E < V_0$

Figure 6.3 shows the different regions around the two turning points r_1 and r_2 for energy $E < V_0$. The regions around r_1 are numbered $2, 3, 4$ and 5 as shown. The primed numbers similarly denote the regions around r_2. We have followed a scheme in numbering these lines that show how the different regions around a turning point transform as we increase the particle's energy. There are two turning points here instead of one; so one has to define two W_{rc}s, one corresponding to r_1 and the other to r_2. In the definition (6.12) the turning point used for defining W_{rc1} is r_1 and that for W_{rc2} is r_2. The approximation for u around r_1 is expressed in terms of W_{rc1} and that around r_2 in terms of W_{rc2}. The constant coefficients to be used in the solution around r_2 are not independent of the ones used in the solution around r_1; there is the

region common to 2 and $5'$ (or 5 and $2'$) and the u expressed in terms of W_{rc1} should match the one expressed in terms of W_{rc2}. From the requirement (5.2) on p_{rc}, as $r \to \infty$ $p_{rc} \to k = \sqrt{E}$, which by our definition of p_{rc}, is positive imaginary for negative energy. Thus for large r, $p_{rc}dr$ is positive or negative imaginary depending on whether dr is positive or negative. The Stokes lines are thus asymptotically horizontal in the complex r plane for negative energy. Similarly the anti-Stokes lines are vertical.

We first obtain the solution in region 2 consistent with the boundary condition (6.10). Close to the point $r = 0$ both the W_{rc}s are proportional to $\ln r$ whose character is positive imaginary on the Stokes line from r_1 that goes into $r = 0$. Thus $\exp(-iW_{rc1}/\hbar)$ is singular at $r = 0$ and its coefficient B_2 must be zero. A_2 is arbitrary. Using these constants A_2 and B_2 we can determine (A_3, B_3), (A_4, B_4) and (A_5, B_5) using the connection formulas (6.14). These constants are

$$\begin{aligned} A_3 &= A_2, \quad A_4 = A_2, \quad A_5 = 0, \\ B_3 &= 0, \quad B_4 = iA_2, \quad B_5 = iA_2. \end{aligned} \tag{6.16}$$

Thus only region 4 around r_1 has an approximate solution u containing both the exponentials $\exp(\pm iWrc1/\hbar)$; Using eq. (6.16) in (6.15) we obtain the poles r_n in this region:

$$W_{rc}(r_n, E, l) = (n - 1/4)\pi\hbar, \tag{6.17}$$

with $n = 1, 2, 3, \ldots$ Since all the poles are located at points where W_{rc} is real it follows that the anti-Stokes line that points south of r_1 is the locus of infinitely many poles. Next, we obtain the solution in region $2'$, which overlaps with 5. The two

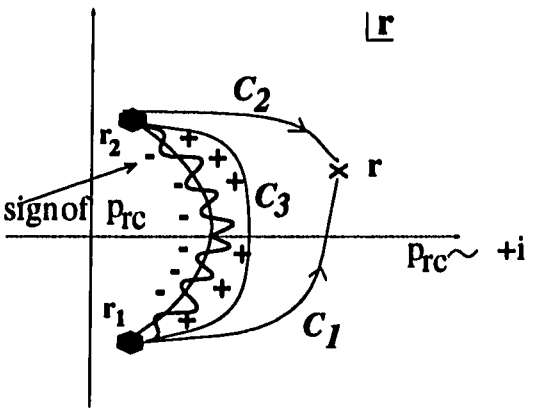

Figure 6.4: Definition of W_{rc1} and W_{rc2}

different representations of u here are

$$u_{2'} \simeq (1/\sqrt{prc})\,[\,A_{2'}\,e^{iW_{rc2}/\hbar} + B_{2'}\,e^{-iW_{rc2}/\hbar}] \tag{6.18}$$

and

$$u_5 \simeq (1/\sqrt{prc})\,[\,A_5\,e^{iW_{rc1}/\hbar} + B_5 e^{-iW_{rc1}/\hbar}], \tag{6.19}$$

which, from (6.16) is

$$u_5 \simeq iA_2\,(1/\sqrt{prc})\,e^{-iW_{rc1}/\hbar}. \tag{6.20}$$

In Figure 6.4

$$\int_{C_1} prc\,dr = \int_{C_2} prc\,dr + \int_{C_3} prc\,dr$$

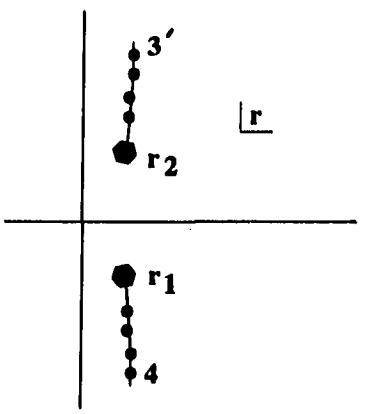

Figure 6.5: Poles in the complex r plane for $E < V_0$

Thus, from the definition (5.10) of the classical radial action J_{rc}, the two W_{rc}s are related by

$$W_{rc1} = \pi J_{rc} + W_{rc2}$$

Equating u_5 and $u_{2'}$ from (6.18) and (6.20), we get

$$A_{2'} = 0 \quad B_{2'} = -i\alpha A_2, \tag{6.21}$$

where

$$\alpha = exp(-i\pi J_{rc}/\hbar).$$

The rest of the primed constants A and B can be obtained using the connection formulas (6.14):

$$A_{3'} = \alpha A_2, \quad A_{4'} = \alpha A_2, \quad A_{5'} = \alpha A_2,$$

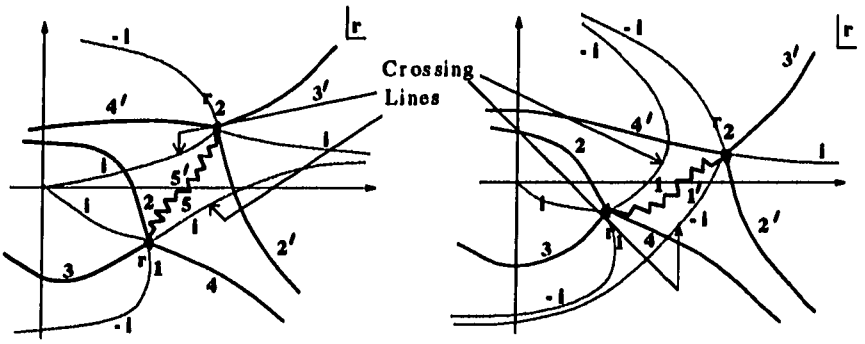

Figure 6.6: Stokes and anti-Stokes lines for $E \approx V_0$

$$B_{3'} = -i\alpha A_2, \quad B_{4'} = 0, \quad B_{5'} = 0. \tag{6.22}$$

We see that region $3'$, with u having two exponentials, has infinitely many poles located on the anti-Stokes line going north of r_2, a result we could have predicted by symmetry. The resulting picture of poles in the complex r plane for $E < V_0$ is shown in Figure 6.5. Anti-Stokes lines 4 and $3'$ go to $r = \infty$. The limit point of the poles located on these anti-Stokes lines is thus $r = \infty$.

Poles for $V_0 < E < 0$

As seen in chapter 5 r_1 and r_2 move onto the positive real axis of the r plane and remain there for $V_0 < E < 0$ corresponding to the region of classical physical bound states. The Stokes and anti-Stokes lines from these two turning points are

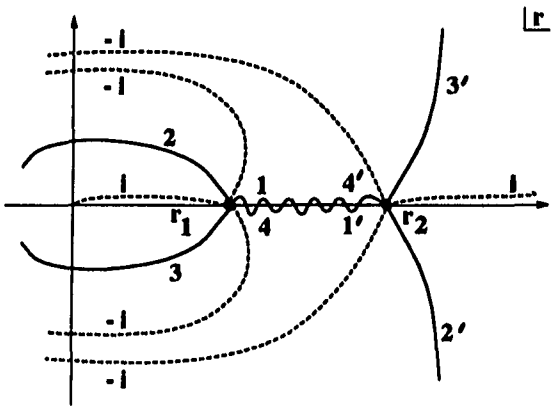

Figure 6.7: Stokes and anti-Stokes lines for $V_0 < E < 0$

shown in Figure 6.7. Figure 6.6 shows the geometry of these lines for energies close to V_0; the first of these is for E slightly less then V_0 and the second for E slightly greater than V_0. The two turning points are near each other for these energies. The transition to the the physically allowed region of $E > V_0$ from the unphysical $E < V_0$ region is characterized by the crossing of two Stokes lines, one each from r_1 and r_2 as shown in the figure; these lines rotate counterclockwise closing region $5'$ and opening region 1 while simultaneously closing region 5 and opening region $1'$. One significant change after this transition is that the set of poles that were south of r_1 (in region 4) which used to follow the motion of r_1 now move to region $2'$ and follow r_2.

We first construct the semiclassical wave function u in region 2; here B_2, the coefficient of the dominant exponential has to vanish to satisfy the boundary condition

Table 6.1: Coefficients A and B of $\exp(\pm iW/\hbar)$

Energy Range	A_1	B_1	A_2	B_2	A_3	B_3	A_4	B_4	A_5	B_5
$E < V_0$			1	0	1	0	1	i	0	i
$V_0 < E < 0$	1	$-i$	1	0	1	0	1	i		
$E > 0$			1	0	1	0	1	i	0	i
	$A_{1'}$	$B_{1'}$	$A_{2'}$	$B_{2'}$	$A_{3'}$	$B_{3'}$	$A_{4'}$	$B_{4'}$	$A_{5'}$	$B_{5'}$
$E < V_0$			0	$-i\alpha$	α	$-i\alpha$	α	0	α	0
$V_0 < E < 0$	$-1/\alpha$	$-i\alpha$	$-1/\alpha$	$-i\beta$	α	$-i\beta$	α	$-i/\alpha$		
$E > 0$			0	$-i\alpha$	α	$-i\alpha$	α	0	α	0

$\alpha = \exp(-i\pi J_{rc}/\hbar)$ $\qquad$ $\beta = \alpha + 1/\alpha$

(6.10) on u at $r = 0$ which lies in this region. The coefficient A_2 of the subdominant solution is arbitrary. The other three sets of constant coefficients of u around r_1 are obtained from the connection formulas. The wave function is then extended to regions around r_2 by matching u in the overlapping regions 4 and $1'$. All the coefficients are listed in Table 6.1. Having determined the semiclassical wave function all over the r plane we now examine the different regions for the presence of poles. A region where u is proportional to the single exponential $\exp(iW_{rc1}/\hbar)$ or $\exp(-iW_{rc1}/\hbar)$ has no poles that move as the energy varies, unlike regions where u has two exponentials.

Poles in between r_1 and r_2

In region 1

$$\begin{aligned} u_1 &\simeq (1/\sqrt{p_{rc}})[e^{iW_{rc1}/\hbar} - ie^{-iW_{rc1}/\hbar}] \\ &\sim (1/\sqrt{p_{rc}})\sin(W_{rc1}/\hbar - \pi/4), \end{aligned} \tag{6.23}$$

which is the form of the solution, up to a constant, in between the turning points r_1 and r_2. The poles occur on the real axis when $W_{rc1} = (n + 1/4)\pi\hbar$, with n an integer. If $E \approx V_0$, $W_{rc1} \approx 0$ for all r in between r_1 and r_2 and there are no poles on the real axis. As the energy increases the absolute value of W_{rc1} also increases and more and more poles appear between r_1 and r_2. We call these 'poles in the well'.

Poles in the southern half plane

In region $2'$ the wave function is of the form (see Table 6.1)

$$\begin{aligned} u_{2'} = &\simeq (1/\sqrt{p_{rc}})[(1/\alpha)e^{iW_{rc2}/\hbar} + i\beta e^{-iW_{rc2}/\hbar}] \\ &\sim (1/\sqrt{p_{rc}})[e^{iW_{rc2}/\hbar} + i(1 + exp(-2i\pi J_{rc}/\hbar)e^{-iW_{rc2}/\hbar}], \quad (6.24) \end{aligned}$$

where $\beta = \alpha + 1/\alpha$. We can deduce the following results from this form of the solution:

(1) The part of the real axis $r > r_2$ is a boundary of the region where the above form of the solution is valid. For the range of energy under consideration J_{rc} is real and positive. For those energies for which $J_{rc} = (n_r + 1/2)\hbar$, for integer n_r the coefficient of the dominant exponential in u vanishes, leaving the wave function a subdominant exponential for $r > r_2$; a normalizable wave function results for these special energies. These energies are the energy eigenvalues in the WKB approximation.

(2) From (6.15) and (6.24) the jth pole r_j of p_r in this region is given by

$$W_{rc2}(r_j, E, l) = [\,(1/2i)\,\ln\,[1 + exp(-2i\pi J_{rc}/\hbar)\,]\,] + (j + 1/4)\pi\,]\,\hbar \quad (6.25)$$

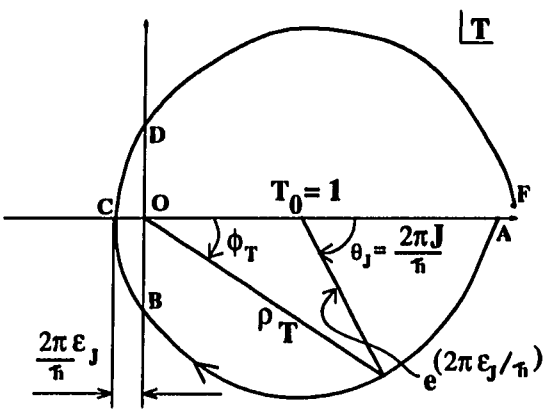

Figure 6.8: Variation of $T(E)$ with energy in T plane

We can write

$$W_{rc}(r, E, l) \simeq [\, kr + O(\ln r)\,], \tag{6.26}$$

for $|r|$ large, with $E = k^2$. We define $k = i\kappa$ with $\kappa > 0$ and define

$$T(E) = \rho_T(E)e^{-i\phi_T(E)} = 1 + exp(-2iJ_{rc}(E, l)/\hbar). \tag{6.27}$$

For large j, from (6.25), (6.26) , and (6.27)

$$r_j = x_j + iy_j \approx [\,-(1/2\kappa)\,[\ln(\rho_T)] + (i/\kappa)\{\phi_T/2 - (j + 1/4)\pi\}]\hbar. \tag{6.28}$$

In this approximation, therefore, all the poles are located along a vertical line south of r_2, with a spacing of $\pi\hbar/\kappa$ between successive poles. As the energy increases, $\kappa = \sqrt{-E}$ decreases and the inter-pole distance increases.

(3) We can use equation (6.28) to study the motion of poles with energy. For $J_{rc}(E + i\epsilon_E) = J + i\epsilon_J$ with $J = Re(J_{rc})$ and $Im(J_{rc}) = \epsilon_J > 0$ the distance in the complex T plane between $T(E)$ and 1 is $|T(E) - 1| = exp(2\pi\epsilon_J/\hbar) > 1$ (see Figure 6.8). As the energy increases from V_0, following definition (6.27), $T(E)$ moves clockwise around the point $T_0 = 1$ because ϕ_T increases (see eq. (6.8)). As $\phi_T \rightarrow \pi$, ρ_T attains its minimum value $\approx 2\epsilon_J/\hbar$ and x_j, which is proportional to $-\ln(\rho_T)$ is maximum. As ϕ_T increases further ρ_T increases and x_j decreases. Thus as the phase ϕ_T passes through π ($B \rightarrow C \rightarrow D$ in the figure) the pole goes out east and then comes back west. Such an eastward excursion of the pole followed by a westward return repeats cyclically for $\phi_T = \pi, 3\pi, 5\pi, \ldots$. If $\epsilon_E = 0$ then $\epsilon_J = 0$ and $\mathrm{Min}(\rho_T) = 0$; the poles would move east all the way to $r = \infty$. This vanishing of T results in u being proportional to a single decaying exponential for $r \rightarrow \infty$ on the real r axis, from (6.24), corresponding to an energy eigenvalue. y_j depends on E through both κ and ϕ_T. The dependence on ϕ_T is significant as $T(E)$ moves from B to D in Figure 6.8. On the curve BCD, $\theta_J = 2\pi J/\hbar \approx \pi$, thus $J(E)$ and hence $\kappa(E)$ is nearly a constant for $T(E)$ on BCD. However for this short range of energy $\phi_T(E)$ varies through π, resulting in the advance of y_j through approximately π/κ_C. As the energy passes by an eigenvalue the pole moves up towards the x axis by about π/κ_C. For the parts $A \rightarrow B$ and $D \rightarrow F$ in figure 6.9 ϕ_T advances by π tending to increase y_j; κ decreases for this variation of E tending to decrease y_j. Of these two counter influences determining the variation of y_j it can be shown that the latter is more significant. During the advance of E in carrying $T(E)$ from A to F, there is a net upward movement of y_j, i.e., the pole comes closer to the x axis. The resulting motion of such a "southern pole" corresponding to $j = 3$ for three cycles of ϕ_T is

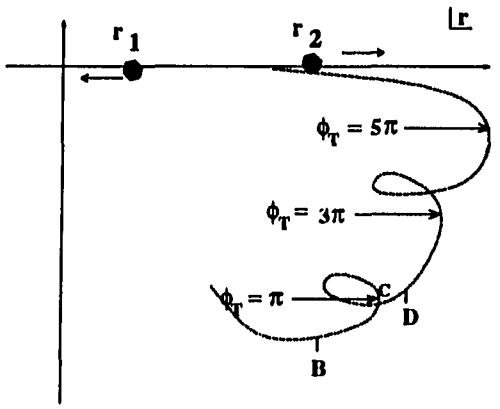

Figure 6.9: Movement of a southern pole with energy

shown in Figure 6.9. These poles eventually become poles in the well, entering the region between r_1 and r_2.

Poles in the northern half plane

Th WKB form of the wave function in region $3'$ is of the form

$$u_{3'} \simeq (1/\sqrt{prc})[(e^{iW_{rc}2/\hbar} - i(1 + \exp(2i\pi J_{rc}/\hbar)e^{-iW_{rc}2/\hbar}]. \qquad (6.29)$$

Defining

$$\begin{aligned} T'(E) &= \rho_{T'}(E)e^{i\phi_{T'}(E)} = 1 + \exp(2i/\pi J_{rc}(E,l)/\hbar) \\ &= 1 + \exp(-2\pi\epsilon_J/\hbar)\exp(2i\pi J(E)/\hbar). \qquad (6.30) \end{aligned}$$

T' varies with E as shown in Figure 6.10. It moves counterclockwise with increasing energy around the point $T_0{}' = 1$. This T' path does not encircle the point $T' = 0$,

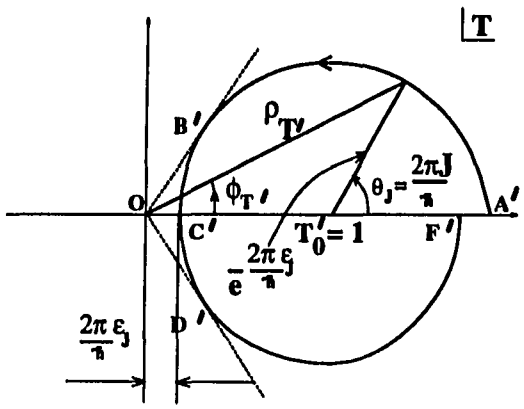

Figure 6.10: Variation of $T'(E)$ with energy in T' plane

since $\exp(-2\epsilon_j/\hbar) < 1$. The location of the jth pole is given by

$$r_j = x_j + iy_j \approx [-(1/2\kappa)\{\ln(\rho_{T'}] + (i/\kappa)[(j-1/4)\pi - \phi_{T'}/2\}]\hbar. \quad (6.31)$$

These poles are thus located on a vertical line going north of r_2. The variation of x_j is similar to the case of southern poles. The variation of y_j is however different; the phase $\phi_{T'}$ does not monotonically increase. It is bounded by the angle OB' and OD' make with the x axis; and $\phi_{T'}$ oscillates between $\angle D'OC'$ and $\angle B'OC'$. κ decreases, and therefore y_j, which is proportional to $1/\kappa$ increases, with increasing negative energy. These "northern poles" do not approach the real axis unlike the southern poles. This lack of symmetry between the poles in the southern and northern half planes arises because of the positive nature of ϵ_J which, in turn, results from

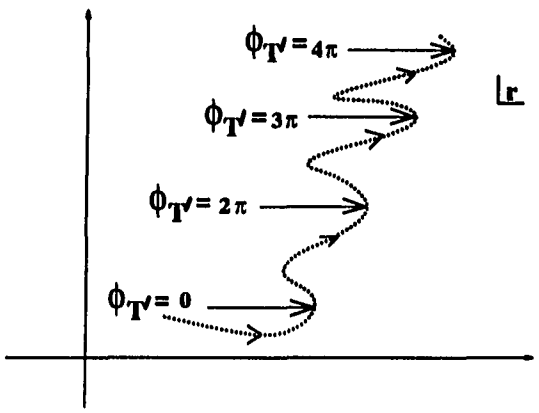

Figure 6.11: Movement of a northern pole with energy

our choice of a positive ϵ_E. The variation of a northern pole with energy is shown in Figure 6.11. Figure 6.12 shows the locations of poles as the energy increases from one negative eigenvalue to the next.

Poles for $E > 0$

As E becomes positive the turning point r_2 moves to the negative real axis of the r plane while r_1 continues to be on the positive real axis. The pictures of Stokes and anti-Stokes lines during this transition are shown in Figure 6.13. As in the transition around $E = V_0$, Stokes lines from the two turning points cross over around $E = 0$, pushing regions 1 and $1'$ out while forming the new regions 5 and $5'$. The important change is in the character of p_{rc} which, for large r, is approximately $\sqrt{E}$ and is,

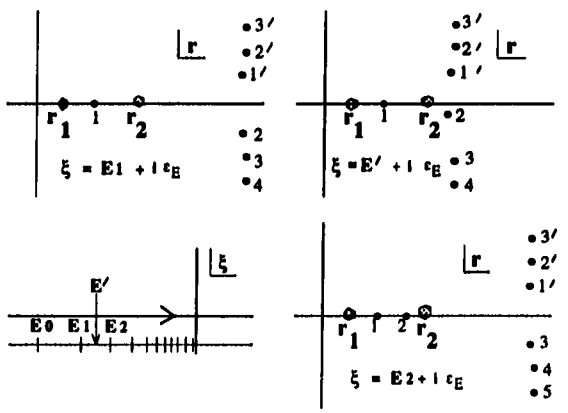

Figure 6.12: Collective movement of poles with energy

by our definition of the classical momentum function, positive for positive E. The Stokes lines, corresponding to the direction of dr that yields imaginary $p_{rc}dr$, point north and south in the r plane asymptotically for negative energy; and the anti-Stokes lines point east and west, ie, they are oriented perpendicular to the Stokes lines asymptotically. After the transition from negative to positive energy the anti-Stokes line 4 assumes the role of $2'$ in that it now is in the center of the region that contains the poles which were located south of r_2 for negative energy. Following the counterclockwise rotation through 90^o of the anti-Stokes line 4 the southern poles also rotate by $\pi/2$ and now move to the real axis. Similarly the northern poles follow the anti-Stokes line $3'$ and move to the negative real axis. This motion of all the poles as the energy changes from negative energy to positive energy after passing through the negative eigenvalues is shown in Figure 6.15. The Stokes and anti-Stokes lines

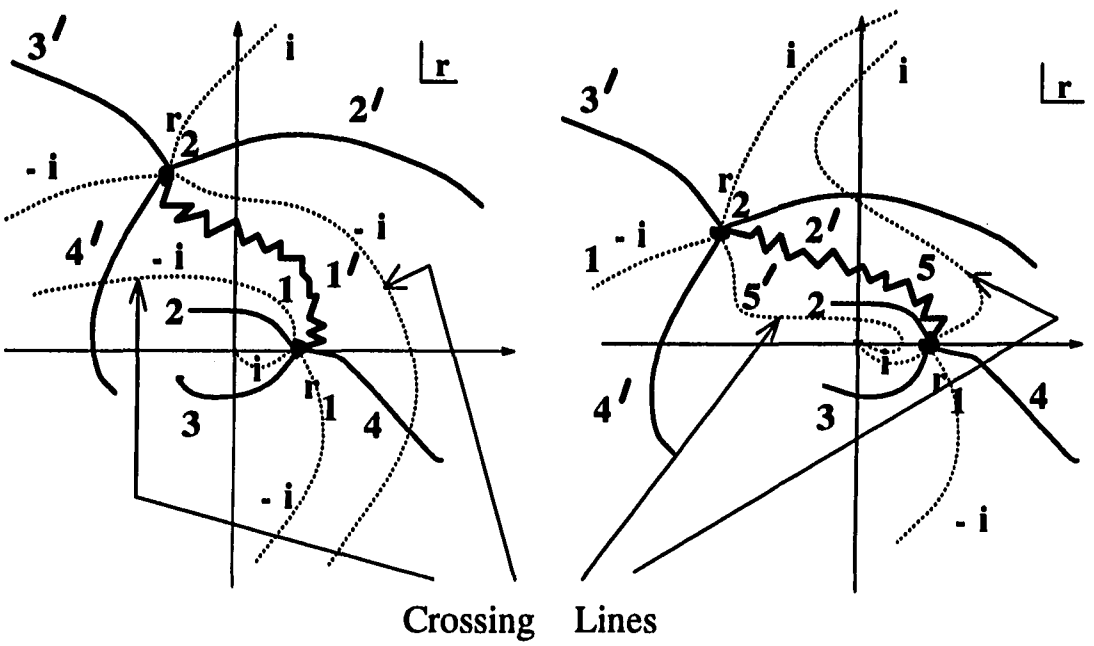

Figure 6.13: Stokes and anti-Stokes lines for $E \approx 0$

for positive energy are shown in Figure 6.14

From Table 6.1 the two regions of pole locations are 4 and $3'$. Using the coefficients A and B from this table we write the wave functions in these two regions:

$$u_4 \simeq (1/\sqrt{p_{rc}}) \sin [\, W_{rc1}/\hbar - \pi/4) \,],$$

$$u_{3'} \simeq (1/\sqrt{p_{rc}}) \cos [\, W_{rc1}/\hbar - \pi/4) \,].$$

The zeroes r_j thus lie to the right of r_1 on the real axis for $W_{rc1}(r_j) = (n + 1/4)\pi\hbar$ and to the left of r_2 on the real axis for $W_{rc2}(r_j) = (n + 1/4)\pi\hbar$, as predicted.

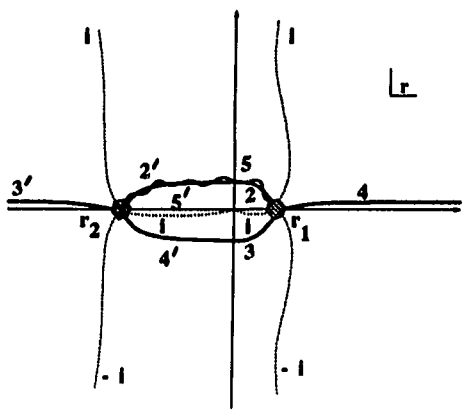

Figure 6.14: Stokes and anti-Stokes lines for $E > 0$

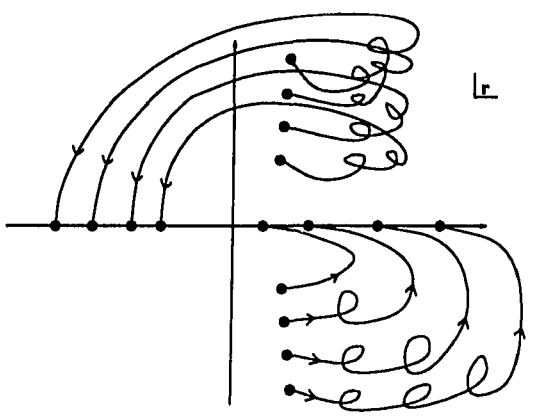

Figure 6.15: Motion of the southern and northern poles with increasing energy

Semiclassical numerical study of the motion of poles with energy

We present here the results of a semiclassical numerical study of the determination of the poles as a function of energy. The equations $u_{2'}(r_j) = 0$ and $u_{3'}(r_j) = 0$ are solved numerically by the Newton-Raphson method. For convenience we have set $\hbar = 1$. The energies used in the calculation are shown in the complex E plane. As seen before, the maxima of $Re(r_j(E))$, where r_j is the jth southern pole, is approximately proportional to $\ln \epsilon_J$. We can thus restrict the rapid variation of the location of a pole around the energy eigenvalues by controlling the magnitude of ϵ_J.

Figures 6.16 and 6.17 show the motion of the three topmost southern poles with energy computed numerically. These figures correspond to successively smaller values of constant ϵ_J (this makes the imaginary part of energy, which is proportional to ϵ_J, also smaller for successive computations). The numbers 1, 2, 3,... in the figure indicate the positions of the poles for $\mathcal{E} = E_1 + i\epsilon_E$, $E_2 + i\epsilon_E$, $E_3 + i\epsilon_E$,... respectively. As predicted the poles go out farther east, as the energy nears an eigenvalue, the smaller ϵ_J is at an energy eigenvalue. The sensitivity of the maximas of $Re(r_j)$ to ϵ_J is logarithmic as is evident from the figures. Also the increase in $Im(r_j)$ as the energy passes by an eigenvalue is the same for every pole; the WKB analysis predicts this increase to be $\pi/\sqrt{-E_n}$, where E_n is the nth energy eigenvalue, which matches the computed increase in $Im(r_j)$. The nth southern pole enters the region of the real axis between r_1 and r_2 as the system's energy equals that of the nth excited state. All the southern poles are on the positive real axis for positive energies. Figure 6.18 shows the first ten southern poles computed for negative energies.

Figures 6.19 and 6.19 show the movement of the northern poles with energy, computed by an identical method. As predicted, these poles perform right-left oscilla-

tions with energy for negative energies, with $Re(r_j)$ displaying the same logarithmic sensitivity to ϵ_E as the southern poles for energies near an eigenvalue. As E becomes positive, the northern poles move counterclockwise and reach the negative real axis. This can be understood by following the rotation of anti-Stokes line $3'$ in Figure 6.13 as E changes sign from negative to positive values. The northern poles have this anti-Stokes line as their asymptote, since W_{rc2} is real on this line; and from equation (6.29) these poles are located where $W_{rc2}(r_j) \approx (j - 1/4)$ for large j. That the line $3'$ rotates counterclockwise around $E = 0$ follows from the character of W_{rc2} far from the origin : $W_{rc2} \approx kr$ there. The phase of $\mathcal{E}$ decreases from π to 0 as the sign of E becomes positive; the phase of $k = \sqrt{\mathcal{E}}$ decreases from $\pi/2$ to 0. The phase of $W_{rc2} \approx kr$ on the anti-Stokes line $3'$ is π and has to retain this character even during the rapid change of phase of k around $E = 0$. This is achieved by the counterclockwise rotation of r, the position of a point on the anti-Stokes line, increasing its phase by $\pi/2$, so that the phase of kr remains π for points on the anti-Stokes line.

We will see in Chapter 7 that the exact positions of these poles and their characteristic variations with energy, as determined by numerically integrating Schrödinger equation, are represented quite accurately by the numerical method based on the WKB approximation of the wave function in the complex r plane presented in this chapter.

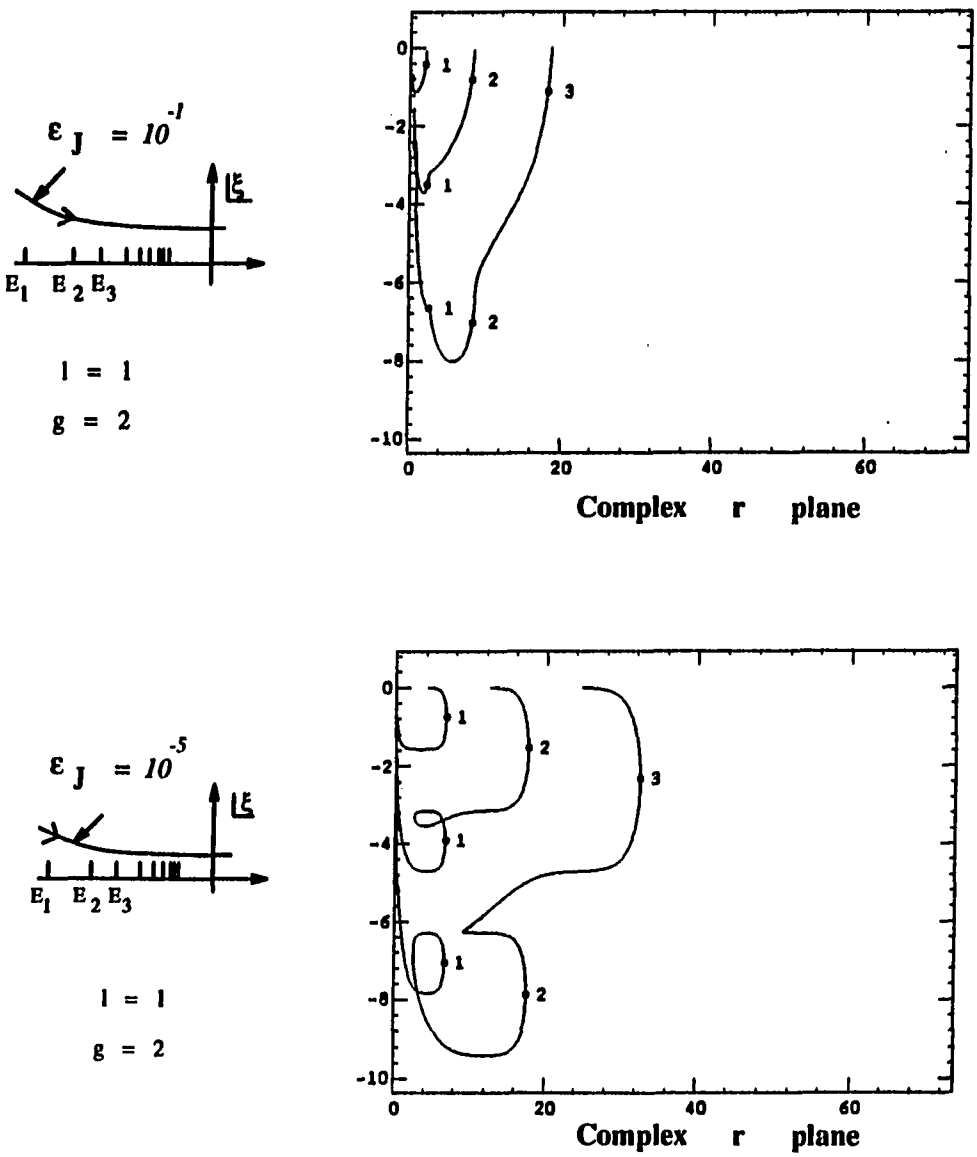

Figure 6.16: First three southern poles of p_r computed using the WKB approximation for the Coulomb wavefunction

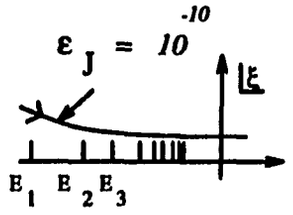

l = 1

g = 2

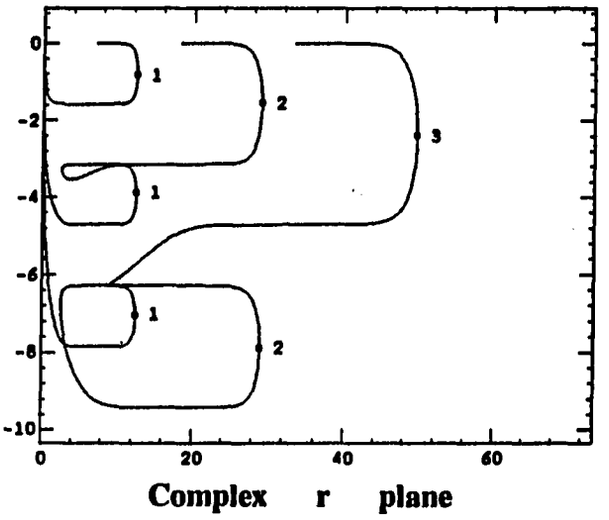

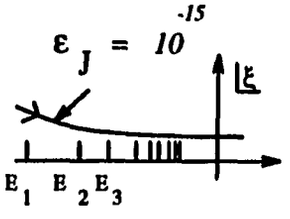

l = 1

g = 2

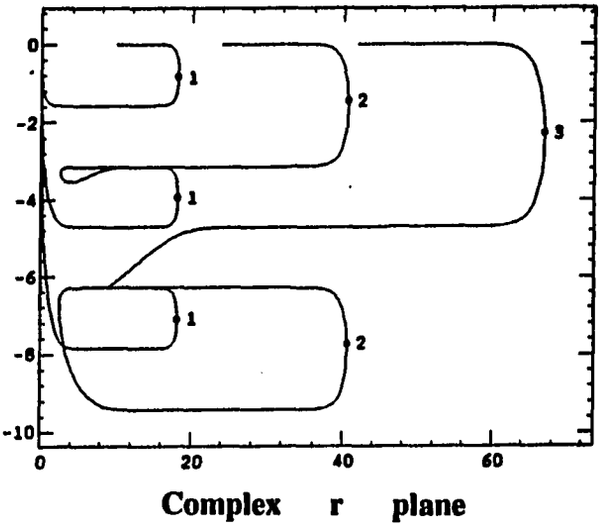

Figure 6.17: First three southern poles of p_l computed using the WKB approximation for the Coulomb wavefunction with smaller ϵ_E

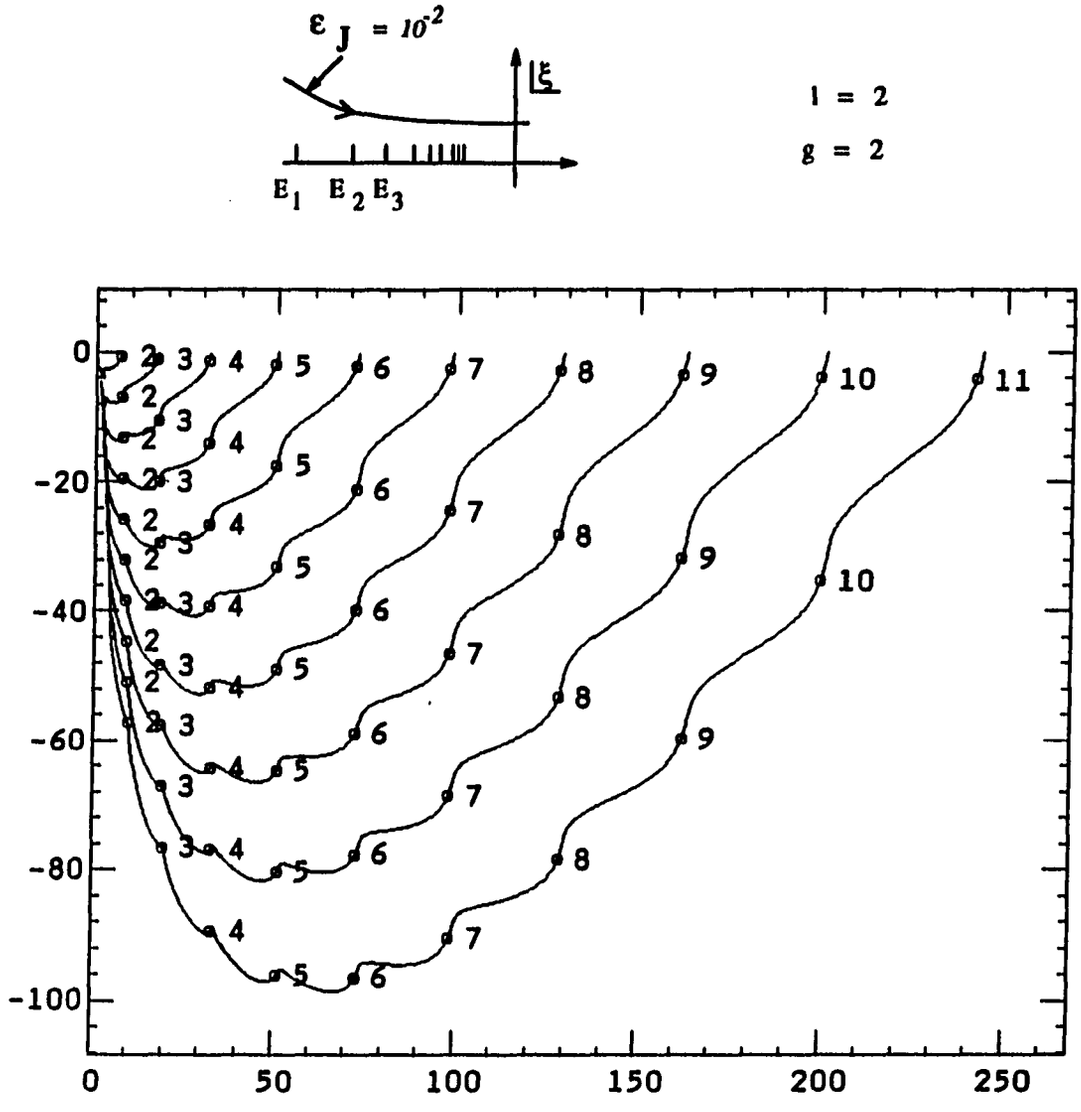

Figure 6.18: Ten southern poles of p_r in the complex r plane computed using the WKB approximation for the Coulomb wavefunction

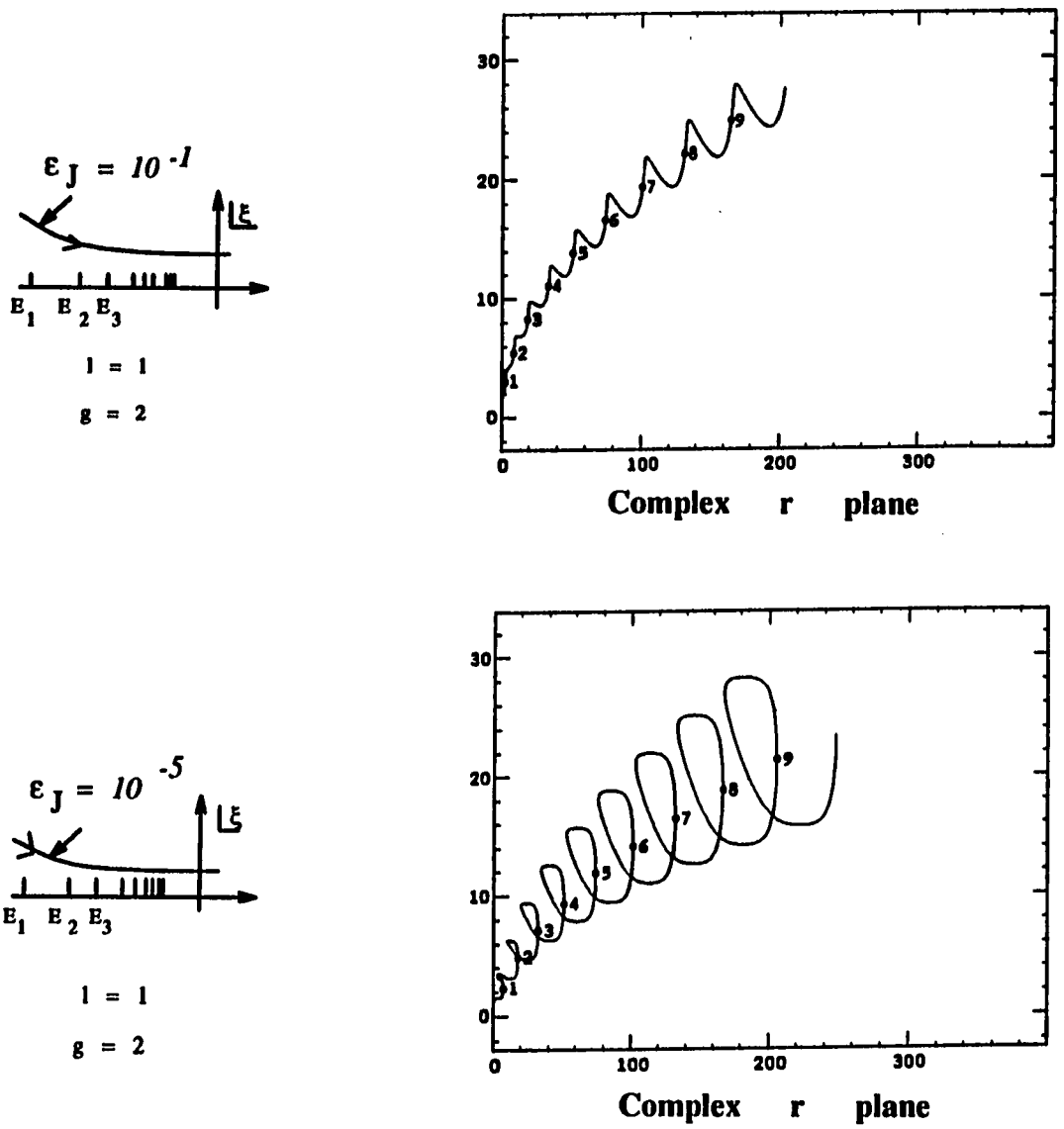

Figure 6.19: First northern pole of p_r computed using the WKB approximation for the Coulomb wavefunction

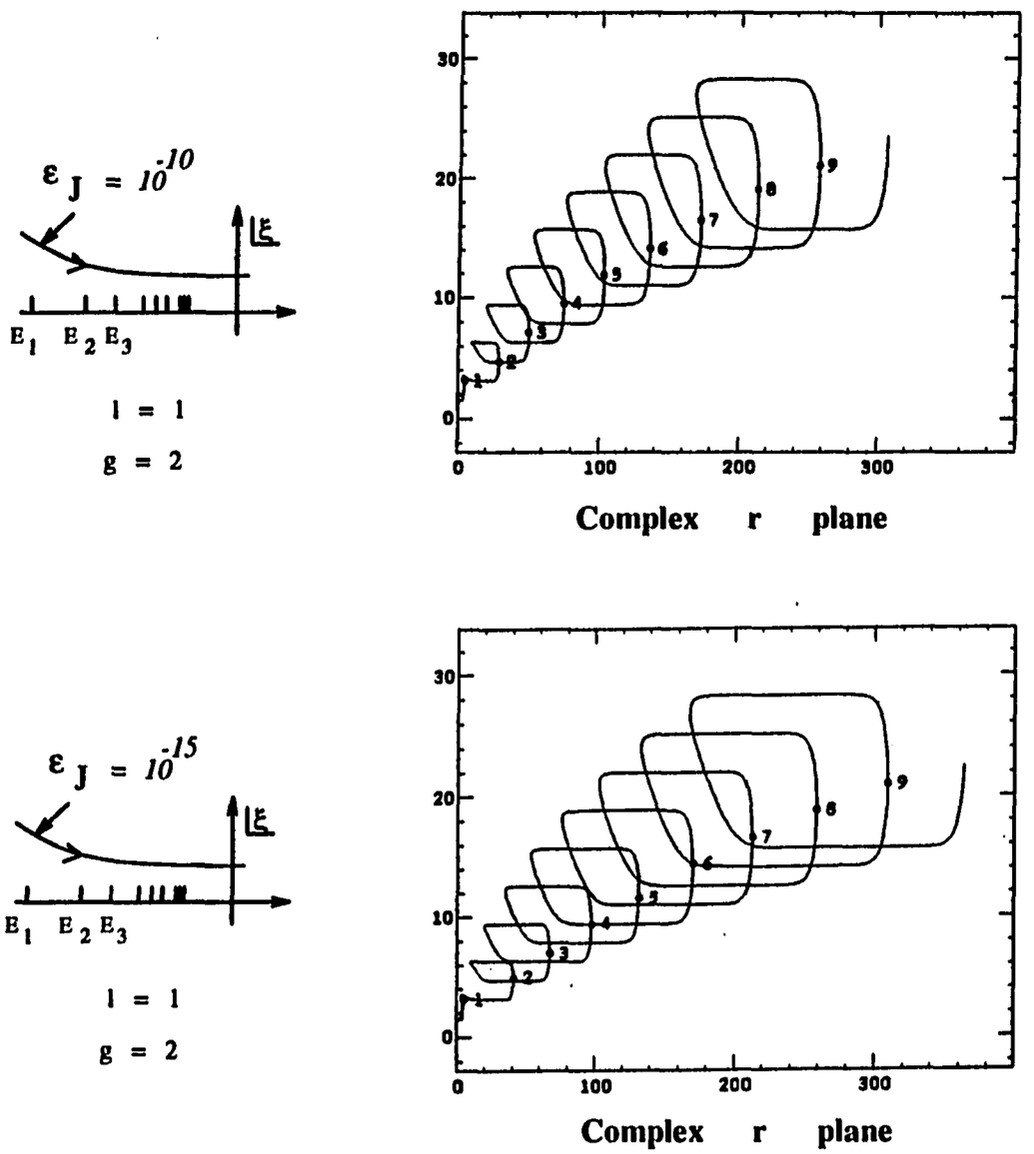

Figure 6.20: First northern pole of p_r computed using the WKB approximation for the Coulomb wave function with smaller ϵ_E

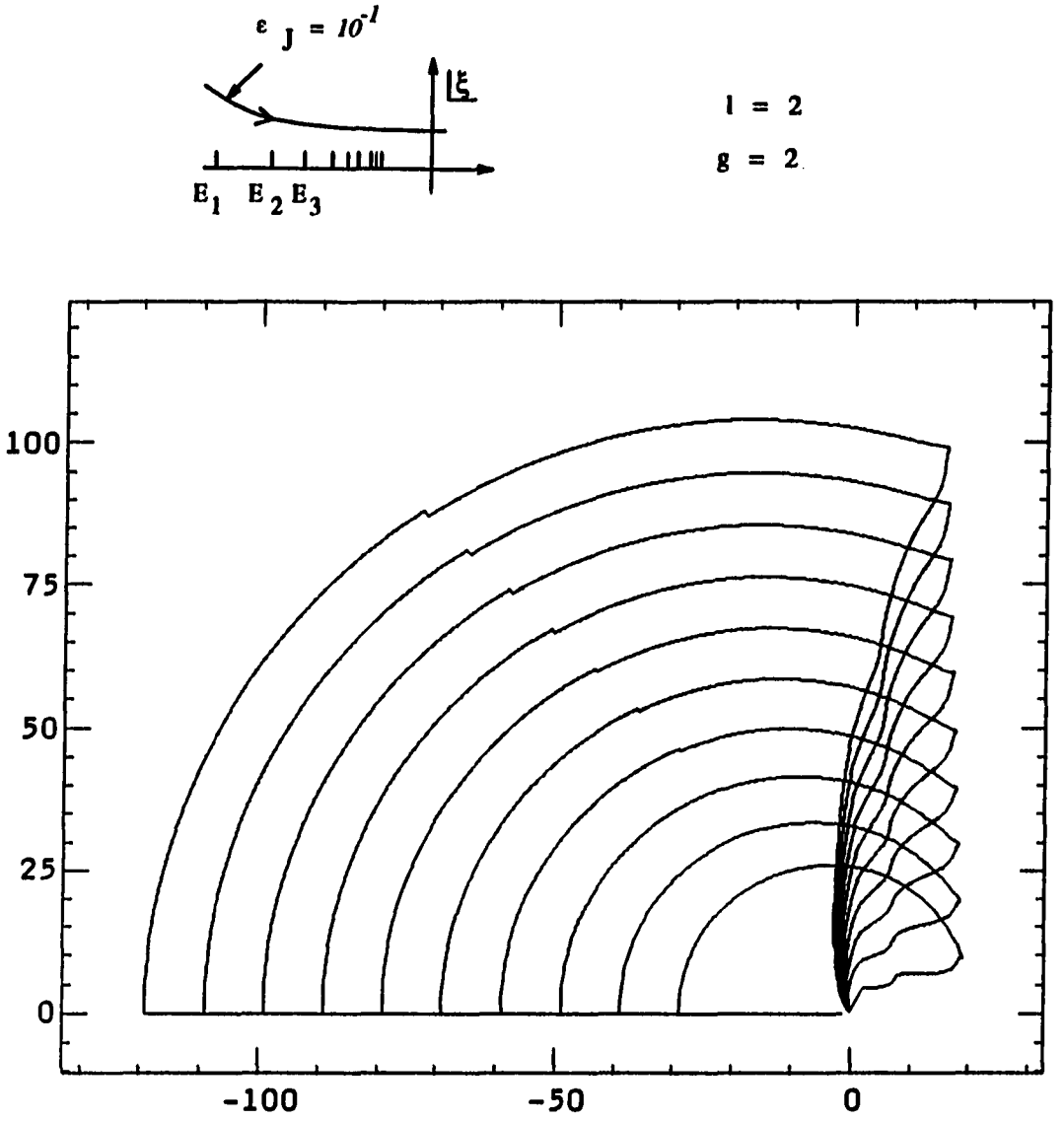

Figure 6.21: Ten northern poles of p_r in the complex r plane computed using the WKB approximation for the Coulomb wavefunction

CHAPTER 7. EXACT STUDY OF THE POLES OF MOMENTUM FUNCTION - COULOMB POTENTIAL

We describe in this chapter a numerical method used to find the poles of the quantun momentum function $p_r(r, \mathcal{E}, L)$ of a particle moving in the Coulomb potential as a function of energy. The results of the computation of the poles is presented along with their comparison with the predictions of the semiclassical analysis of Chapter 6.

Computation of the poles of $p_r(r, \mathcal{E}, L)$

From the semiclassical analysis of the locations of the poles of $p_r(r, \mathcal{E}, L)$ for a particle moving in a Coulomb potential we know that for $E = E_{high} >> 0$ the zeroes of $u(r, \mathcal{E}, L)$ are located to the right of r_1 and to the left of r_2 on the real axis in the complex r plane. We first find the approximate location of these zeroes r_j by solving equations (6.25) numerically. We then numerically integrate the Schrödinger equation (6.8) from the initial point $r_0 = (\epsilon_{r0}, 0)$, with initial conditions $u(r_0, E_{high}, l) = {\epsilon_{r0}}^{l+1}$, $u'(r_0, E_{high}, l) = (l+1){\epsilon_{r0}}^{l}$, with $\epsilon_{r0} << 1$, to the point $r = r_j$. These initial conditions are consistent with (6.10). Having obtained $u(r_j, E_{high}, l)$ and $u'(r_j, E_{high}, l)$ we search for the zero closest to $r_j(E_{high}, l)$. The integration is performed by a 4th order Runge-Kutta method and the search for a zero is carried out using the Newton- Raphson method. Once we have the zero

$r_j(E_{high}, l)$ the energy is incremented by $-\Delta E$ and the search for $r_j, E_{high} - \Delta E, l)$ done as before. This procedure is repeated for an energy range that extends up to $E = E_{low} << 0$.

Results of numerical computation of poles and their comparison with semiclassical results

Figures (7.1) and (7.2) show the first three northern poles computed as functions of energy. Figure (7.3) is similar; the energies used for this computation had a constant imaginary part unlike the previous two figures where the imaginary part of energy was varied to keep ϵ_J constant. If the energy were purely real those poles not on the real axis move all the way to $r = \infty$ for energy eigenvalues. By our choice of a complex energy we have avoided this situation; these figures show the sensitivity of $Re(r_j)$ to ϵ_J. The variation of these poles with energy is very similar to that predicted by the WKB analysis of Chapter 6. The numbers n in the figures represent the location of the poles when $E = E_n$. The maxima of $Re(r_j)$ are attained on energy eigenvalues. The nth southern pole enters the region between r_1 and r_2 for $E = E_n$. Thus every pole comes on to the real axis for some negative energy. As the energy is increased the number of poles in the well increases by one when $\mathcal{E}$ passes by an eigenvalue. For positive E all the southern poles are on the real axis.

Figure (7.4) shows the motion of the second southern pole with energy for successively increasing total angular momentum l. As l increases, from equation (6.7), $|E(n_r, l)|$ decreases, and the WKB expression (6.28) predicts the maxima of $Re(r_j)$ to be inversely proportional to $\sqrt{|E(n_r, l)|}$. This explains the greater eastward motion of the poles around eigenvalues for higher l.

Figure (7.5) represents the computed locations of the northern poles. These are again consistent with the corresponding pictures of chapter 6 based on the WKB analysis. The passage of E from negative to positive values brings these northern poles onto the negative real axis to the left of r_2, by moving them in an arc in the r plane.

Effectiveness of the WKB method

All the features observed in the motion of of the poles of $p_r(r, \mathcal{E}, L)$ with $\mathcal{E}$ can be explained using the semiclassical expressions of Chapter 6. Instead of finding an exact expression for the wave function for all energies of the system we can make use of the approximate wave function to locate the poles; the location of the poles of the quantum momentum function and their variation with energy is accurately predicted by the WKB analysis, as our comparison of the precisely computed pole locations with the corresponding ones obtained by the semiclassical analysis reveals. Our study of the momentum function for the Yukawa potential will parallel this analysis.

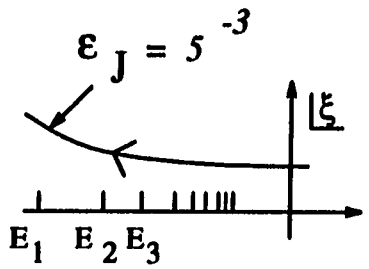

l = 0

g = 2

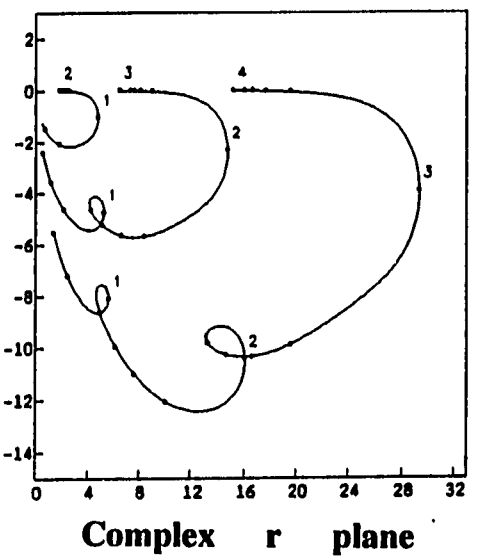

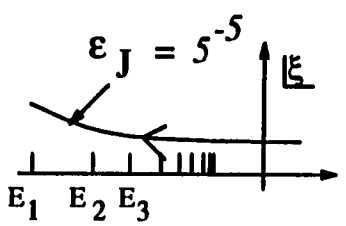

l = 0

g = 2

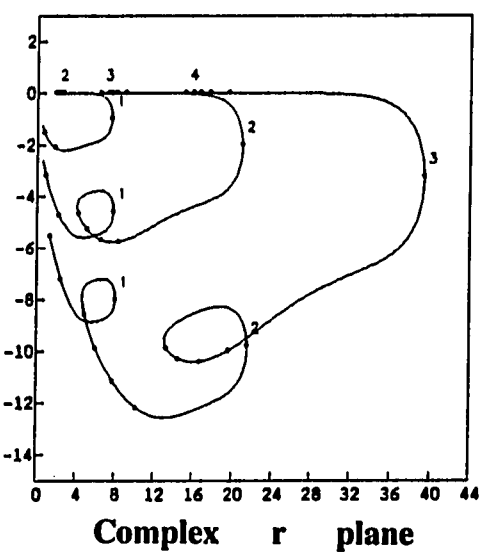

Figure 7.1: First three southern poles of p_r obtained by numerical integration of the Schrödinger equation for the Coulomb potential

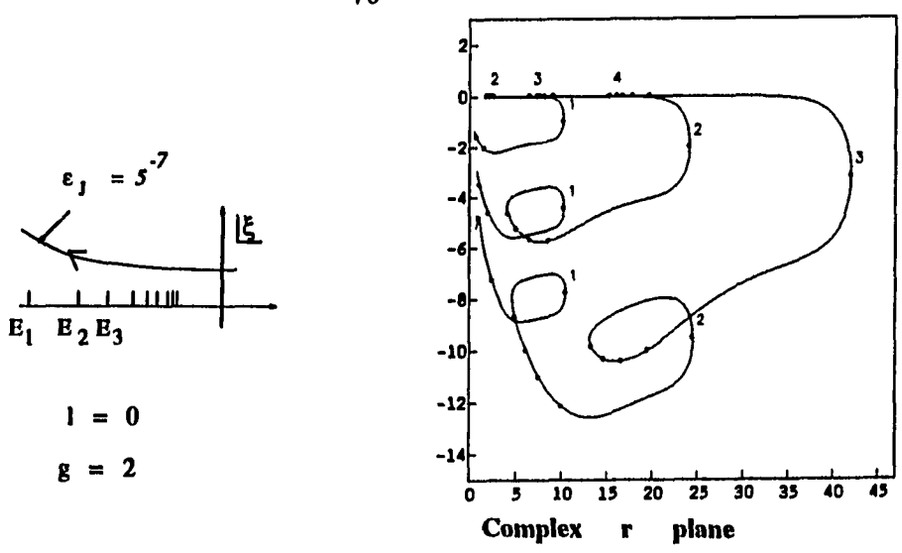

Figure 7.2: First three southern poles of p_r obtained by numerical integration of the Schrödinger equation for the Coulomb potential

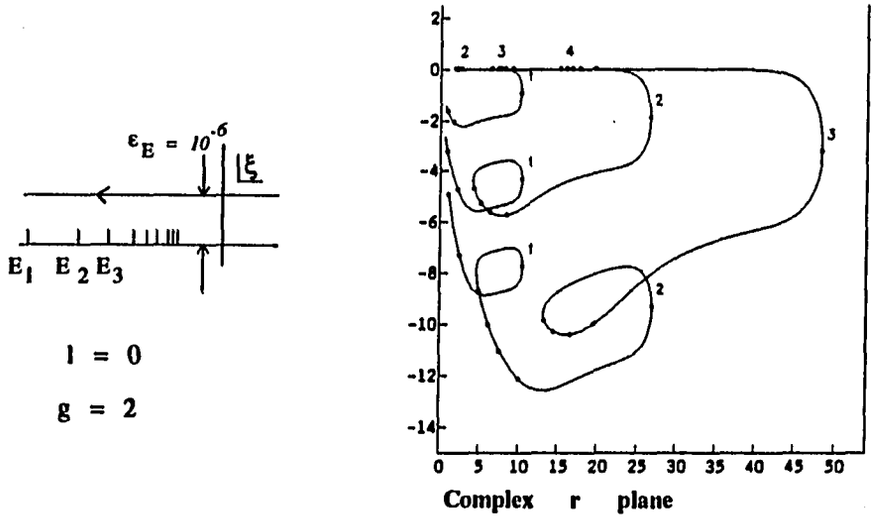

Figure 7.3: First three southern poles of p_r with constant ϵ_E

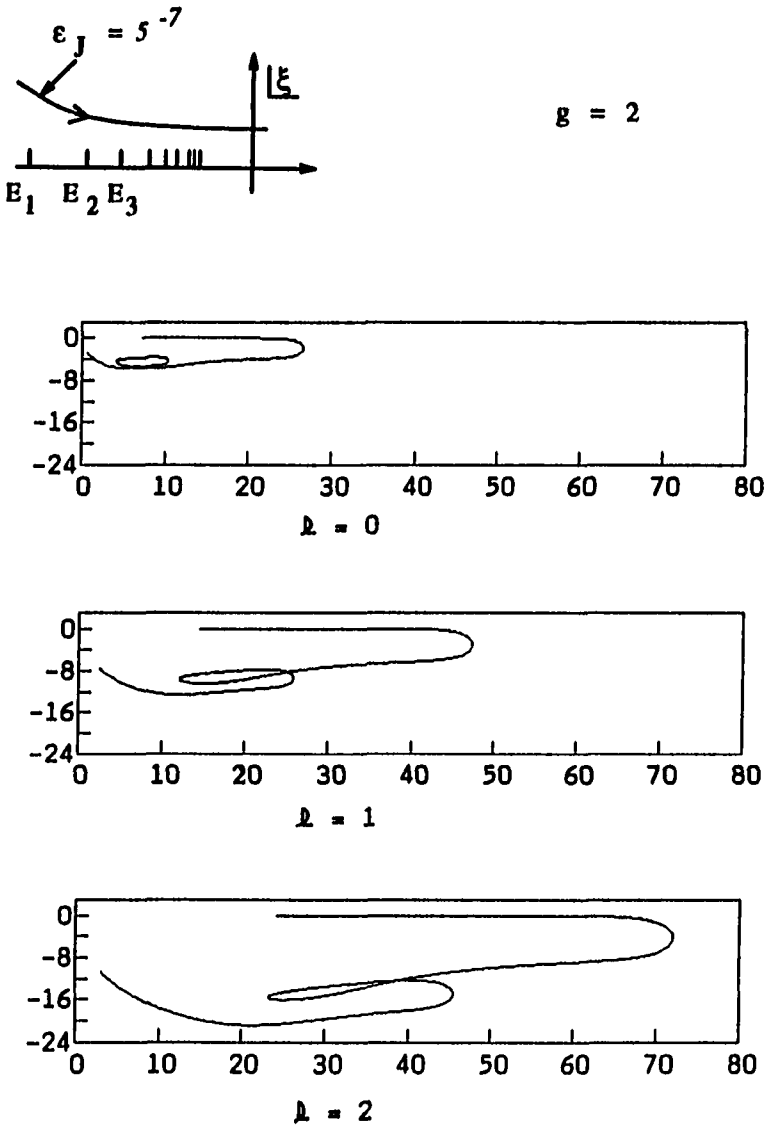

Figure 7.4: Second southern pole of p_r for three successively higher values of angular momentum

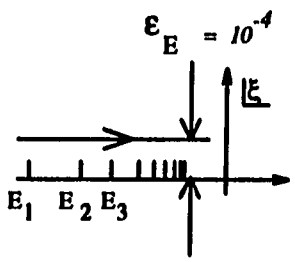

l = 0

g = 2

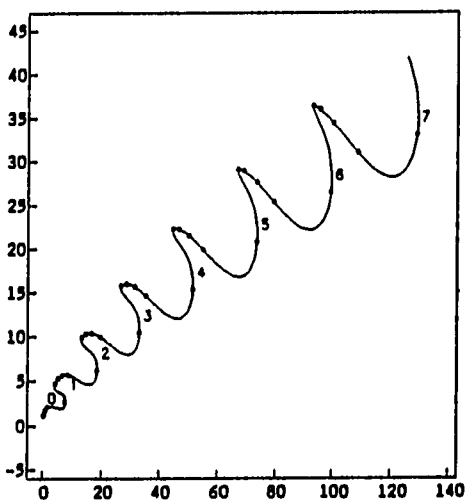

first northern pole in r plane

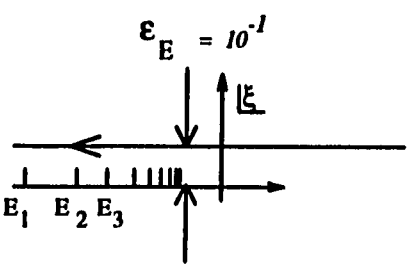

l = 0

g = 2

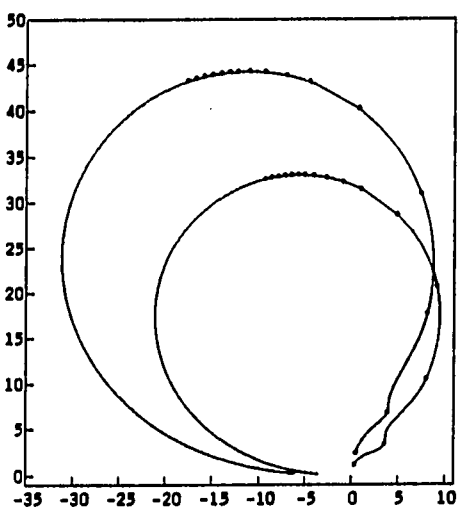

first two northern poles in r plane

Figure 7.5: Northern poles of p_r obtained through numerical integration of the Schrödinger equation for the Coulomb potential

CHAPTER 8. DEFINITION OF J_r FOR COULOMB POTENTIAL

The definition of the analytically extended quantum radial action variable has to meet the following requirements:

(*i*) J_r must be a continuous function of energy, smoothly interpolating between physical bound states.

(*ii*) Its definition should have the same form for states of all energy, negative and positive.

(*iii*) The definition should agree with the contour integral definition of J_r for bound states.

(*iv*) The form of the definition in the quantum case should correspond to the definition in the classical case.

We provide in this chapter such a definition of J_r for a particle moving in the Coulomb potential. Our definition (6.3) of J_r for quantum bound states is an integral of the form $(1/2\pi)\oint p_r dr$ over a contour in the complex r plane that enclosed the dynamical poles in the potential well. The integral has contributions from two fixed poles of the integrand, one at $r = 0$ and the other at $r = \infty$. We have seen in Chapters 6 and 7 that, for non-negative energy eigenvalues and for positive energies, there is an additional family of infinite poles whose limit point is $r = \infty$; thus the point $r = \infty$ cannot play the role of an isolated pole of the integrand for non-energy eigenvalues

and for positive energy. We now describe a contour integral definition of J_r, due to Nanayakkara [2], that overcomes this problem. It involves a modification of the integrand on the lines of the one introduced in the definition of the classical radial action variable in chapter 5.

Definition of J_r by modifying the integrand

The definition of J_r for all energy is

$$\begin{aligned} \tilde{J}_r(\epsilon_r) &= \frac{1}{2\pi} \oint_{C'} p_r(r, \mathcal{E}, L)\, dr \,/\, [1 - \epsilon_r\, r]^2, \\ J_r &= \lim_{\epsilon_r \to 0} \tilde{J}_r(\epsilon_r) \end{aligned} \tag{8.1}$$

with a positive imaginary ϵ_r, and the clockwise contour C', defined in Figure (8.1), encloses the points $r = 0$ and $r = 1/\epsilon_r$. The dynamical poles of p_r (whose location is a function of energy) are in the exterior of C' for all energies. We now show that the integrand in (8.1) has two fixed poles, one at $r = 0$ and another at $r = 1/\epsilon_r$. Thus the integral around C' is done by distorting the contour into C_0 and C_∞. Around $r = 0$ the integrand $\sim -(i/2\pi)(l+1)\hbar/r$ as the denominator $(1 - \epsilon_r r)^2$ is ≈ 1 and $p_r \sim -i(l+1)\hbar/r$, from (6.4). The contribution to J_r from C_0 is, therefore, $-(l+1)\hbar$. Next, the denominator in the integrand has a second order zero at $r = 1/\epsilon_r$. This results in a second order pole for the integrand at that point if $p_r(r = 1/\epsilon_r, \mathcal{E}, l)$ is non-zero and finite. We obtain a semiclassical expression for p_r at $r = 1/\epsilon_r$ and show that it indeed has such a character.

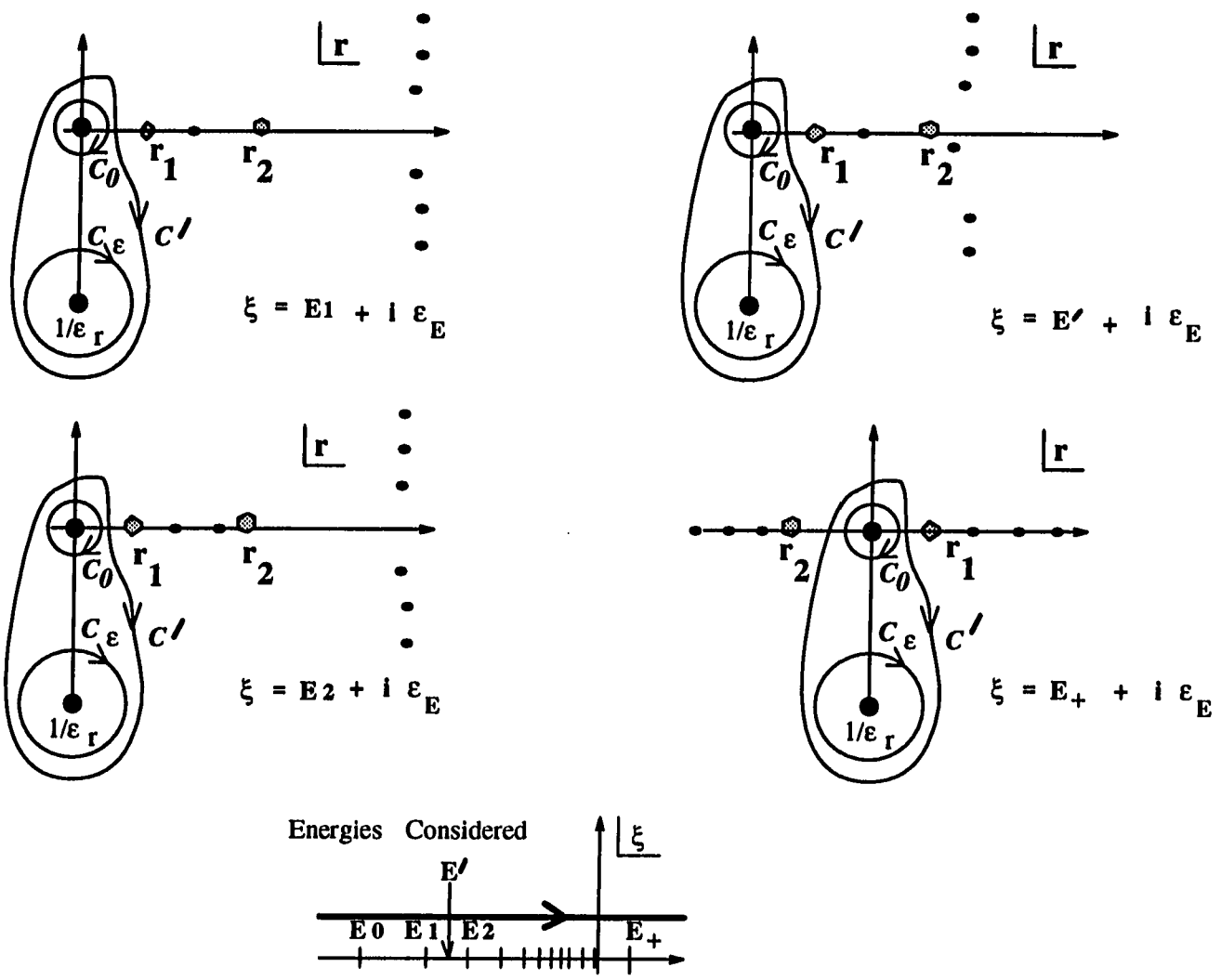

Figure 8.1: Contour C' for the definition of J_γ for all energies

Semiclassical expression for p_r near $r = 1/\epsilon_r$

For $E < 0$ the WKB wave function u in the region containing $r = 1/\epsilon_r$ is of the form

$$u \approx (1/\sqrt{p_{rc}})[\exp(iW/\hbar) + G\exp(-iW/\hbar)],$$

where G is a constant and W is W_{rc1} if $E < V_0$ and W_{rc2} if $V_0 < E < 0$ (region 4 in Figure (6.3) and Table 6.1). The form of W for large r is

$$\begin{aligned} W &= \int_{r_0}^{r} [E + g/r - (l+1/2)^2\hbar^2/r^2]^{1/2} dr \\ &= \int_{r_0}^{r} [k + (g/2k)/r + \ldots] dr \\ &\approx c + kr + (g/2k)\ln(r) + O(1/r^2), \end{aligned}$$

where r_0 is an appropriate turning point, $k = i\kappa = \sqrt{E}$ with $\kappa > 0$ for $E < 0$ and c a constant. Since $\epsilon_r = i|\epsilon_r|$, $\exp(iW/\hbar)$ at the point $r = 1/\epsilon_r$ is proportional to $[1/|\epsilon_r|]^{g/2\hbar\kappa|\epsilon_r|}$. This is large compared to $[\,|\epsilon_r|\,]^{g/2\hbar\kappa|\epsilon_r|}$ to which the other exponential $\exp(-iW/\hbar)$ is proportional to. Thus around $r = 1/\epsilon_r$, for $E < 0$,

$$u \approx (1/\sqrt{p_{rc}})\,\exp(iW/\hbar). \tag{8.2}$$

For $E > 0$, the point $1/\epsilon_r$ lies in a region where u has the form $(1/\sqrt{p_{rc}})\exp(iW/\hbar)$ (region 4 in Figure (6.3), region $2'$ in Figure (6.7 and region 3 in Figure (6.14); see Table 6.1)). Using (8.2) and the connection $p_r = -i\hbar u'/u$ between u and p_r we obtain

$$p_r \approx p_{rc} + O(1/r^2) \text{and } p'_r = p'_{rc} + O(1/r^3). \tag{8.3}$$

for all energy E. Noting that $p'_{rc} \sim O(1/r^2)$ and that p'_r is equal p'_{rc} to the leading order in r we see that the contribution, to the zeroth order in ϵ_r of C_ϵ to J_r is identical

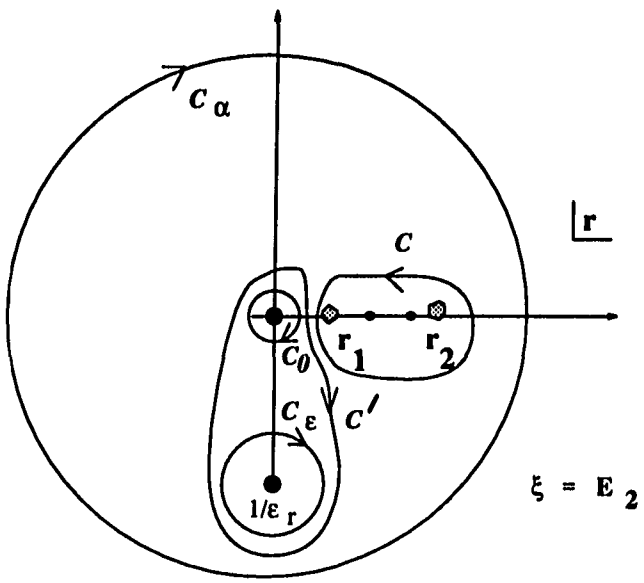

Figure 8.2: Poles of p_r for eigenvalue $E = E_2$

to that in the corresponding classical case, viz, $g/2\sqrt{-E}$. This is the contribution of C_∞ in eq. (5.12) to J_r when the energy of the system is a negative eigenvalue. J_r is again given by eq. (6.6) as a function of E and l for all energies of the system.

Definition of J_r by modifying the integrand

If the energy of the system is a negative eigenvalue (with $\epsilon_E = 0$) then the only poles of the integrand in (8.1) exterior to C' will be the poles in the well, equal in number to the excitation n_r of the system; the northern and southern poles recede to $r = \infty$ (see Figure (8.2)). The contour C' can then be distorted into C and

C_∞ for evaluating the integral in (8.1). The denominator in the integrand, being a quadratic, and the numerator, to the leading order in r, a constant on C_∞, means the integral over C_∞ vanishes. The contribution from C, to the leading order in ϵ_r, is $n_r\hbar$. Definition (8.1) thus correctly reduces to our previous definition (6.3) of J_r on negative energy eigenvalues. It also analytically extends the definition of the quantum radial action variable to all physically allowed energies of the system while also interpolating between physically allowed bound states.

Significance of quantum Coulomb radial action variable

Analogous to the classical radial excitation families which consist of orbits having the same angular momentum but different values of the radial action variable and energy, we can classify quantum states of a particle by their common angular momentum. The J_r of such states with a common angular momentum is a function of energy; its energy dependence for Coulomb states is shown in Figure (8.3). For negative energies the physical bound states are characterized by integral J_r only; this is unlike in the classical case where any real $J_{rc} > 0$ corresponded to a bound orbit. This quantization of J_r thus quantizes the physical negative energies of the particle. The variation of J_r with energy is shown in Figure (8.4). The quantum radial action variable, so defined by the same contour integral for all energies, while bringing out the significance of the physical bound states, also interpolates between these states smoothly by assuming noninteger values for the unphysical negative energy states. Such a definition, valid for all energies of the particle (including positive energy), is useful in the study of quantum resonances which, though unbound, are special positive energy states. The Coulomb potential does not admit resonances because it does

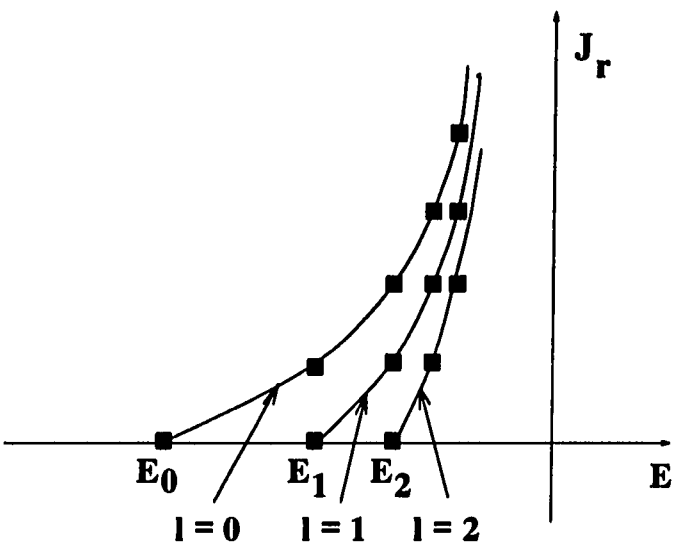

Figure 8.3: Common angular momentum states for Coulomb potential

not have a potential well of finite width; a study of resonances thus has to await the construction of J_r for a potential of the Yukawa type which does have resonances. This will be the focus of the next four chapters.

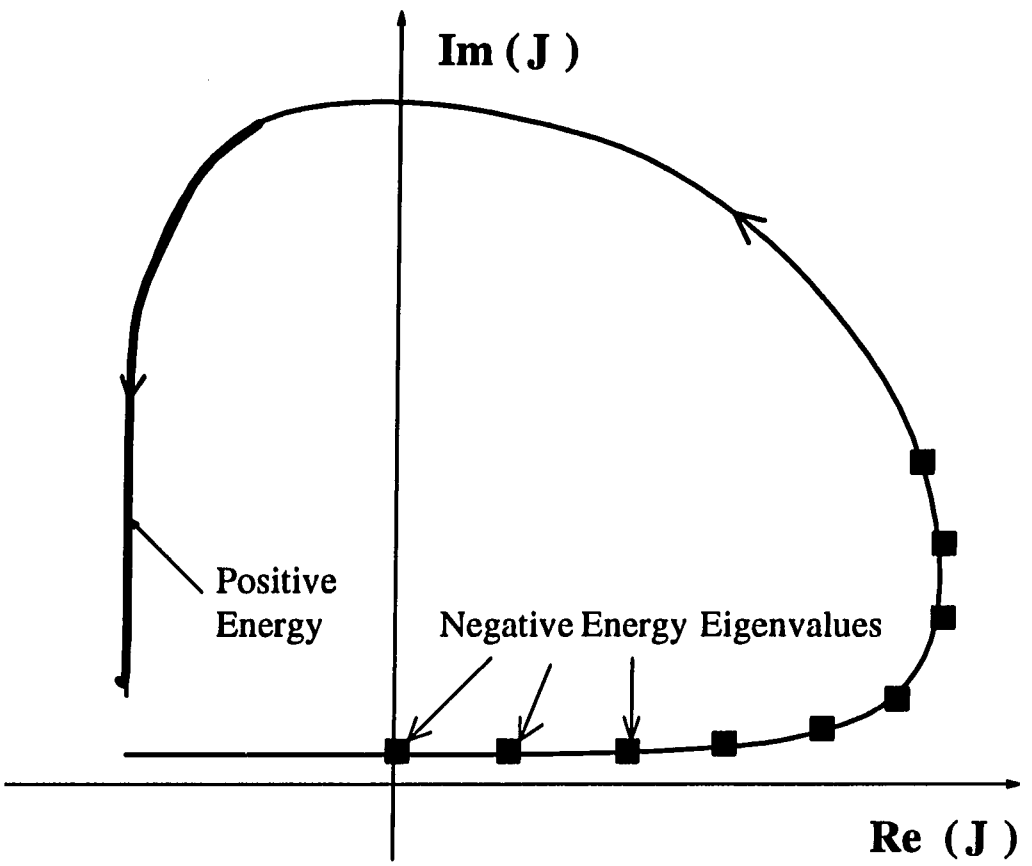

Figure 8.4: Variation of J_T with energy for Coulomb potential

CHAPTER 9. CLASSICAL ACTION VARIABLE - YUKAWA POTENTIAL

The Yukawa potential is a model potential for the strong interaction between hadrons. It is attractive and dominant at short distances, providing strong binding. It is of the form $-(g/r)\exp(-r/R)$ where g, as in the Coulomb case, represents the square of the coupling constant and R is the range of the force. The mediation of a force between two particles by a massive particle of mass μ produces a force of range $\propto 1/\mu$. In the limit of zero μ a potential of infinite range, like the Coulomb potential, results. A plot of the effective Yukawa potential, that includes the angular momentum barrier L^2/r^2, is shown in figure 9.1. We consider Yukawian potentials with g and R such that

$$L^2/g \; < \; 0.42R. \tag{9.1}$$

It can be shown that this results in both a potential well and a potential hill for non-zero L ; the former is essential for the existence of bound states. It has a minimum strength of V_0, which is the depth of the well, at $r = r_0$ shown in figure 9.1. For a given radial distance r from the attractive center, the strength of the effective Yukawa potential is weaker than the corresponding Coulomb potential due to the presence of $\exp(-r/R)$. There is, therefore, a potential well of finite width; the effective potential cuts off to zero rapidly after attaining a maximum V_h at r_h.

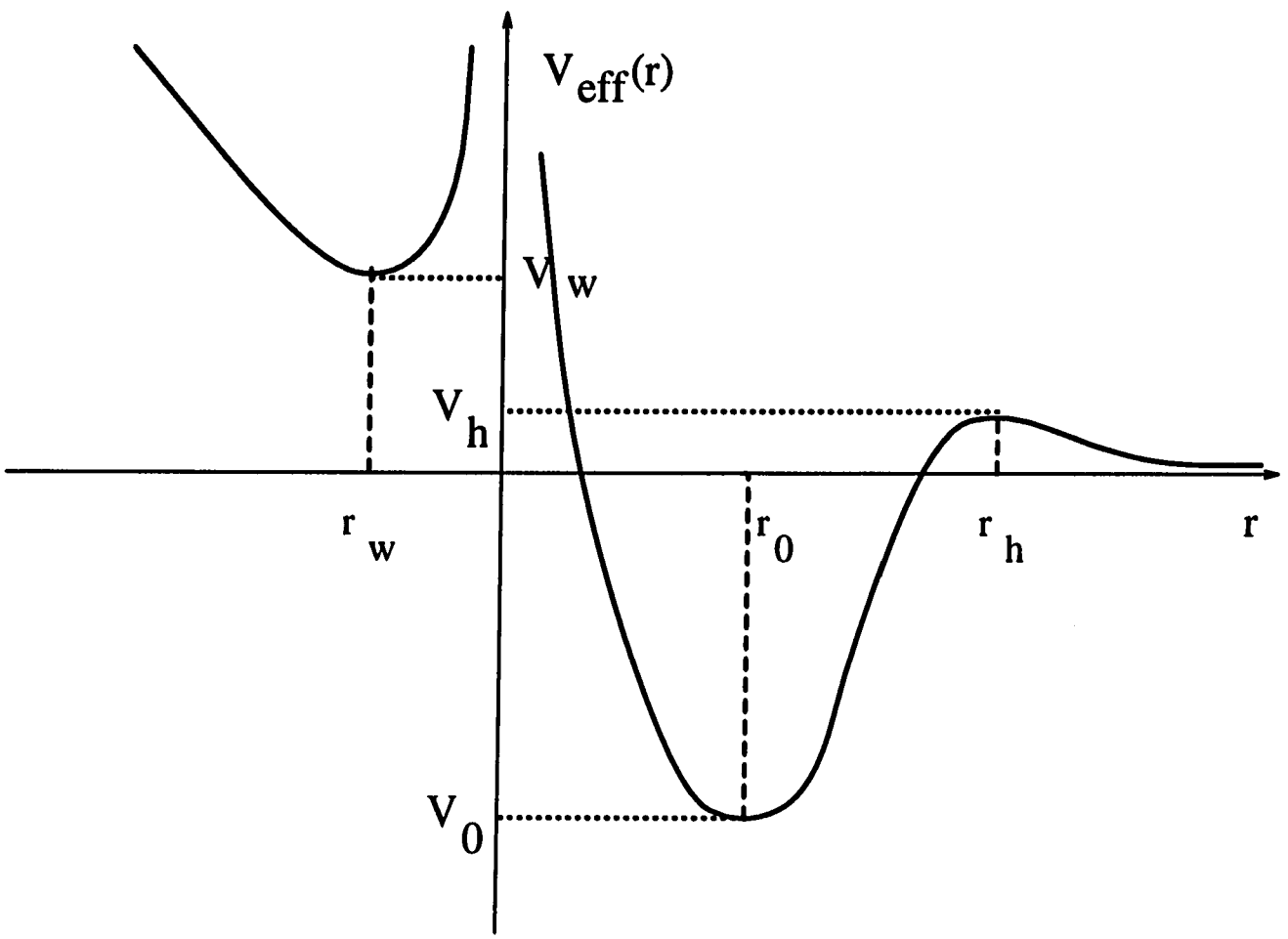

Figure 9.1: Effective Yukawa potential as a function of real r

In this chapter we define the radial action variable for a classical bound state of the Yukawa potential and extend it analytically to all energies of the system, negative and positive.

Location of classical turning points

We first locate the classical turning points to define the classical momentum function $p_{rc}(r, \mathcal{E}, L)$ as a suitable branch of $\sqrt{\mathcal{E} - V_{eff}(r)}$ in the complex r plane. Unlike in the case of the Coulomb potential, the Yukawa potential has an infinite number of turning points with branch cuts of $p_{rc}(r, \mathcal{E}, L)$ originating from each one of them. The classical momentum function is

$$p_{rc}(r, \mathcal{E}, L) \;=\; [\,\mathcal{E} + (g/r)\exp(-r/R) - L^2/r^2\,]^{\frac{1}{2}}. \tag{9.2}$$

The turning points r_j, which are functions of $\mathcal{E}$, L and g, are obtained from

$$\begin{aligned} p_{rc}(r_j, \mathcal{E}, L) \;&=\; 0 \\ \Rightarrow\; \mathcal{E}{r_j}^2 + g\exp(-r_j/R)\, r_j - L^2 \;&=\; 0. \end{aligned} \tag{9.3}$$

Equation (9.3), being transcendental, can be solved only approximately or numerically. We try an approximate solution first and then compare the answer with a numerical solution.

Case (i): $E << -g^2/4L^2$ **and** $|r_j| << L^2/g$

We rewrite eq. (9.3) as

$$r_j \;=\; (-g/2\mathcal{E})\exp(-r_j/R) \;\pm\; \sqrt{[g\exp(-r_j/R)/2\mathcal{E}]^2 \;+ L^2/\mathcal{E}}. \tag{9.4}$$

For $|r_j| << L^2/g$, which from eq. (9.1), is $< R$, the exponential is approximately 1, so

$$r_j \simeq (-g/2\mathcal{E}) \pm \sqrt{[g/2\mathcal{E}]^2 + L^2/\mathcal{E}}, \tag{9.5}$$

which is identical in form to the corresponding Coulomb equation (5.5). For $E << -g^2/4L^2$ (= potential energy minimum V_0 in the Coulomb case), the first term in the square root can be ignored. Then r_j has a real part that increases, and an imaginary part that increases in magnitude, as the negative E increases. We conclude that there are two turning points r_1 and r_2 around $r = 0$ which move with energy like their Coulomb counterparts; this motion is shown in Figure 9.2a.

Case (ii): $E \approx -g^2/4L^2$ and $r_j \approx r_0 \approx 2L^2/g$

Now, an equation of the form (9.4) still holds locally around $r = r_0$, with g replaced by $g' = g\ exp(-r_0/R)$. This defining relation for turning points, being Coulombic in nature, moves the turning points r_1 and r_2 along paths shown in Figure 9.2b, similar to those of the corresponding Coulomb turning points. Alternately, the potential energy is quadratic in $(r - r_0)$ at the bottom of the potential well locally and for such a quadratic potential, the equation $E - V_{eff}(r) = 0$ has two roots of the form $r_{1,2} = r_0 \mp \Delta_0$, with Δ_0 positive imaginary if $E < V_{eff}(r_0)$ and positive if $E > V_{eff}(r_0)$. As the energy enters the physically allowed region of $E > V_0$, r_1 moves to the left of r_0 and r_2 to the right of r_0 on the real axis, as shown in Figure 9.2c. We see from this figure that for any higher energy, r_1 is on the real axis and approaches $r = 0$ as $E \to \infty$. r_2 moves eastward along the real axis till it comes close to r_h for $E \simeq V_h$, the potential hill peak. Figure 9.3 shows the computed motion of r_1 and r_2 with energy for $l = 1$, $g = 55$, $R = 1$; here, $V_0 = -702$.

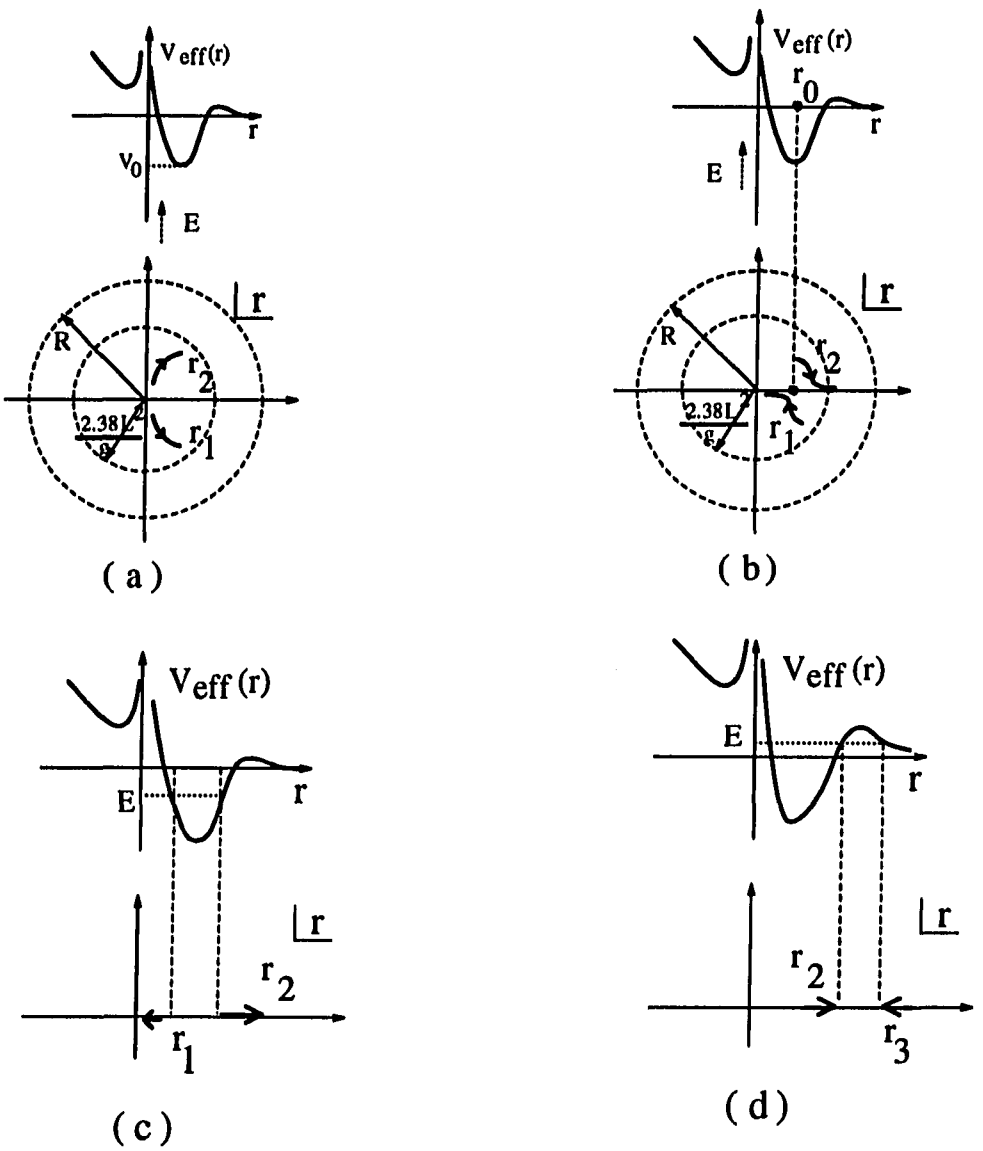

Figure 9.2: Motion of r_1 and r_2 with energy

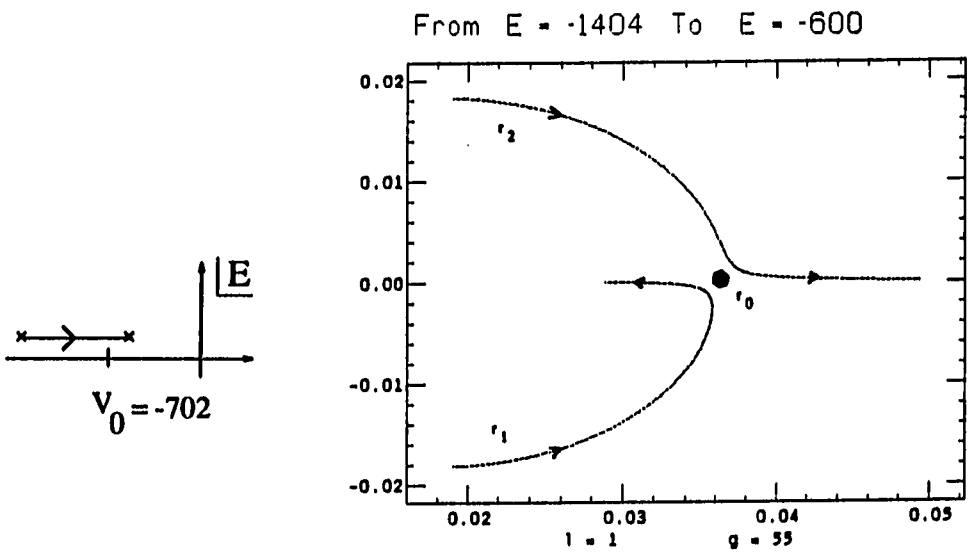

Figure 9.3: Computed motion of r_1 and r_2 with energy for the range $E = 2\,V_0$ to $E \geq V_0$ with $R = 1$

Case (iii): $E \approx E_h$ and $r_j \approx r_h$

For energies $0 < E < E_h$, there are two turning points, r_2 and r_3, one on each side of r_h. This is shown in Figure 9.2d. Approximating the potential by a quadratic in $(r - r_0)$ around $r = r_h$ yields two turning points near r_h of the form $r_{2,3} = r_h \mp \Delta_h$ with Δ_h positive for $E < E_h$ and negative imaginary if $E > E_h$. Thus r_2 moves into the upper half and r_3 into the lower half of the complex r plane for $E > E_h$. This is shown in Figure 9.4a.

Case (iv): $E_h < E < E_w$ and $|r_j| \approx r_h$

For this range of energy r_2 moves along a counterclockwise arc in the upper half plane; r_3, its complex conjugate moves in the lower half plane (see Figure 9.4b). The

two approach each other near $r = r_w$ for $E \simeq E_w$ where there is the second minimum of the potential energy. The quadratic approximation for $V_{eff}(r)$ at $r = r_w$ again shows that for $E > E_w$, r_2 is to the right and r_3 to the left of r_w. The motion of r_2 and r_3 for the energy range $E > E_h$ is shown in Figure 9.4c. It is clear that for energies higher than V_w, r_2 and r_3 will be on the negative real axis, with $r_2 \rightarrow 0$ and $r_3 \rightarrow -\infty$ as $E \rightarrow \infty$. Figure 9.5 shows the computed motion of r_2 and r_3 with energy for the range $E = 2\,V_0$ to $E \geq V_w$. The motion of r_3 for the energy range $E < V_0$ to $E \approx 0$ requires a study of the region $Re(r) < 0$.

Case (v): $Re(r) < 0$

For $Re(r/R) << 0$ we can ignore the last term in eq. (9.3) and write

$$\mathcal{E} r_n + g \exp(-r_n/R) \simeq 0. \tag{9.6}$$

Writing $r_n = r_{nR} + i\, r_{nI}$ and $\mathcal{E} = |\mathcal{E}|\, \exp(i\, \theta_{\mathcal{E}})$ and substituting these in eq. (9.6) we get

$$|\mathcal{E}|\, \cos(\theta_{\mathcal{E}})\, r_{nR} - |\mathcal{E}|\, \sin(\theta_{\mathcal{E}})\, r_{nI} \simeq -g\, exp(-r_{nR}/R)\, \cos\,(r_{nI}/R), \tag{9.7}$$

$$|\mathcal{E}|\, \sin(\theta_{\mathcal{E}})\, r_{nR} + |\mathcal{E}|\, \cos(\theta_{\mathcal{E}})\, r_{nI} \simeq g\, exp(-r_{nR}/R)\, \sin\,(\, r_{nI}/R\,). \tag{9.8}$$

These two equations can be rewritten as

$$r_{nR} \simeq \frac{-g\, exp(-r_{nR}/R)}{|\mathcal{E}|}\, \cos\,[\, r_{nI}/R + \theta_{\mathcal{E}}\,], \tag{9.9}$$

$$r_{nI} \simeq \frac{-g\, exp(-r_{nI}/R)}{|\mathcal{E}|}\, \cos\,[\, r_{nI}/R + \theta_{\mathcal{E}}\,], \tag{9.10}$$

$$\text{or,} \quad \frac{r_{nI}}{r_{nR}} \simeq -\tan\,[\, r_{nI}/R + \theta_{\mathcal{E}}\,]. \tag{9.11}$$

If $|r_{nI}/r_{nR}| >> 1$, then from eq. (9.11),

$$r_{nI}/R + \theta_{\mathcal{E}} \simeq (n + 1/2)\,\pi, \quad n = 0, \pm 1, \pm 2, \ldots. \tag{9.12}$$

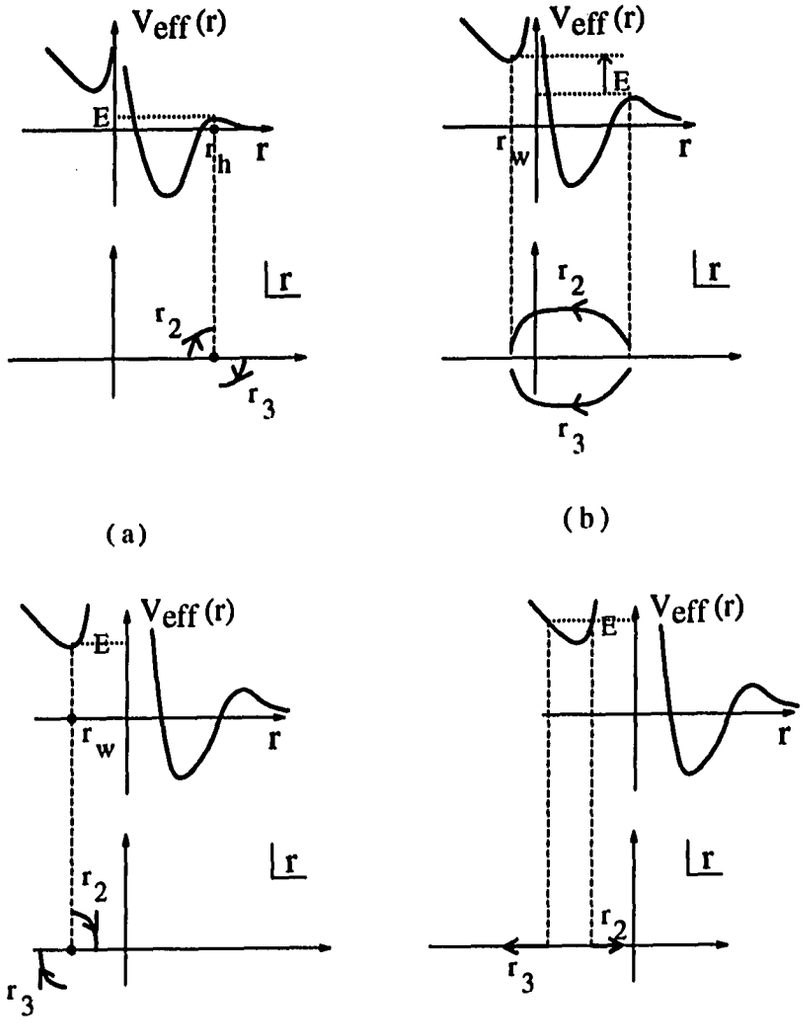

Figure 9.4: Motion of r_2 and r_3 with energy

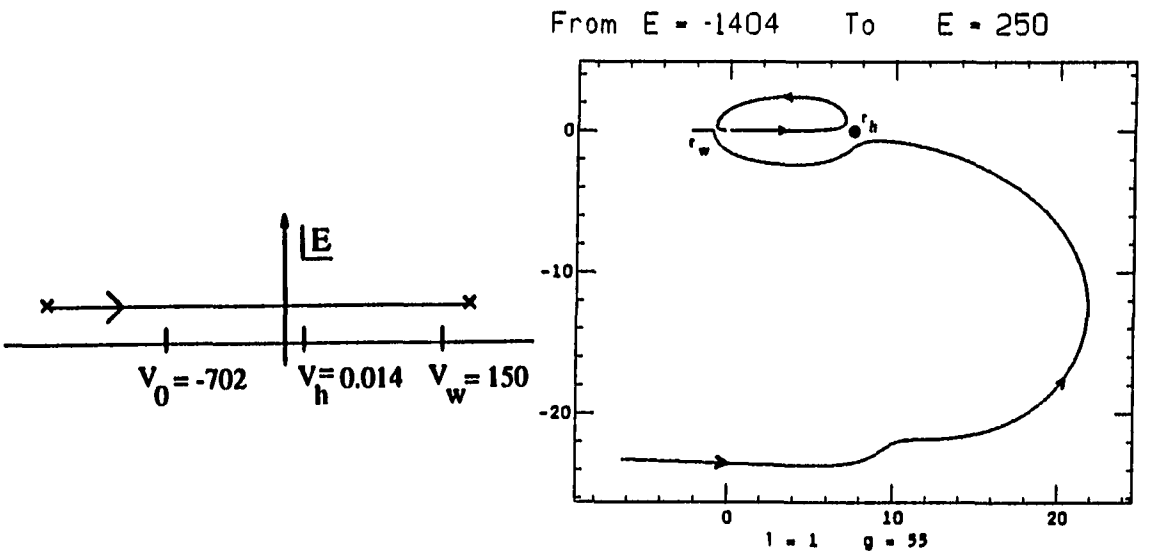

Figure 9.5: Computed motion of r_2 and r_3 with energy for the range $E = 2\,V_0$ to $E \geq V_w$ with $R = 1$

From eq. (9.11) and (9.12),

$$\exp(-r_{nR}/R) \simeq (-1)^n \frac{|\mathcal{E}|}{g} r_{nI} \tag{9.13}$$

For $r_{nI} > 0$, from eqs. (9.12) and (9.10)we have ,

$$r_{nI}/R \simeq (2n + 1/2)\,\pi - \theta_{\mathcal{E}}, \quad n = 1,\, 2,\, 3, \ldots, \tag{9.14}$$

$$r_{nR}/R \simeq -\ln\,[\,(\frac{|\mathcal{E}|R}{g})\{(2n + 1/2)\pi - \theta_{\mathcal{E}}\}\,], \tag{9.15}$$

and for $r_{nI} < 0$,

$$r_{nI}/R \simeq (2n + 3/2)\,\pi - \theta_{\mathcal{E}}, \quad n = -1,\, -2,\, -3, \ldots, \tag{9.16}$$

$$r_{nR}/R \simeq -\ln\,[\,(\frac{|\mathcal{E}|R}{g})\{(2n + 3/2)\pi - \theta_{\mathcal{E}}\}\,]. \tag{9.17}$$

Thus, the imaginary parts of these "western turning points" is relatively insensitive to the energy; their real parts depend on the energy logarithmically. As the energy

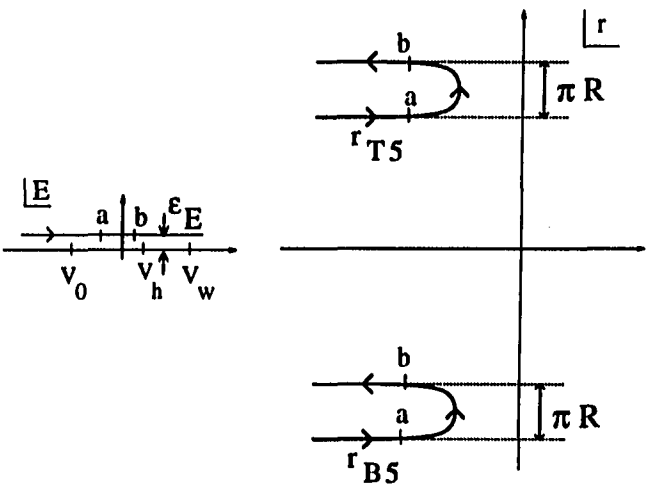

Figure 9.6: Motion of the western turning points with energy

increases, these turning points move east for $E < 0$ and move west for $E > 0$. The phase of the energy, $\theta_{\mathcal{E}}$ decreases from π to 0 as E changes sign from $-$ to $+$; thus the western turning points move northwards by $\pi\ R$ around $\mathcal{E} = 0$. These predicted motions of the western turning points are shown in Figure 9.6. The turning points in the second quadrant are denoted by r_{Tn} and those in the third by r_{Bn}, for "top" and "bottom" respectively. The exactly computed turning points are shown in Figure 9.7. The results agree with the above conclusions except for the first four turning points in the south.

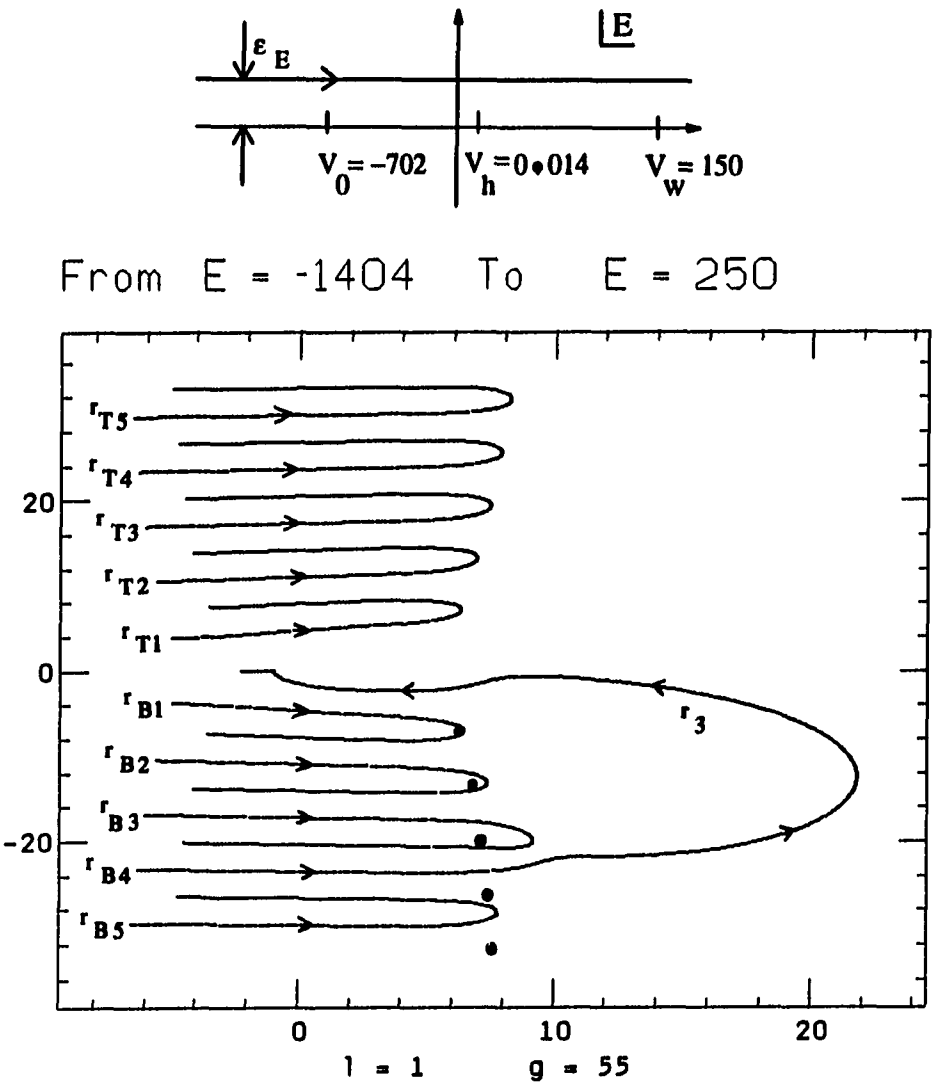

Figure 9.7: Computed motion of the western turning points with energy for the range $E = 2\,V_0$ to $E \geq V_w$ with $R = 1$

Case (vi): Western turning points for $E \approx 0$

To understand the motion of the first three western turning points r_{B1}, r_{B2} and r_{B3} around $E \approx 0$ in Figure 9.7, we construct the following model. The zeroes r_{0n} of the potential energy $V_{eff}(r)$ are given by

$$g\, r_{0n}\, \exp(-r_{0n}/R) - L^2 \;=\; 0 \tag{9.18}$$

An approximate solution of (9.18) is

$$r_{0n} \;\simeq\; [\,\ln(g/L^2) + \ln(2n\pi)\,] + i\,(2n + 1/2)\pi \quad n = 0, 1, 2, \ldots$$

and their complex conjugates. They are in the first and the fourth quadrants; Figure 9.8a shows their locations. We recast Equation (9.3) into the form

$$\exp(-\delta_n) \;=\; \frac{1 - (\mathcal{E} {r_{0n}}^2/L^2)\,\{1 + \delta_n R/r_{0n}\}^2}{1 + \delta_n R/r_{0n}}, \tag{9.19}$$

where $\delta_n = (r_n - r_{0n})/R$, r_{0n} being the zero of the effective potential nearest to the turning point r_n. Assuming that the turning points are very nearly equal to the zeroes of V_{eff} for $\mathcal{E} \approx 0$, ie., $|\delta_n/r_{0n}| << 1$, we can write, using eq. (9.19),

$$\begin{aligned} \exp(-\delta_n) \;&\simeq\; 1 \;-\; \frac{\mathcal{E} {r_{0n}}^2}{L^2} \\ \delta_n \;&\simeq\; -\ln\,[1 - \frac{\mathcal{E} {r_{0n}}^2}{L^2}\,]. \end{aligned} \tag{9.20}$$

If $|\mathcal{E} {r_{0n}}^2/L^2| << 1$, which is true for turning points for low n and $\mathcal{E} \approx 0$, we can expand the logarithm in (9.20) yielding,

$$\delta_n \;\approx\; [\mathcal{E} {r_{0n}}^2/L^2] + \frac{1}{2}[\mathcal{E} {r_{0n}}^2/L^2]^2. \tag{9.21}$$

Figures 9.8b through 9.8g illustrate the use of eq. (9.21) to obtain the dependence on $\mathcal{E}$ of the turning points r_{Bn} near the real axis. By using the phases of r_{0n} and

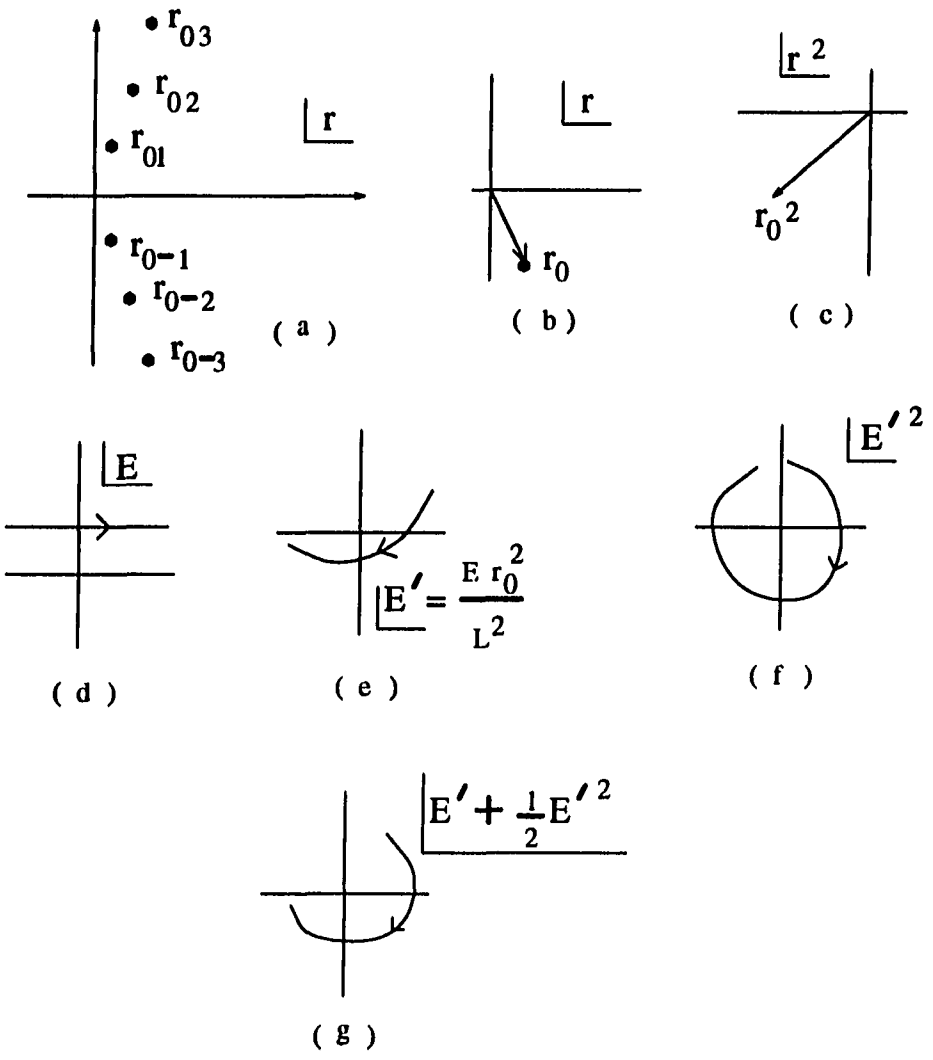

Figure 9.8: Motion of the western turning points with energy for $E \approx 0$

E we can find the phase of $E' = E\, {r_0}^2/L^2$; and from the phase of E', we get the phase of δ_n. Since $(r_n - r_{0n})$ is proportional to δ_n, the turning point r_n goes around the zero of $V_{eff}(r)$ clockwise. In Figure (9.7) we see r_{B1}, r_{B2} and r_{B3} display this behavior; the points in this figure indicate the locations of r_{0n} in the fourth quadrant.

Using eq. (9.19) we can also explain the motion of r_{B4} which moves in an arc rapidly for $E \approx 0$. A self consistent solution of eq. (9.19) is obtained by

$$1 - (\mathcal{E} {r_{0N}}^2/L^2)\,\{1 + \delta_N R/r_{0N}\}^2 \;\approx\; 0 \tag{9.22}$$

for some $n = N$; it leads to

$$\delta_N \;=\; \frac{1}{R}[-r_{0N} + L/\sqrt{\mathcal{E}}]. \tag{9.23}$$

It makes this particular turning point $r_{BN} = r_{0N}$ move in an arc counterclockwise through an angle $\pi/2$ as $\theta_{\mathcal{E}}$ changes through π, and moving it onto the real axis to the right of r_h where it becomes the turning point r_3. Which of the western turning points moves in an arc and reaches the real axis to become r_3 for positive E thus depends on the magnitude of ϵ_E; the smaller ϵ_E is, the lower is the western turning point that transforms itself into r_3, since $|\mathcal{E}|$ in eq. (9.22) is $\approx \epsilon_E$.

Definitions of the classical momentum function $p_{rc}(r, \mathcal{E}, L)$ and J_{rc}

We choose branch cuts for $p_{rc}(r, \mathcal{E}, L)$ for different energies as shown in Figures 9.9 through 9.11. One cut connects the turning points r_1 and r_2. The cuts from the western turning points go west to $r = \infty$. We choose + sign for p_{rc} just below the cut connecting r_1 and r_2 for energies $V_0 < E < 0$ that correspond to classical bound

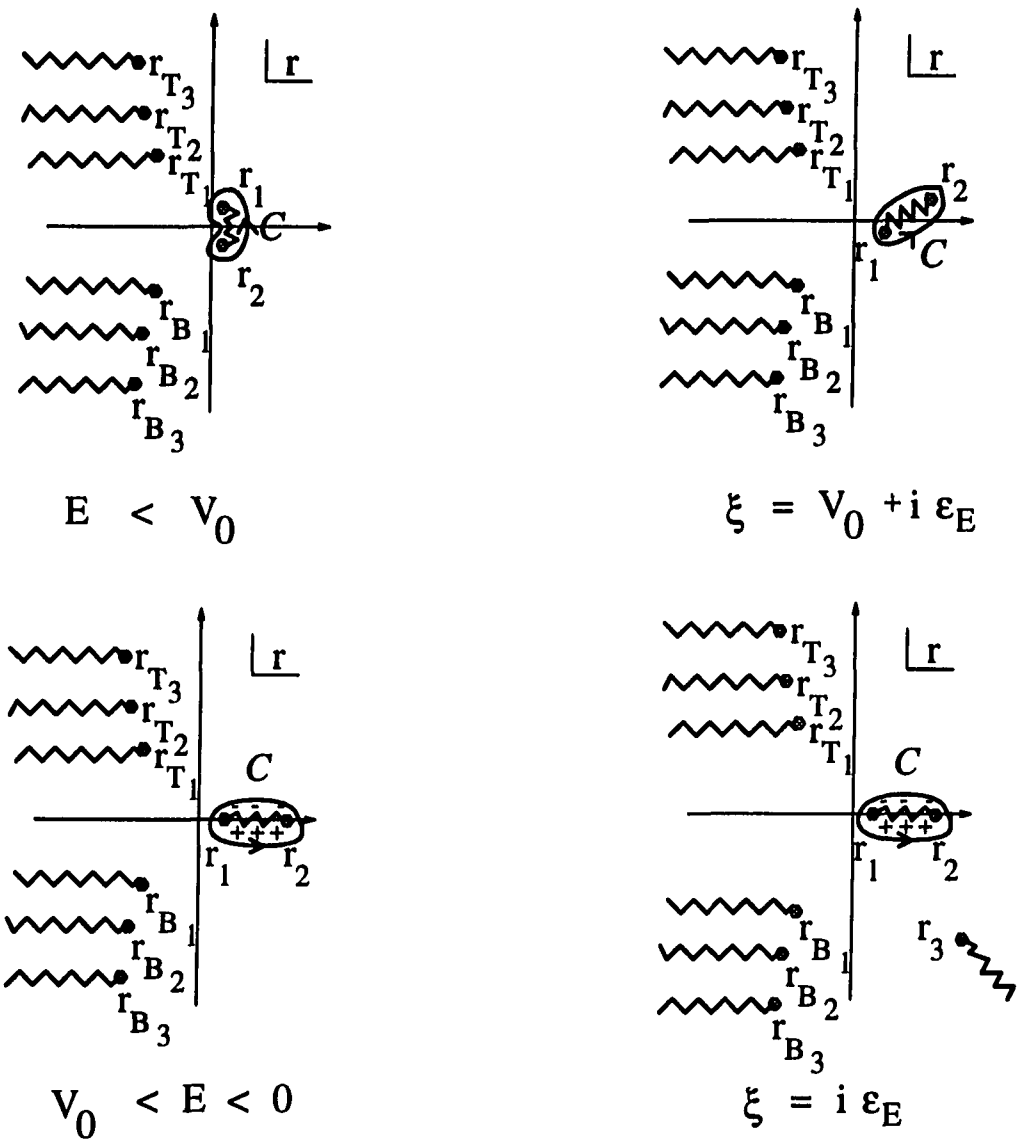

Figure 9.9: Branch cuts of $p_{rc}(r, \mathcal{E}, L)$ and the contour C for for $E < E_h$

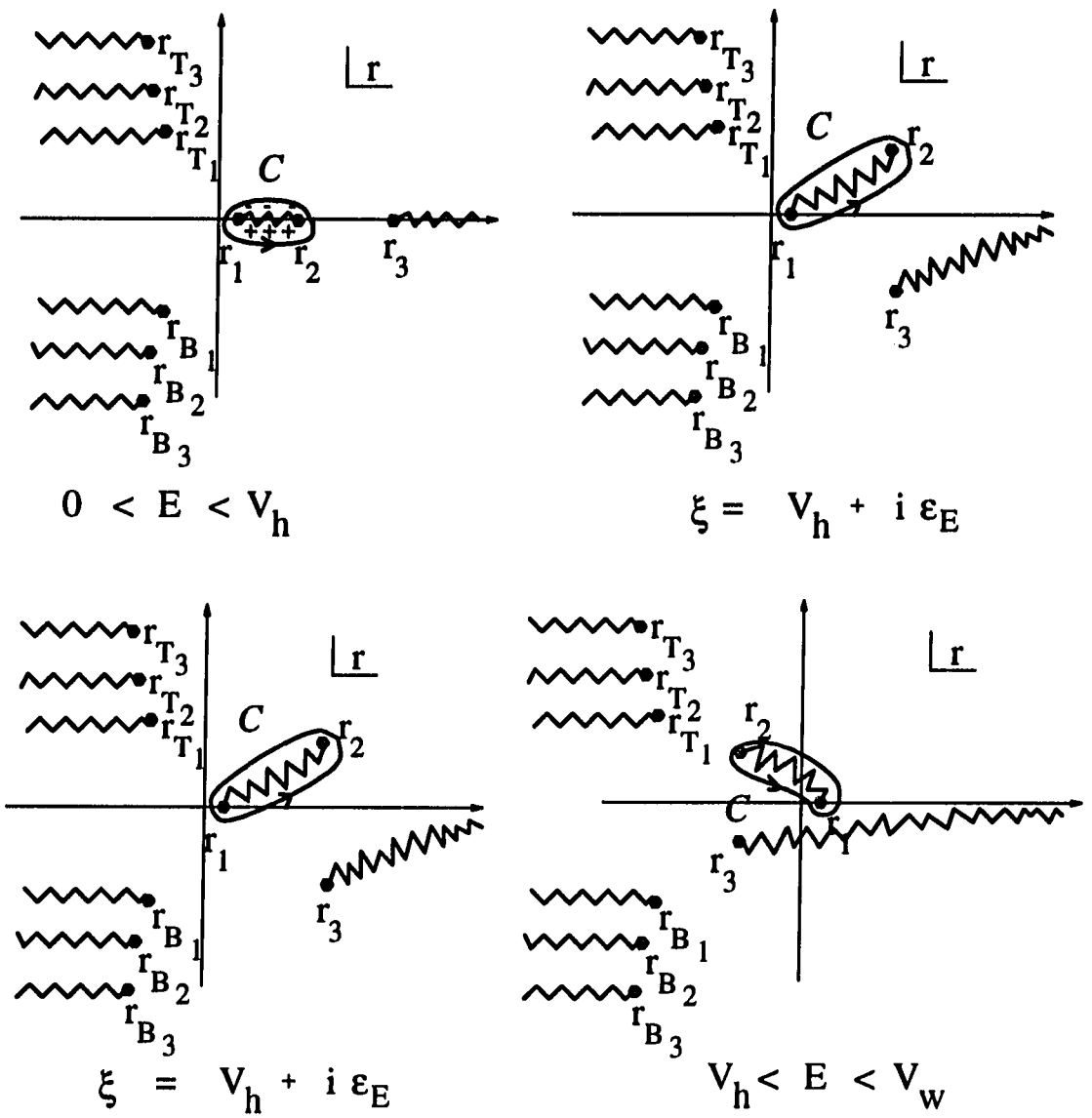

Figure 9.10: Branch cuts of $p_{rc}(r, \mathcal{E}, L)$ and the contour C for for $0 < E < E_w$

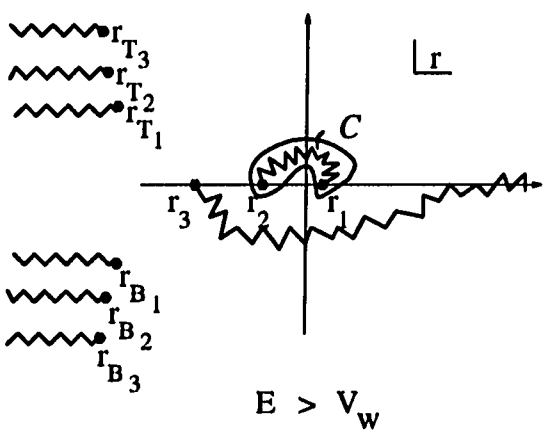

Figure 9.11: Branch cuts of $p_{rc}(r, \mathcal{E}, L)$ and the contour C for for $E > E_w$

states. For all energies the counterclockwise contour C encloses the turning points r_1 and r_2 and the cut joining them. We define J_{rc}, the classical action variable, by

$$J_{rc} = \frac{1}{2\pi} \oint_C p_{rc}(r, \mathcal{E}, L)\, dr. \tag{9.24}$$

The evaluation of the integral in eq. (9.24) can be done using the perturbation theory developed in [7]. Writing the square of the classical momentum function as

$$p_{rc}{}^2 = -\frac{L^2}{r_1 r_2} \frac{(r-r_1)(r-r_2)}{r^2} f^2(r) \tag{9.25}$$

with

$$f^2(r) = 1 + \sum_{n=1}^{\infty} v_n r^n, \tag{9.26}$$

we can show (see Appendix B) that

$$v_n \sim (\frac{r_2}{R})^{n+1}. \tag{9.27}$$

Using

$$f(r) = 1 + \sum_{n=1}^{\infty} t_n r^n, \tag{9.28}$$

squaring it to get the expansion for $f^2(r)$ and comparing that expansion with the one in eq. (9.27), we get

$$t_n = \frac{1}{2}[v_n - \{\sum_{j=1}^{n-1} t_j t_{n-j}\}], \tag{9.29}$$

$$\sim (\frac{r_2}{R})^{n+1}. \tag{9.30}$$

Thus, $p_{rc}(r, \mathcal{E}, L)$ for the Yukawa potential has the same form as the one for the Coulomb potential (see eq. 5.4) in the zeroth order in (r_2/R). From equations (9.24)

and (9.25) we can write J_{rc} as a series:

$$J_{rc} = J_{rc}(\text{Coulomb}) + \sum_{n=1}^{\infty} P(r_1, r_2, n+1)\, t_n, \tag{9.31}$$

where

$$P(r_1, r_2, n) = \sum_{j=0}^{n} b_j b_{n-j}\, r_1^j r_2^{n-j}, \tag{9.32}$$

b_j being the coefficients in the binomial expansion

$$[1-x]^n = \sum_{j=0}^{\infty} b_j x^j. \tag{9.33}$$

In the limit of $R \to \infty$ (which turns the Yukawa potential into the infinite range Coulomb potential), all the t_n (from eq. (9.30)) vanish and we recover the expression (5.8) for J_{rc}.

Alternate definition of J_{rc}

A classical Lagrangian of the form

$$\mathcal{L} = \frac{1}{4}\left[\frac{\dot{r}^2}{(1-\epsilon_r r)^4} + r^2\dot{\theta}^2 + r^2\sin^2\theta\,\dot{\phi}^2\right] - V(r), \tag{9.34}$$

with ϵ_r a positive number, reduces to the correct Lagrangian for a particle moving in a central potential $V(r)$ in the limit of $\epsilon_r \to 0$. The Lagrange equations of motion separates in the r, θ and ϕ coordinates and the equation of motion for r is

$$\frac{d}{dt}\left[\frac{1}{2}\frac{\dot{r}}{(1-\epsilon_r r)^4}\right] = -V'(r) + \frac{2L^2}{r^3}. \tag{9.35}$$

Here $(1-\epsilon_r\, r)^{-4}$ appears as the "effective mass" of the particle. The θ and ϕ equations of motion do not contain ϵ_r. The Hamiltonian that corresponds to the

Lagrangian (9.34) is

$$H = (1-\epsilon_r r)^4 \mathcal{P}_{rc}^2 + \frac{p_{\theta c}^2}{r^2} + \frac{p_{\phi c}^2}{r^2 \sin^2\theta} + V(r) \tag{9.36}$$

Since H does not explicitly depend on time it is a constant, $\mathcal{E}$, of the motion. Also the total angular momentum L is a constant of the motion. The classical momentum function $\mathcal{P}_{rc}$ of such a particle at the radial coordinate r is

$$\mathcal{P}_{rc}(r,\mathcal{E},L) = \frac{\sqrt{\mathcal{E}-V(r)-L^2/r^2}}{(1-\epsilon_r r)^2}. \tag{9.37}$$

The classical turning points of the motion are independent of ϵ_r; thus they continue to be at the locations given in Figures 9.9 through 9.11. We define $\tilde{J}(\mathcal{E},L,\epsilon_r)$ by

$$\tilde{J}_{rc}(\mathcal{E},L,\epsilon_r) = \frac{1}{2\pi}\oint_{C'} \mathcal{P}_{rc}(r,\mathcal{E},L)\,dr, \tag{9.38}$$

where the counterclockwise contour C' encloses the turning points r_1 and r_2 and the point $r = 1/\epsilon_r$, as shown in Figure 9.12, and the action variable is defined by

$$J_{rc} = \lim_{\epsilon_r \to 0} \tilde{J}(\mathcal{E},L,\epsilon_r). \tag{9.39}$$

The integral over C' can be performed by distorting the contour C' into two contours C and C_ϵ. The integral over the former yields

$$\frac{1}{2\pi}\oint_C \sqrt{\mathcal{E}-V(r)}\,dr + O(\epsilon_r), \tag{9.40}$$

since the denominator in eq. (9.37) can be expanded, using the binomial theorem, in positive powers of ϵ_r. The integral over C_ϵ is done using Cauchy's integral formula:

$$\frac{1}{2\pi}\oint_C \frac{\sqrt{\mathcal{E}-V(r)}}{(1-\epsilon_r r)^2}\,dr = i\frac{1}{\epsilon_r^2}\left[g\epsilon_r^2\left(1+\frac{1}{\epsilon_r R}\right)\exp(-1/\epsilon_r R) - 2L^2\epsilon_r^3\right]. \tag{9.41}$$

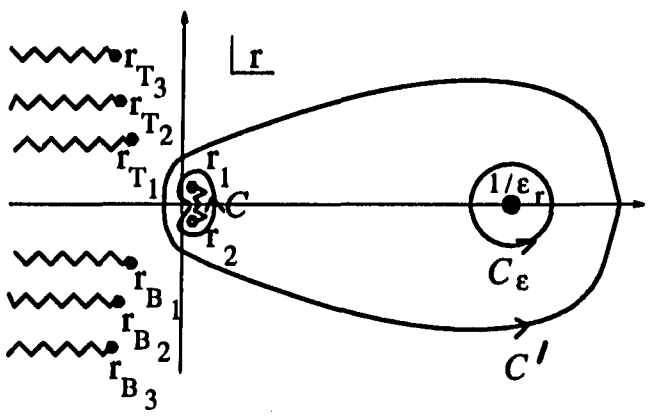

Figure 9.12: Contour C' for the definition of $\tilde{J}_{rc}$

$\tilde{J}(\mathcal{E}, L, \epsilon_r)$, which is the sum of the integrals in (9.40) and (9.41), thus becomes J_{rc} defined in eq. (9.24) in the limit of $\epsilon_r \to 0$.

The usefulness of this alternate definition of J_{rc} by a contour integral over C' rather than C will be evident when we consider the corresponding quantum problem. The interior of C' has an infinite number of poles of the quantum momentum function $\mathcal{P}_r(r, \mathcal{E}, L)$ that vanish into the point $r = 1/\epsilon_r$ on negative energy eigenvalues and an analytic continuation of J_r for energies other than negative eigenvalues requires that we use a modified Hamiltonian of the type (9.36). We have demonstrated here that such a modification of the Hamiltonian leads to a definition of J_{rc} that parallels the corresponding quantum definition.

Features of the Yukawa J_{rc}

We saw in chapter 5 the energy dependence of J_{rc} for the Coulomb potential; the Coulomb turning point r_2 moves all the way to $r = \infty$ as $\mathcal{E}$ approaches 0 resulting in $J_{rc} \to \infty$ in this limit. The period of the bound radial Coulomb motion, as a consequence, grows indefinitely. For the Yukawa potential, on the other hand, the action variable J_{rc} is finite as $\mathcal{E} \to 0$; there is a bound r_h for the turning point r_2. This makes the integral in eq. (9.24) finite for $\mathcal{E} = 0$. A consequence of this, as we will see in chapter 11, is that the quantum bound states for the Yukawa potential, unlike for the Coulomb potential, are finite in number.

CHAPTER 10. SEMICLASSICAL STUDY - YUKAWA POTENTIAL

We study in this chapter the energy dependence of the locations of the poles of the quantum momentum function for the Yukawa potential using the WKB wave functions. We find that the structure of these poles bears similarity to those found in the case of the Coulomb potential. It also displays features that are distinctly different; instead of one family of infinite poles there are infinitely many such families, a result of the presence in the potential of the exponential which is periodic in the imaginary part of its argument. The short range nature of the potential which has a well of finite width curtails the total number of bound states to a finite number, unlike the Coulomb potential. The semiclassical method, due to its reliance on the turning points, which are infinitely many in this case, also poses problems that are peculiar to the Yukawa potential.

Nature of $W_{rc}(r, \mathcal{E}, L)$ west of the western turning points

From our study of the Yukawa potential we know that there are an infinite number of western turning points, in addition to the Coulomb like turning points r_1 and r_2. There are Stokes and anti-Stokes lines radiating outwards from these turning points, dividing the complex r plane into regions in each of which one uses a WKB wave function which has the form of two exponentials $\exp(\pm i W_{rc}/\hbar)$; the

coefficients of the exponentials in each region are chosen so that the WKB solutions on the two sides of the boundary separating the two regions are relatively smooth, allowing for a discontinuity only in the subdominant exponential on the boundary (which is a Stokes line). A particularly simple insight into the nature of the Stokes and anti-Stokes lines originating at the western turning points is available. Consider a point r west of the western turning points at which there is a Stokes line. To know the direction along which the Stokes line proceeds from this point r, we approximate the classical momentum function by

$$p_{rc}(r, \mathcal{E}, L) \simeq \sqrt{\frac{g}{r}} \exp(-r/R);$$

this is justified since the exponential has a real part $\exp(-Re(r)/R)$ that dominates the other two terms in $p_{rc}(r, \mathcal{E}, L)$. The phase of $p_{rc}(r, \mathcal{E}, L)$ is $-1/2\,(Im(r)/R + \theta_r)$, where θ_r is the phase of r. Since $|\theta_r| << |Im(r)|$ for $|r/R| << 1$ (very far west,) the phase of $p_{rc}(r, \mathcal{E}, L)$ is $\simeq -Im(r)/2R$. Thus for $Im(r) = (2n+1)\pi R$, n being an integer, p_{rc} is imaginary and the line element dr along the Stokes line must be real. This shows that there are Stokes lines, west of the turning points, going west, with vertical spacing of $2\pi R$, with $Im(r) = (2n+1)\pi R$. Similarly there are anti-Stokes lines going west in the western half plane with $Im(r) = 2n\pi R$. This is true for all energies, positive and negative. We choose the branch cuts of $p_{rc}(r, \mathcal{E}, L)$ originating at the western turning points to lie along these anti-Stokes lines. In the right half plane, on the other hand, the pattern of Stokes and anti-Stokes lines depends on the sign of the energy. For $Re(r)$ large and positive, $p_{rc} \simeq \sqrt{E}$; therefore, W_{rc}, which is the integral of $p_{rc}(r, \mathcal{E}, L)$ is imaginary along paths going east of the western turning points for negative energy, hence the Stokes lines go east of the western turning points for $E < 0$; similarly the anti-Stokes lines go north and south. For $E > 0$, this

situation reverses; Stokes lines go north and south and anti-Stokes lines go east. We now study the different regions for the presence of poles by mapping the Stokes and anti-Stokes lines around each turning point and constructing the WKB wave function in each region.

Poles for $E < V_0$

Figure 10.1 shows the division of the r plane into different regions with the Stokes lines (represented by the dashed lines) forming the boundaries of regions within which we can use a WKB wave function $u(r, \mathcal{E}, L)$ with a particular set of coefficients of $\exp(\pm iWrc/\hbar)$. The nature of W along a Stokes line ($\pm i$ like) is also shown (W here refers to the the W defined with respect to the turning point at which that particular Stokes line starts). The constant coefficients A, B in the different regions surrounding a turning point are related by the connection formulas (6.14). Since the pattern of Stokes and anti-Stokes lines around the turning points r_1 and r_2 is identical to the corresponding picture in the Coulomb case (see figure 10.1), the coefficients $A_2, B_2, A_3, B_3, A_4, B_4, A_5, B_5$ and $A_{2'}, B_{2'}, A_{3'}, B_{3'}, A_{4'}, B_{4'}$ are the same as the ones listed in table 6.1, with J_{rc} for the Coulomb potential replaced by the one for the Yukawa potential. The difference from the Coulomb case is that region $3'$ does not extend all the way to ∞ north but is bounded by the Stokes line going east from r_{T1}, the first western turning point on top of the real axis. This is because the the WKB solution $u(r, \mathcal{E}, L)$ in the region $3'$ surrounding the turning point r_2, expressed in terms of $\exp(\pm iW_{rc2}/\hbar)$ has to match the $u(r, \mathcal{E}, L)$ written in terms of $\exp(\pm iW_{T1}/\hbar)$ in the region 2 around r_{T1}; this matching is done in the region labeled "strip 2", which is part of both these regions. The subscripts on the Ws here

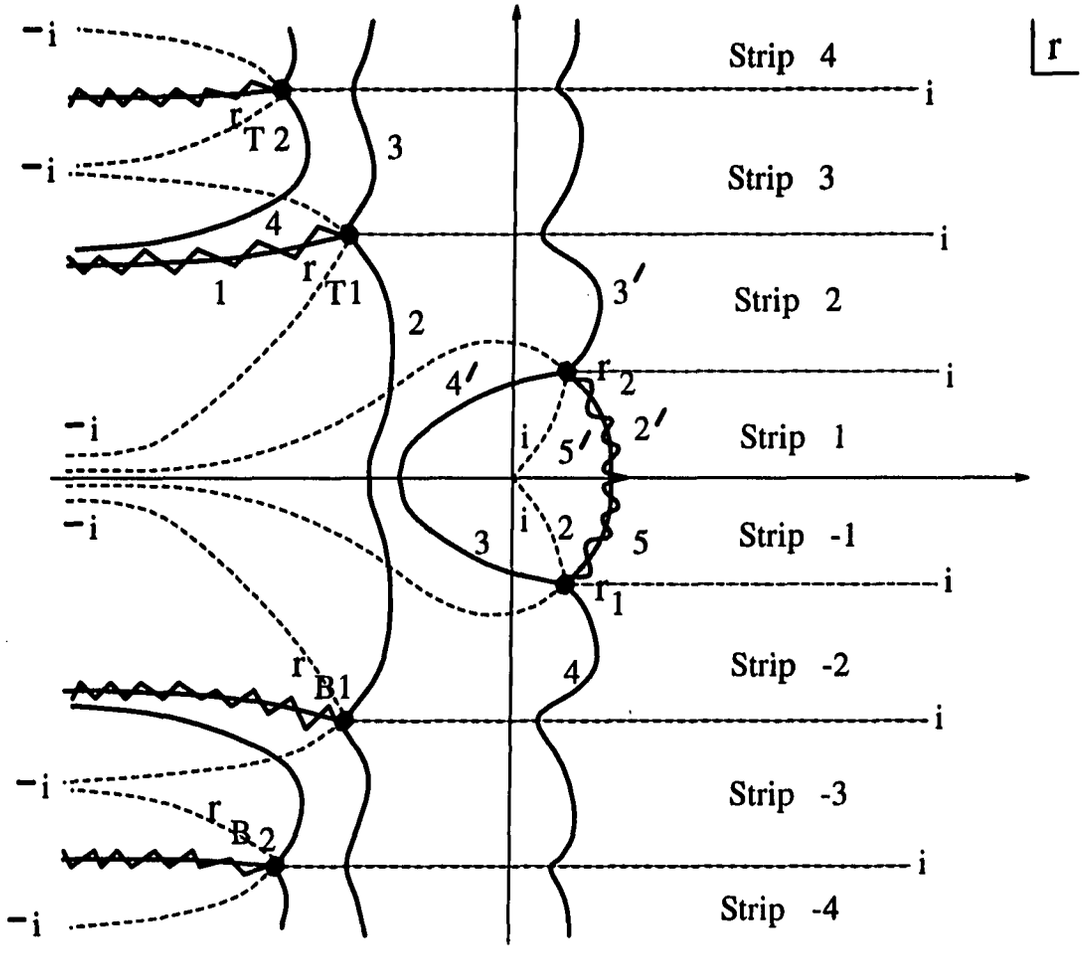

Figure 10.1: Stokes and anti-Stokes lines for $E < V_0$

denote the turning points with respect to which these extended classical characteristic functions are defined, eg., W_{T1} is $\int_{r_{T1}} p_{rc}(r,\mathcal{E},l)\,dr$ (see eq. (6.12)). Similar strips numbered $2,3,4,\ldots$ occupy the entire region to the east of the top western turning points, each strip numbered $n+1$ representing the region where the wave function expressed in terms of $W_{T\,n}$ has to match the wave function expressed in terms of $W_{T\,n-1}$. This matching of the different WKB representations of $u(r,\mathcal{E},L)$ restricts us to use the W_{T1} form of u in strip 3 instead of the W_{rc2} form, though both forms coincide in strip 2. Similar restrictions apply in the southern half plane.

The WKB solution u is first obtained in region $5'$ by imposing the boundary condition (6.10). This solution is extended to regions $2', 3'$ and $4'$ around r_2 using the connection formulas (6.14). The solution in region 2 around r_{T1} is then obtained by matching it with the solution in region $3'$ near r_2. The connection formulas are again used to obtain the solution all around r_{T1}. One continues this procedure of extending the solution from regions surrounding a top turning point to the regions surrounding the next higher turning point. The solution in the southern half plane is similarly obtained. Table 10.1 shows the coefficients (A,B) of $\exp(\pm iW/\hbar)$ for the regions around r_2 and r_{T1}. We identify regions where u has the form of two exponentials in order to locate the zeroes of u. As in the Coulomb case region $3'$ (strip 2) has zeroes north of r_2. Similarly strip 3 has zeroes since region 3 near r_{T1} has a u of the double exponential form. Every strip has zeroes, by extension. The spacing between these zeroes is of the order of $\pi\hbar/\sqrt{|E|}$, which follows from an equation of the form (6.28).From this near constant spacing between the zeroes we can deduce that every strip has only finitely many zeroes, as these zeroes are near the anti-Stokes lines which run perpendicular to the strips and there is only a finite

Table 10.1: Coefficients A and B of $\exp(\pm iW/\hbar)$ for $E < V_0$

A_2 1	B_2 0	A_3 1	B_3 0
A_4 1	B_4 i	A_5 0	B_5 i
$A_{2'}$ 0	$B_{2'}$ $-i\alpha$	$A_{3'}$ α	$B_{3'}$ $-i\alpha$
$A_{4'}$ α	$B_{4'}$ 0	$A_{5'}$ α	$B_{5'}$ 0
A_{1T1} $\alpha\gamma_{2T1}$	B_{1T1} $-2i\alpha\cos(I_{2T1}/\hbar)$	A_{2T1} $\alpha\gamma_{2T1}$	B_{2T1} $-i\alpha/\gamma_{2T1}$
A_{3T1} $2\alpha\cos(I_{2T1}/\hbar)$	B_{3T1} $-i\alpha/\gamma_{2T1}$	A_{4T1} $2\alpha\cos(I_{2T1}/\hbar)$	B_{4T1} $i\alpha/\gamma_{2T1}$

$$\alpha = \exp(-i\pi J_{rc}/\hbar) \qquad \beta = \alpha + 1/\alpha$$

$$I_{2T1} = \int_{r_2}^{r_{T1}} p_{rc}(r, \mathcal{E}, L)\, dr = W_{rc2}(r = r_{T1})$$

$$\gamma_{2T1} \quad \exp\{iW_{rc2}(r = r_{T1})/\hbar\}$$

length of the anti-Stokes line in any strip. The zeroes in the northern plane east of the western turning points is thus infinitely many, there being an infinite number of strips. These zeroes are very similar to the northern zeroes one encounters in the case of the Coulomb potential. A similar set of southern zeroes are present south of r_1. The other region around r_{T1} that has zeroes is region 4; The zeroes in this region have the anti-Stokes line west of r_{T1} as their asymptote. These are infinitely many; the spacing between them decreases exponentially as one goes west, since, from eq. (6.15),

$$W_{T1}(r_{n+1}) - W_{T1}(r_n) = \pi\hbar,$$

$$\Rightarrow \quad r_{n+1} - r_n \simeq \pi\hbar/p_{rc}(r = r_n) \propto \frac{\sqrt{r_n}\pi\hbar}{\exp(-r_n/2R)}.$$

There is a similar train of zeroes west of every western turning point. These "western zeroes" of $u(r, \mathcal{E}, L)$ or "western poles" of $p_r(r, \mathcal{E}, L)$ grouped into infinitely many trains, with each train containing an infinite number of zeroes, are a new feature of the Yukawa potential. As the energy increases, these western zeroes move east along with the western turning points. This eastern motion with energy increase becomes less pronounced as one follows the motion of farther zeroes. The northern and southern zeroes have a motion similar to their Coulomb counterparts; they steadily get farther apart with energy increase. The pattern of the zeroes is shown in Figure 10.2.

Poles for $V_0 < E < 0$

As E increases beyond V_0 the turning points r_1 and r_2 come onto the real axis. The plot of Stokes and anti-Stokes lines is shown in figure 10.3. The WKB coefficients (A, B) for regions around r_2, r_{T1} and r_{B1} can be found as before. We obtain $u(r, \mathcal{E}, L)$ by matching the WKB wave functions expressed in terms of W_{rc}s corresponding to neighboring turning points, following the sequence

$$r_1 \rightarrow r_2 \rightarrow r_{T1} \rightarrow r_{T2},$$
$$r_1 \rightarrow r_2 \rightarrow r_{B1} \rightarrow r_{B2}.$$

The pattern of the lines around r_2 is similar to the one in the Coulomb case. The solution in every strip contains an exponential of the form $\exp(-iW/\hbar$ whose coefficient is proportional to $\cos(\pi J_{rc}/\hbar)$. This exponential is the dominant of the two exponentials in the solution on the Stokes lines east of the western turning points.

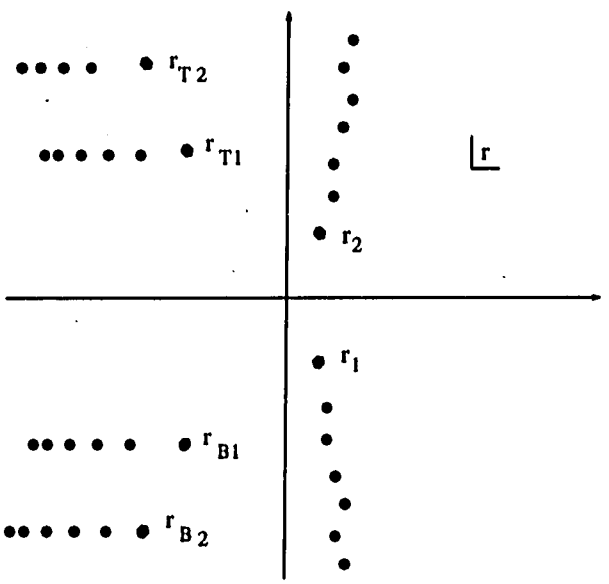

Figure 10.2: Poles of p_r for $E < V_0$

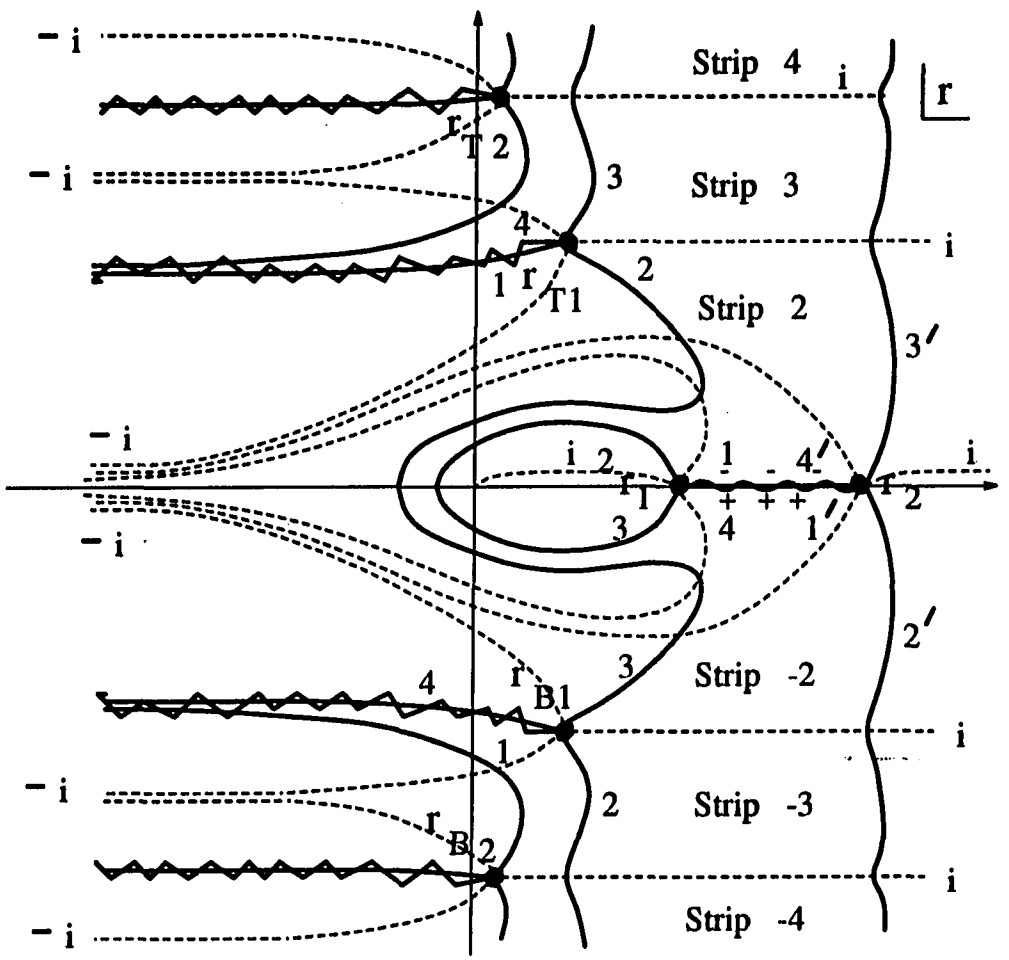

Figure 10.3: Stokes and anti-Stokes lines for $V_0 < E < 0$

Table 10.2: Coefficients A and B of $\exp(\pm iW/\hbar)$ for $V_0 < E < 0$

$A_{1'}$ $-1/\alpha$	$B_{1'}$ $-i\alpha$	$A_{2'}$ $-1/\alpha$	$B_{2'}$ $-i\beta$
$A_{3'}$ α	$B_{3'}$ $-i\beta$	$A_{4'}$ α	$B_{4'}$ $-i/\alpha$
A_{1T1} $\alpha\gamma_{2T1}$	B_{1T1} $-i(\beta/\gamma_{2T1} + \alpha\gamma_{2T1})$	A_{2T1} $\alpha\gamma_{2T1}$	B_{2T1} $-i\beta/\gamma_{2T1}$
A_{3T1} $\alpha\gamma_{2T1} + \beta/\gamma_{2T1}$	B_{3T1} $-i\beta/\gamma_{2T1}$	A_{4T1} $\alpha\gamma_{2T1} + \beta/\gamma_{2T1}$	B_{4T1} $i\alpha/\gamma_{2T1}$
A_{1T2} $\gamma_{2T1}\gamma_{T1T2}\alpha - i\gamma_{2T1}\gamma_{T1T2}\alpha$ $+\gamma_{T1T2}\beta/\gamma_{2T1}$	B_{1T2} $\gamma_{2T1}\gamma_{T1T2}\alpha$ $-i\{1/(\gamma_{2T1}\gamma_{T1T2})$ $+\gamma_{T1T2}/\gamma_{2T1}\}\beta$	A_{2T2} $-i\beta/(\gamma_{2T1}\gamma_{T1T2})$ $+\gamma_{T1T2}\beta/\gamma_{2T1}$	B_{2T2}
A_{3T2} $\gamma_{2T1}\gamma_{T1T2}\alpha$ $+\{1/(\gamma_{2T1}\gamma_{T1T2})$ $+\gamma_{T1T2}/\gamma_{2T1}\}\beta$	B_{3T2} $-i\beta/(\gamma_{2T1}\gamma_{T1T2})$	A_{4T2} $\gamma_{2T1}\gamma_{T1T2}\alpha$ $+\{1/(\gamma_{2T1}\gamma_{T1T2})$ $+\gamma_{T1T2}/\gamma_{2T1}\}\beta$	B_{4T2} $i(\gamma_{2T1}\gamma_{T1T2}\alpha$ $+\gamma_{T1T2}\beta/\gamma_{2T1}$

$$\alpha = \exp(-i\pi J_{rc}/\hbar) \qquad \beta = \alpha + 1/\alpha$$

$$I_{2T1} = \int_{r_2}^{r_{T1}} p_{rc}(r, \mathcal{E}, L)\, dr = W_{rc2}(r = r_{T1})$$

$$I_{T1T2} = \int_{r_{T1}}^{r_{T2}} p_{rc}(r, \mathcal{E}, L)\, dr = W_{rcT1}(r = r_{T2})$$

$$\gamma_{2T1} = \exp\{iW_{rc2}(r = r_{T1})/\hbar\}$$
$$\gamma_{T1T2} = \exp\{iW_{rcT1}(r = r_{T2})/\hbar\}$$

The energy eigenstates in the semiclassical approximation are characterized by this dominant exponential vanishing, for $J_{rc}(E,l) = (n+1/2)\hbar$ for integral n. For such energies $\mathcal{E} = E_n + i\epsilon_E$ the northern and southern poles go out east and move back west, with their eastern most location during this looping motion proportional to $\ln(\epsilon_J$. This is identical to the behavior of the Coulomb zeroes near energy eigenvalues. The southern zeroes move north steadily and at each energy eigenvalue the topmost southern zero enters the potential well, increasing by 1 the number of zeroes in between r_1 and r_2. The northern poles move north steadily. The important difference in the motion of the northern and southern poles with energy between the Coulomb and Yukawa potentials is the following. Since J_{rc} can increase without bound as one approaches $\mathcal{E} = 0$ in the Coulomb case the relation $J_{rc} = (n+1/2)\hbar$ is satisfied for infinitely many energies, thus the Coulomb potential admits of an infinite number of bound states. The Yukawa potential, on the other hand, sets an upper bound to J_{rc} by restricting the turning point r_2 to a finite value (see figure 9.1), resulting in a finite number of bound states. A finite number of zeroes enter the potential well for negative energies. The western zeroes move east as in the case of $E < V_0$. Unlike the northern and southern poles they display no sensitivity to eigenvalues. It can be shown, by using the WKB wave function in region 4 around r_{B2} that the train of zeroes west of that turning point never recede to $r = \infty$; it is a result of the integral I_{2B1} not being real for any $\mathcal{E}$. The pattern of zeroes for $V_0 < E < 0$ is shown in Figure 10.4

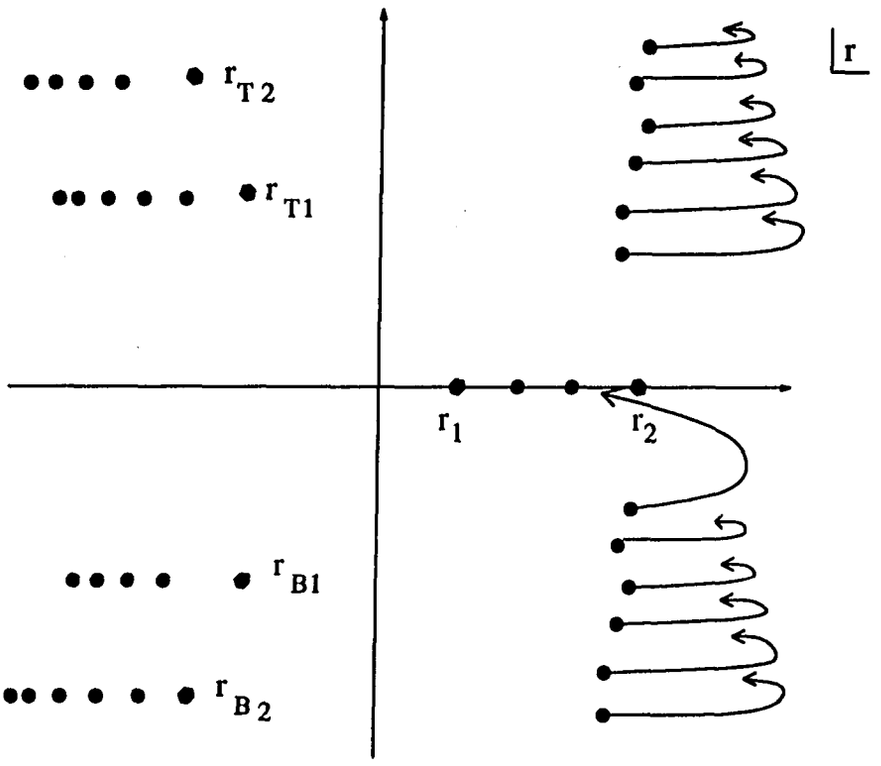

Figure 10.4: Poles of p_r for $V_0 < E < 0$

Poles for $E \approx 0$

The pattern of Stokes and anti-Stokes lines for $E \approx 0$ is shown in Figure 10.5. The turning point r_{B4} breaks out of the sequence of southwestern turning points and arcs counterclockwise onto the real axis for positive energy to become r_3. As seen in Chapter 9, which of the southwestern turning points becomes r_3 depends on the magnitude of ϵ_E. The southern zeroes, that have not entered the potential well follow the motion of r_3 and come onto the real axis. The poles and their motion for $E \approx 0$ is shown in Figure 10.4. The western zeroes move down while the western turning points move up by πR as the energy changes sign from negative to positive.

Poles for $0 < E < V_0$

Figure 10.7 shows the Stokes and anti-Stokes lines for energies in the range $0 < E \prec E_h$. The semiclassical approach of Furry fails for this range for the following reason. There is a Stokes line connecting r_2 and r_3. W_{rc2} is $+i$ like along the line from r_2 to r_3 while W_{rc3} is $-i$ like along the line from r_3 to r_2. If u in region marked I in Figure 10.7 is written as

$$u_{\rm I} = (1/\sqrt{prc}) \left[A_{\rm I} \exp(iW_{rc2}/\hbar) + B_{\rm I} \exp(-iW_{rc2}/\hbar)\right]. \qquad (10.1)$$

We can also express $u_{\rm I}$ in terms of W_{rc3} as

$$u_{\rm I} = (1/\sqrt{prc}) \left[A'_{\rm I} \exp(iW_{rc3}/\hbar) + B'_{\rm I} \exp(-iW_{rc3}/\hbar)\right]. \qquad (10.2)$$

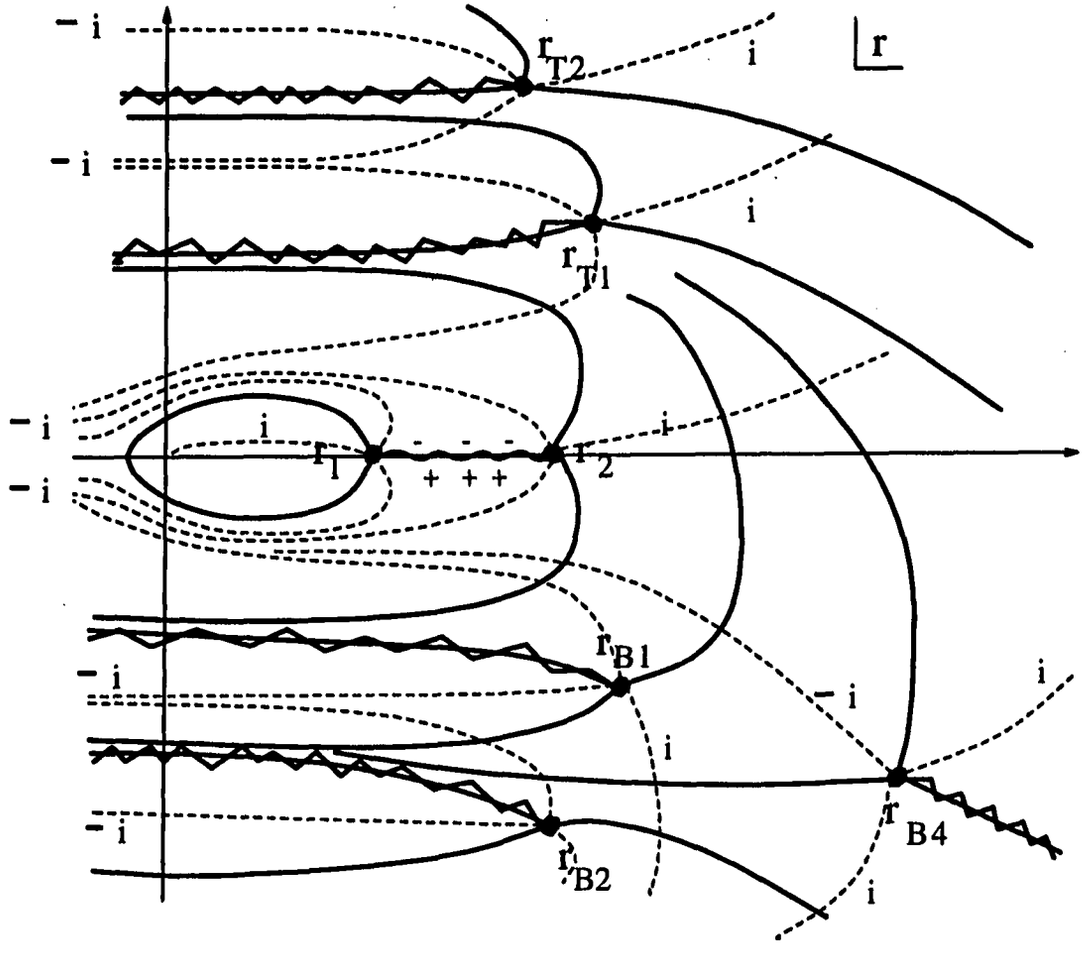

Figure 10.5: Stokes and anti-Stokes lines for $E \approx 0$

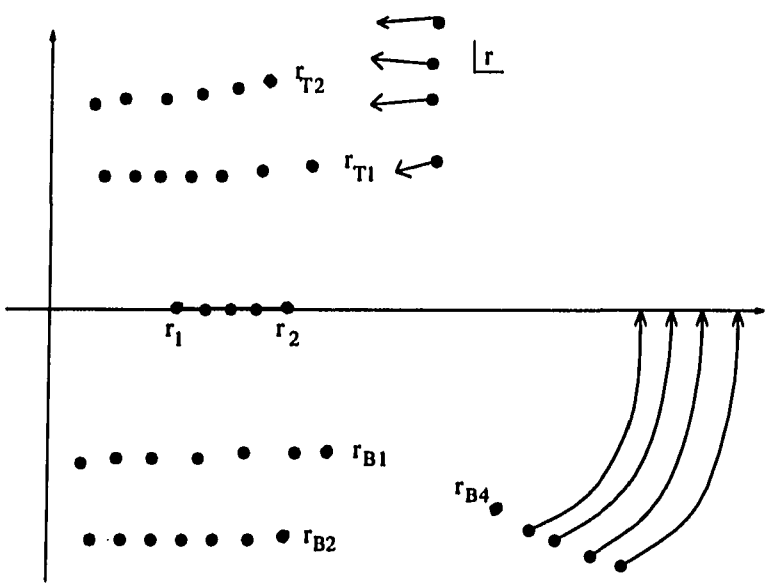

Figure 10.6: Poles of p_r for $E \approx 0$

Expressing W_{rc2} in terms of W_{rc3} we obtain the constant coefficients $A'_{\rm I}$, $B'_{\rm I}$ in terms of $A_{\rm I}$, $B_{\rm I}$:

$$A'_{\rm I} = A_{\rm I}\,\gamma_{23}, \quad B'_{\rm I} = B_{\rm I}\,/\gamma_{23} \tag{10.3}$$

where

$$\gamma_{23} = \exp(i\int_{r2}^{r3} p_{rc}\,dr/\hbar).$$

We can similarly write the wave function in the region marked II using the two Ws:

$$\begin{aligned} u_{\rm II} &= (1/\sqrt{p_{rc}})\left[A_{\rm II}\exp(iW_{rc2}/\hbar) + B_{\rm II}\exp(-iW_{rc2}/\hbar)\right], \\ u_{\rm II} &= (1/\sqrt{p_{rc}})\left[A'_{\rm II}\exp(iW_{rc3}/\hbar) + B'_{\rm II}\exp(-iW_{rc3}/\hbar)\right], \end{aligned} \tag{10.4}$$

with

$$A'_{\rm II} = A_{\rm II}\,\gamma_{23}, \quad B'_{\rm II} = B_{\rm II}\,/\gamma_{23}. \tag{10.5}$$

Using the connection formulas (6.14) to relate the coefficients of region II with those in region I, we can show that for all the As and the Bs to be not identically zero, $\gamma_{23} \equiv 0$, which is impossible. Thus the semiclassical method is not applicable in this case.

Poles for $V_h < E < V_w$

For the energy range $V_h < E < V_w$ the turning points r_2 and r_3 are complex and are complex conjugates of each other as shown in Figure 10.8. The regions where u has the form of two exponentials is to the right of r_1 which is now filled with the southern zeroes, north of r_2, south of r_3 and west of every western turning point. All these regions contain poles as shown in Figure 10.9. The northern poles get closer to the western poles for this energy range.

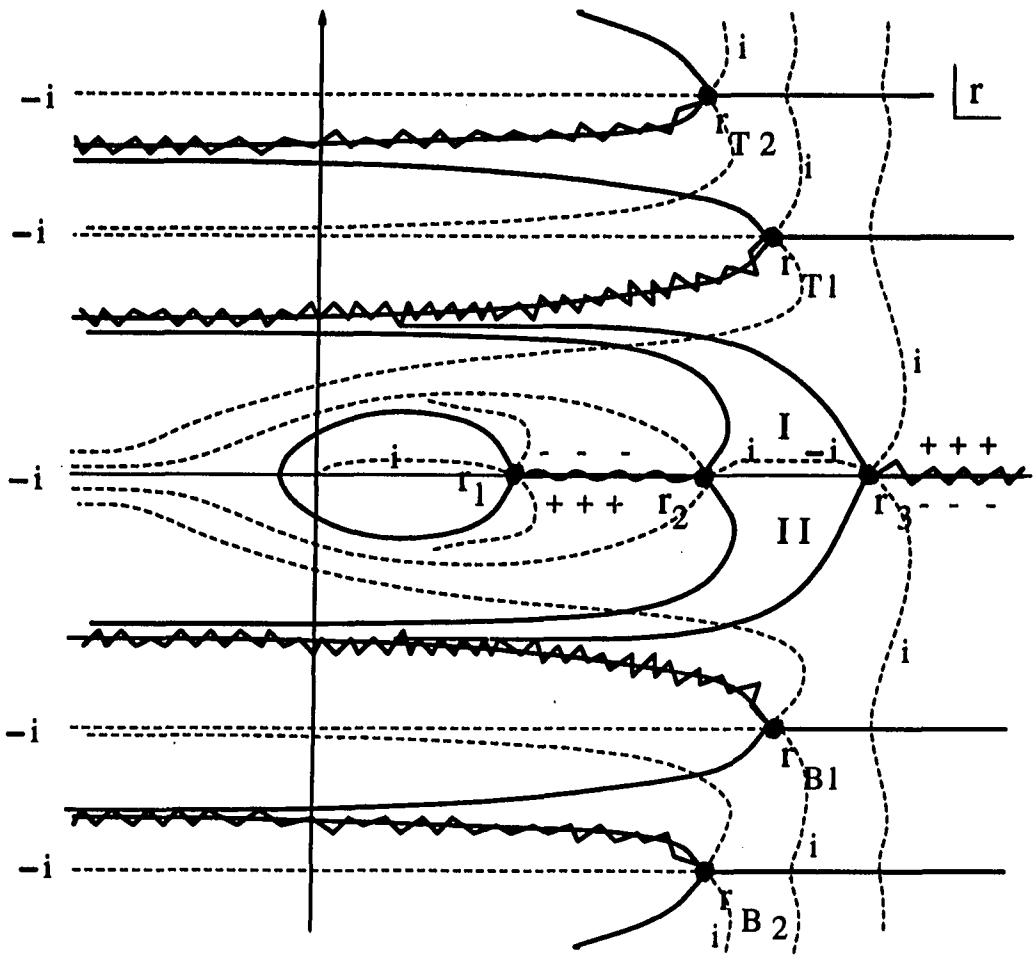

Figure 10.7: Stokes and anti-Stokes lines for $0 < E < V_0$

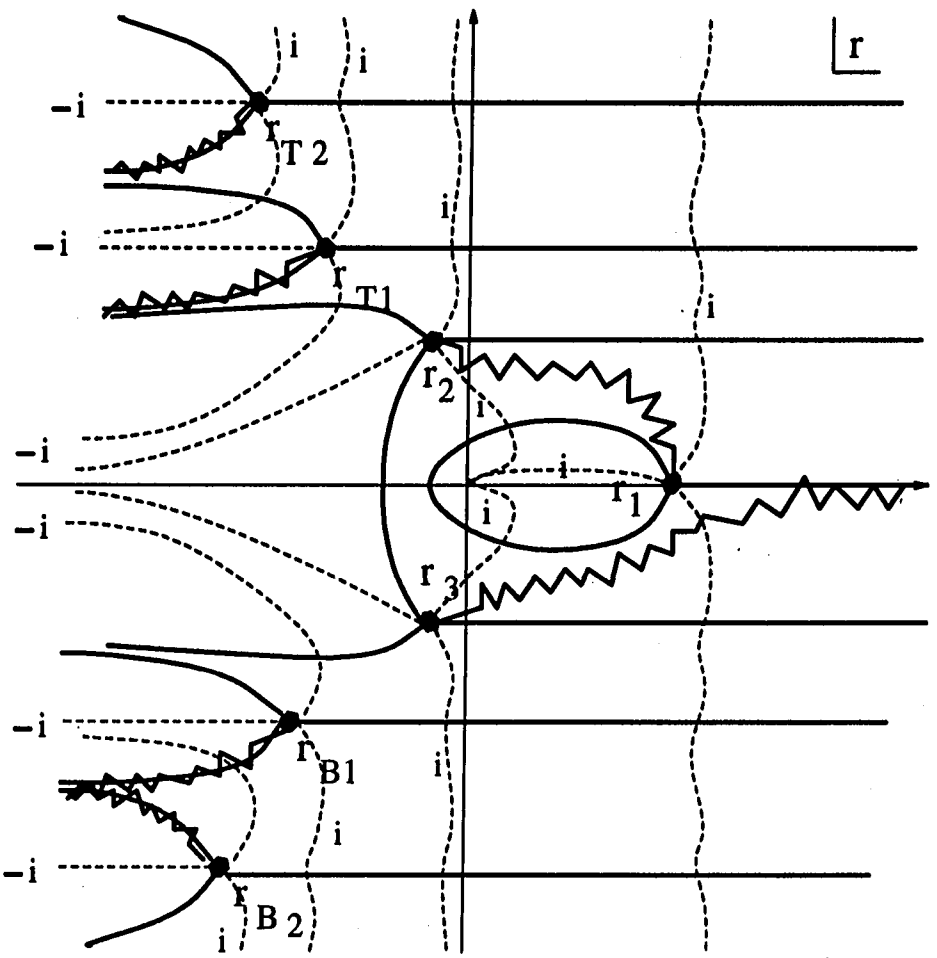

Figure 10.8: Stokes and anti-Stokes lines for $V_h < E < V_w$

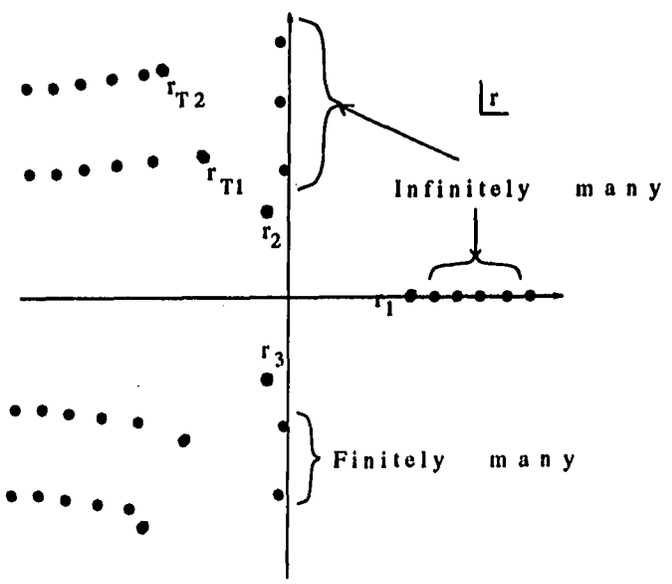

Figure 10.9: Poles of p_r for $V_h < E < V_w$

Poles for $E > V_w$

For $\mathcal{E} \approx V_w$ the turning points r_2 and r_3 are very close to each other; For $E > V_w$ these two turning points become real as shown in Figure 10.10. The wave function u is oscillatory inside the western unphysical potential well. The poles from the first northwestern train fill up this well just as the southern poles fill up the physical potential well. The poles east of r_1 get closer as the energy increases. The poles for $E > V_w$ are shown in Figure 10.11.

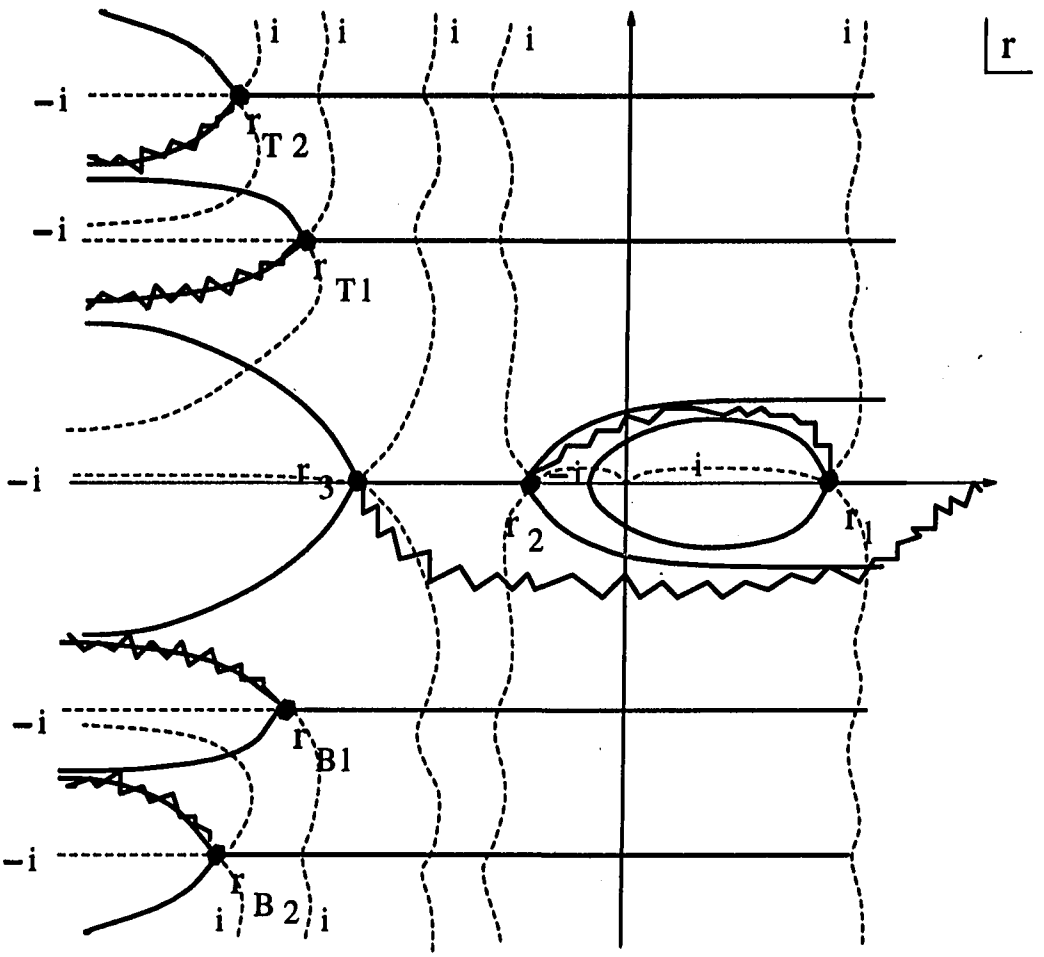

Figure 10.10: Stokes and anti-Stokes lines for $E > V_w$

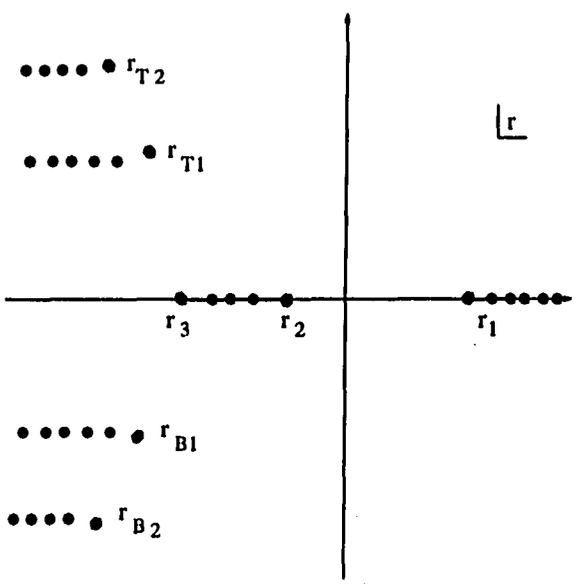

Figure 10.11: Poles of p_r for $E > V_w$

CHAPTER 11. EXACT STUDY OF THE POLES OF MOMENTUM FUNCTION - YUKAWA POTENTIAL

We present in this chapter the results of numerical computations of the motion of the poles of p_r for the Yukawa potential. The technique is similar to the one used for the Coulomb potential. To locate a western pole we integrate, from $r = 0$ to the western turning point at the eastern extremity of the pole train and start our Newton-Raphson search for the zeroes of u west of that turning point.

Discussion of the numerical results

We denote the northern and southern poles by a single index, positive for northern poles and negative for southern poles. The western poles are denoted by r_{ij} with i a positive integer denoting the western pole train of which it is a part (positive integer if the pole is in the upper half of the plane and negative if in the lower half) and j indicating the rank of the pole within the train starting with 1 for the pole which is eastern most for negative energy.

Figures 11.1 and 11.2 show the motion of the first two southern poles with energy for $l = 1$, $g = 23$. This system has two negative energy eigenvalues and no resonances in the scattering region. The four computations were done with four successively smaller values of ϵ_E. The poles move farther out east if ϵ_E, and therefore

ϵ_J, is smaller which is consistent with the prediction, based on the WKB approximation, of the logarithmic dependence on ϵ_J of the real parts of the jth southern pole r_j. In Figure 11.2, the figure corresponding to $\epsilon_E = 2\text{x}10^{-5}$, shows the large displacement of the first pole around the first energy eigenvalue with very little change in energy.

Figure 11.3 shows the first five southern poles move with energy with $\epsilon_E = 0.1$. The first pole, comes onto the real axis after an eastern excursion around the ground state energy. Poles r_{-2} through r_{-5} shown in the figure move in an arc around $E \approx 0$ and come onto the positive real axis. This behavior is unlike the motion of the southern poles for the Coulomb potential all of which reach the positive real axis for a negative energy.

Figures 11.4 through 11.6 show poles for three systems, each with $g = 55$ and l of 1, 2 and 3 (we have set $\hbar = 1$ in the computation). The $l = 1$ system has 4 negative energy eigenvalues, the $l = 2$ system 3 eigenvalues and the $l = 3$ system one eigenvalue and a resonance state. The one with $l = 2$ has the first three southern poles landing on the real axis but the fourth pole moves west around $E \approx 0$ and joins the western poles. It is observed that if a system has n bound states, then the first $(n-1)$ southern poles reach the positive real axis for positive energy while a finite number of southern poles immediately below the first $(n-1)$ join the train of western poles. The remaining ones of this group (infinitely many) arc around and come onto the positive real axis. The third of these systems is very interesting. It has the first southern pole come onto the positive real axis while the rest of the southern poles have an arcing eastward movement around the energy of resonance (determined by a phase shift analysis). This excursion of these southern poles for a positive energy

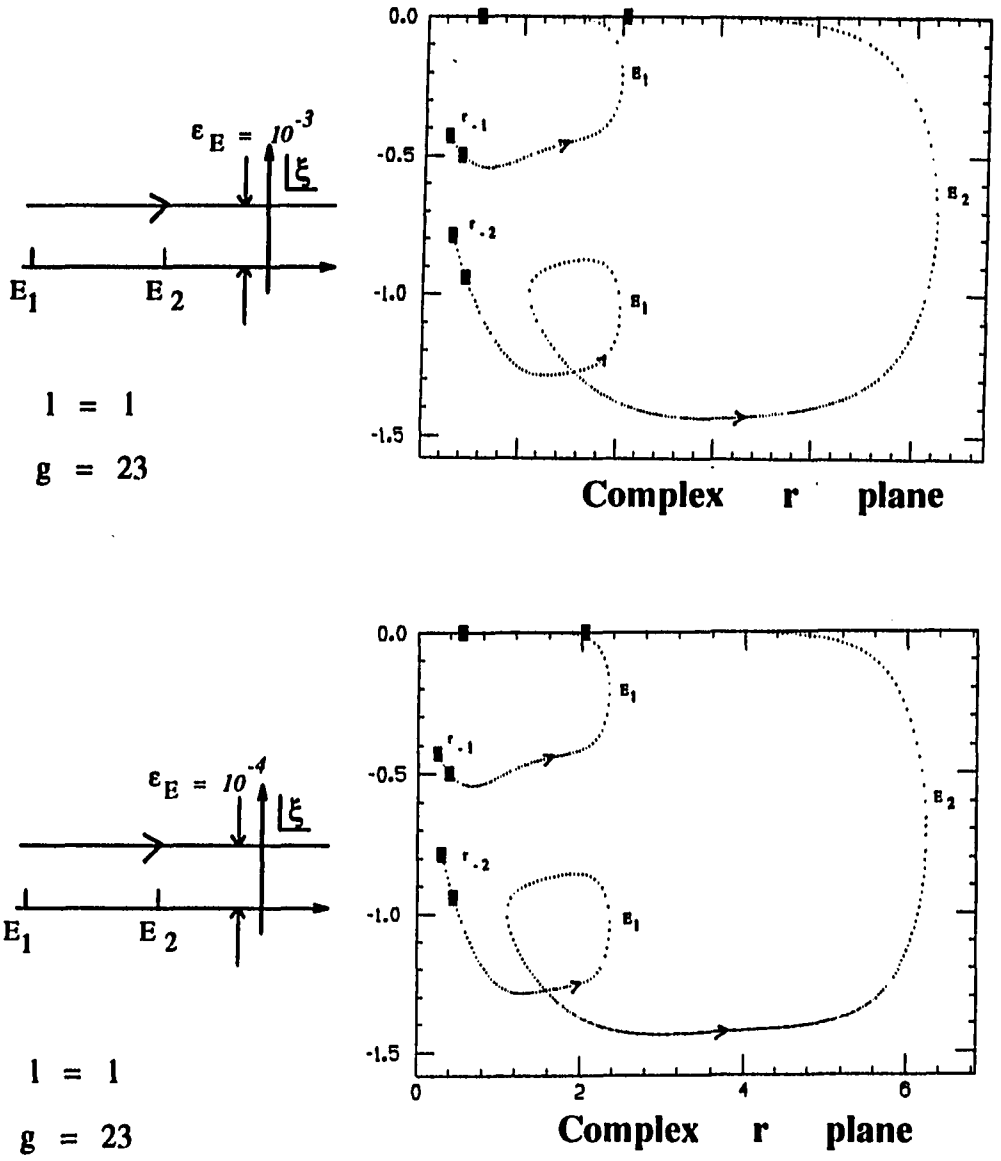

Figure 11.1: First two southern poles of $p_r(r, \mathcal{E}, l)$ for $V_0 < E < V_w$ and $l = 1, \quad g = 23$

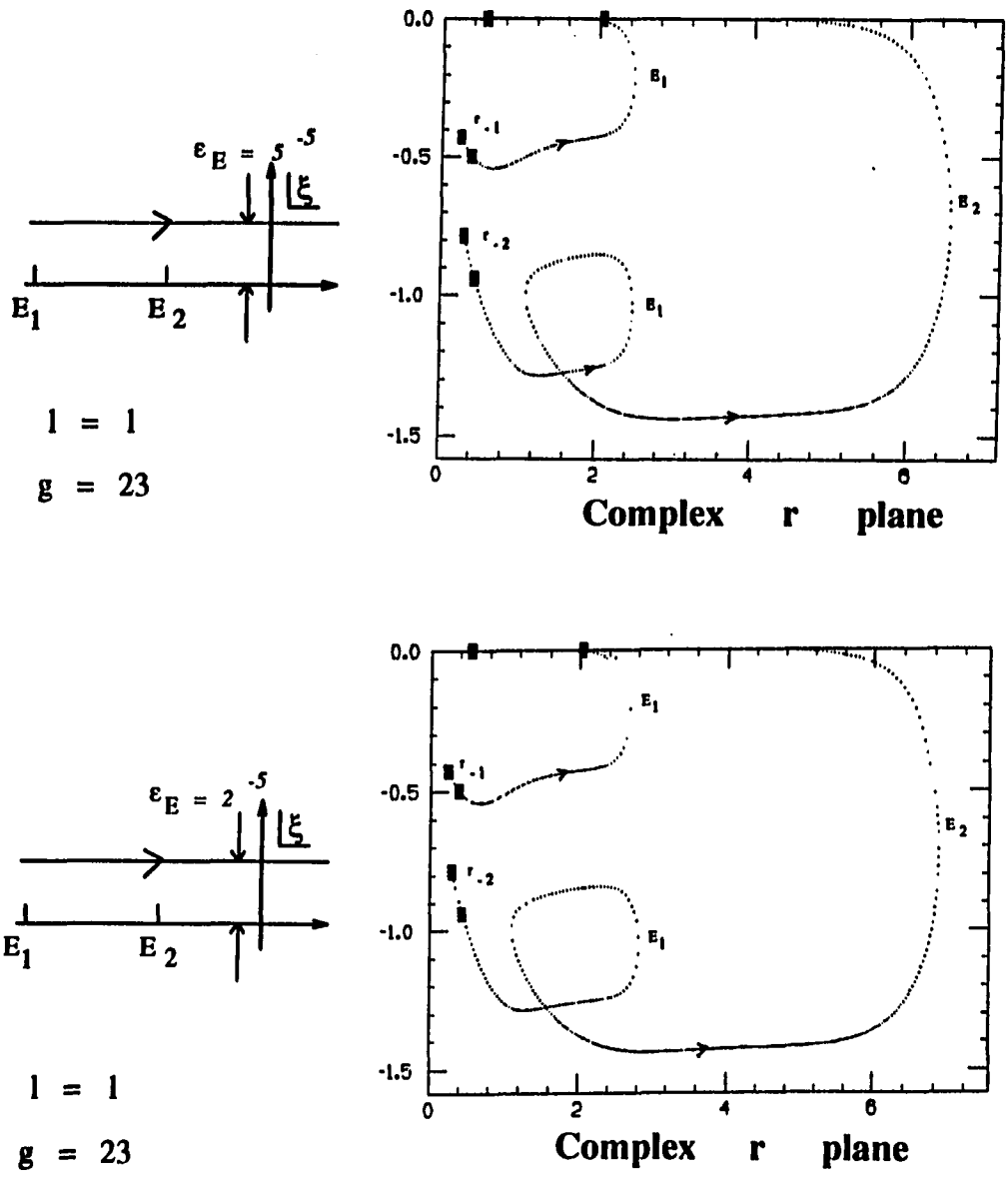

Figure 11.2: First two southern poles of $p_r(r, \mathcal{E}, l)$ for $V_0 < E < V_w$ and $l = 1, \quad g = 23$

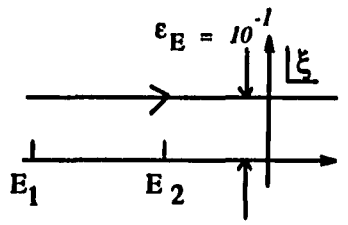

l = 1

g = 23

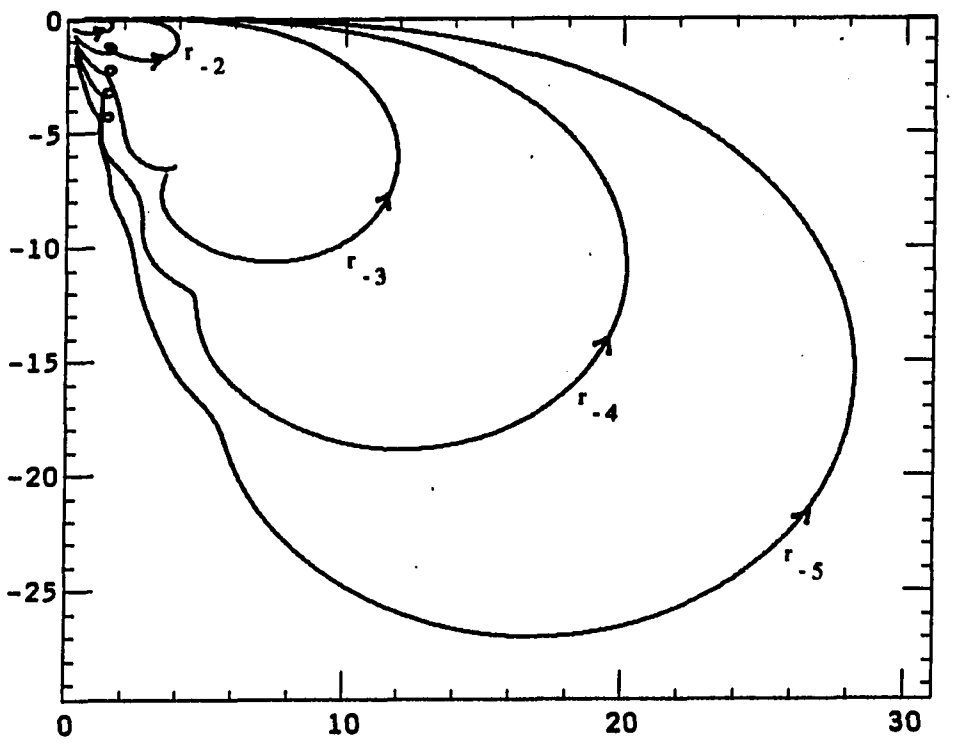

Figure 11.3: First five southern poles of $p_r(r, \mathcal{E}, l)$ for $V_0 < E < V_w$ and $l = 1, \quad g = 23$

is very similar to their behavior around negative energy eigenvalues. The second one, after displaying negative eigenvalue like behavior of rapid motion around the resonant energy, moves west. This behavior of those southern poles that move west instead of coming onto the real axis requires further study. The WKB method, with limited regions of validity of the solutions, is not particularly suited to the study of the behavior of poles for $E \approx 0$.

Figure 11.7 shows the motion of northern and northwestern poles with energy for an $l = 1$, $g = 20$ system which has two bound states. The northern poles are sensitive to energy eigenvalues, like their southern counterparts, performing rapid motion with energy around energy eigenvalues. All except the first northern pole join the western train of poles for positive energy. The northwestern poles are insensitive to energy eigenvalues and move west for increasing negative energy. Around $E \approx 0$ they start a south and westward motion and come down vertically by about πR; the western turning points, for the same energy increment, move up vertically by πR. The vertical spacing between the turning points is $2\pi R$. Thus the poles which follow the eastward motion of a turning point for negative energy switch to following the motion of the turning point one below for positive energy while moving westward. The first northwestern train of poles (two poles r_{11} and r_{12} are shown in the figure) come down to the negative real axis. They fill the western potential well very much like the southern poles filled the physical eastern potential well.

Summary of the motion of poles with energy

(i) A system described by a Yukawa potential that admits n bound states has $n-1$ southern poles coming onto the region of the physical potential well. As the

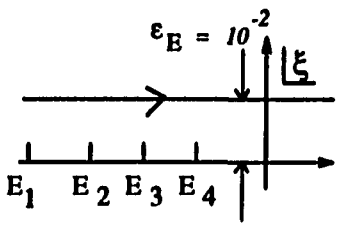

l = 1

g = 55

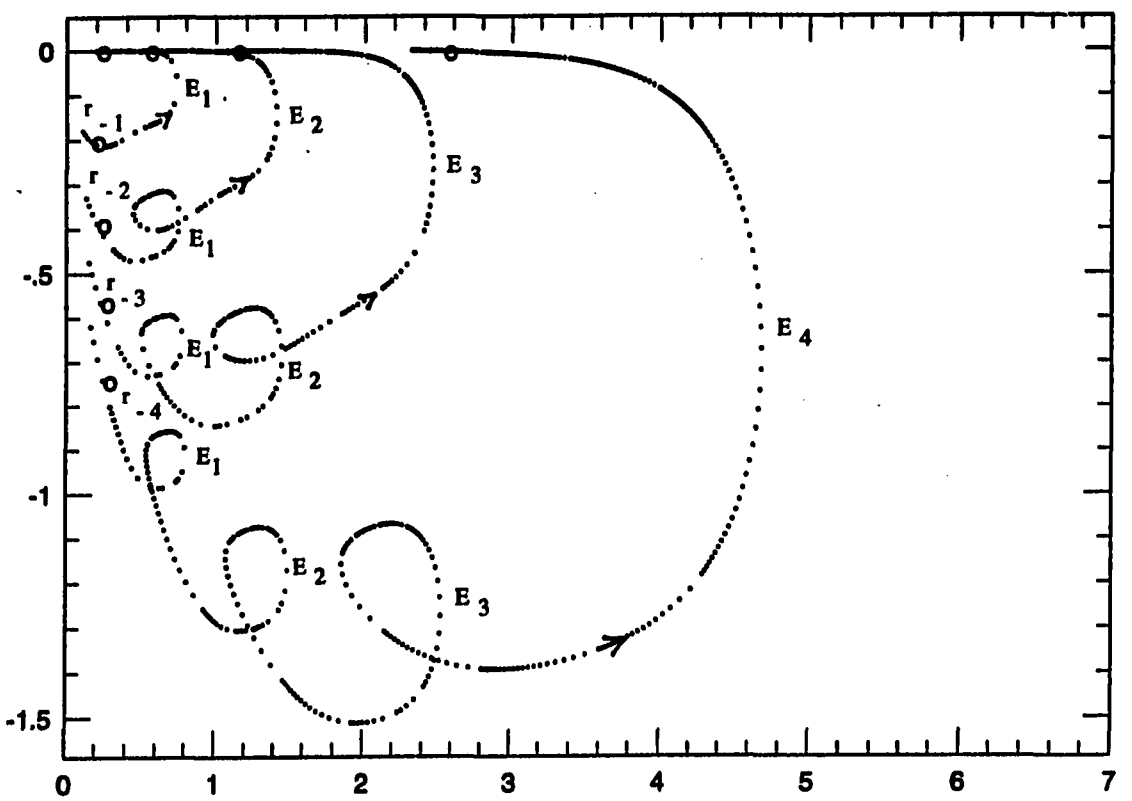

Figure 11.4: First four southern poles of $p_r(r, \mathcal{E}, l)$ for $V_0 < E < V_w$ and $l = 1$, $g = 55$, with four bound states

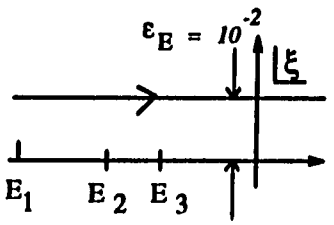

l = 2

g = 55

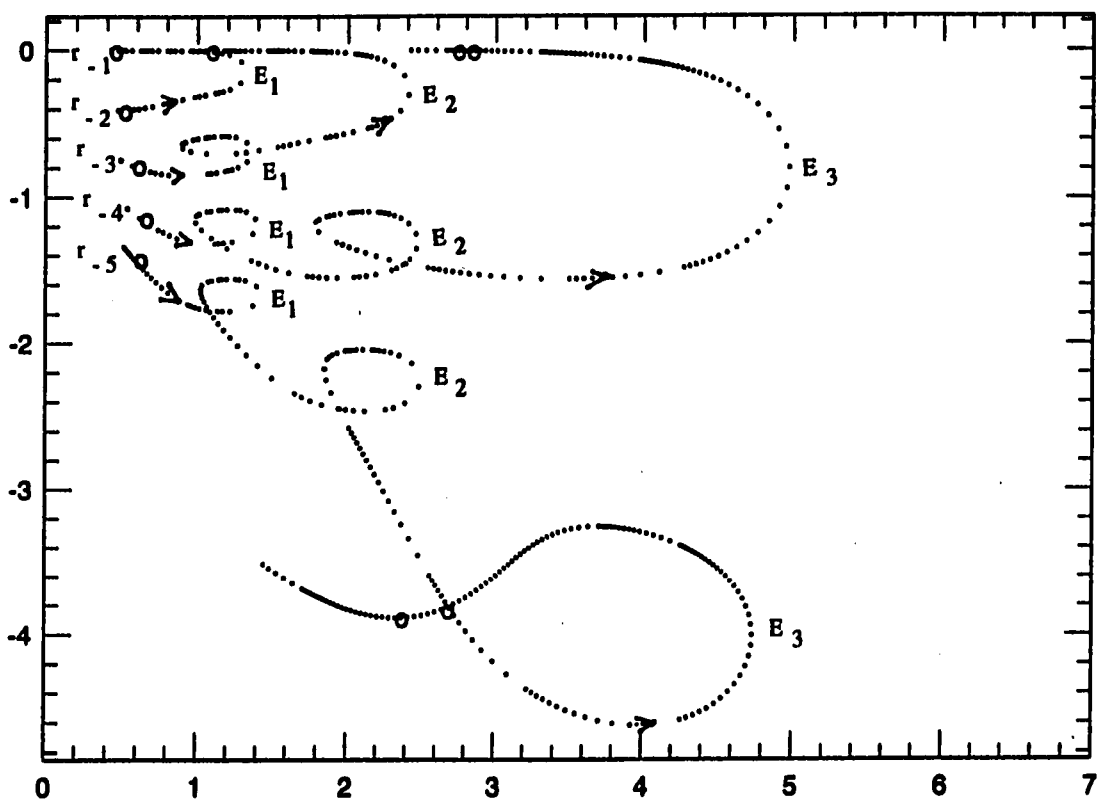

Figure 11.5: First five southern poles of $p_r(r, \mathcal{E}, l)$ for $V_0 < E < V_w$ and $l = 2$, $g = 55$ with three bound states

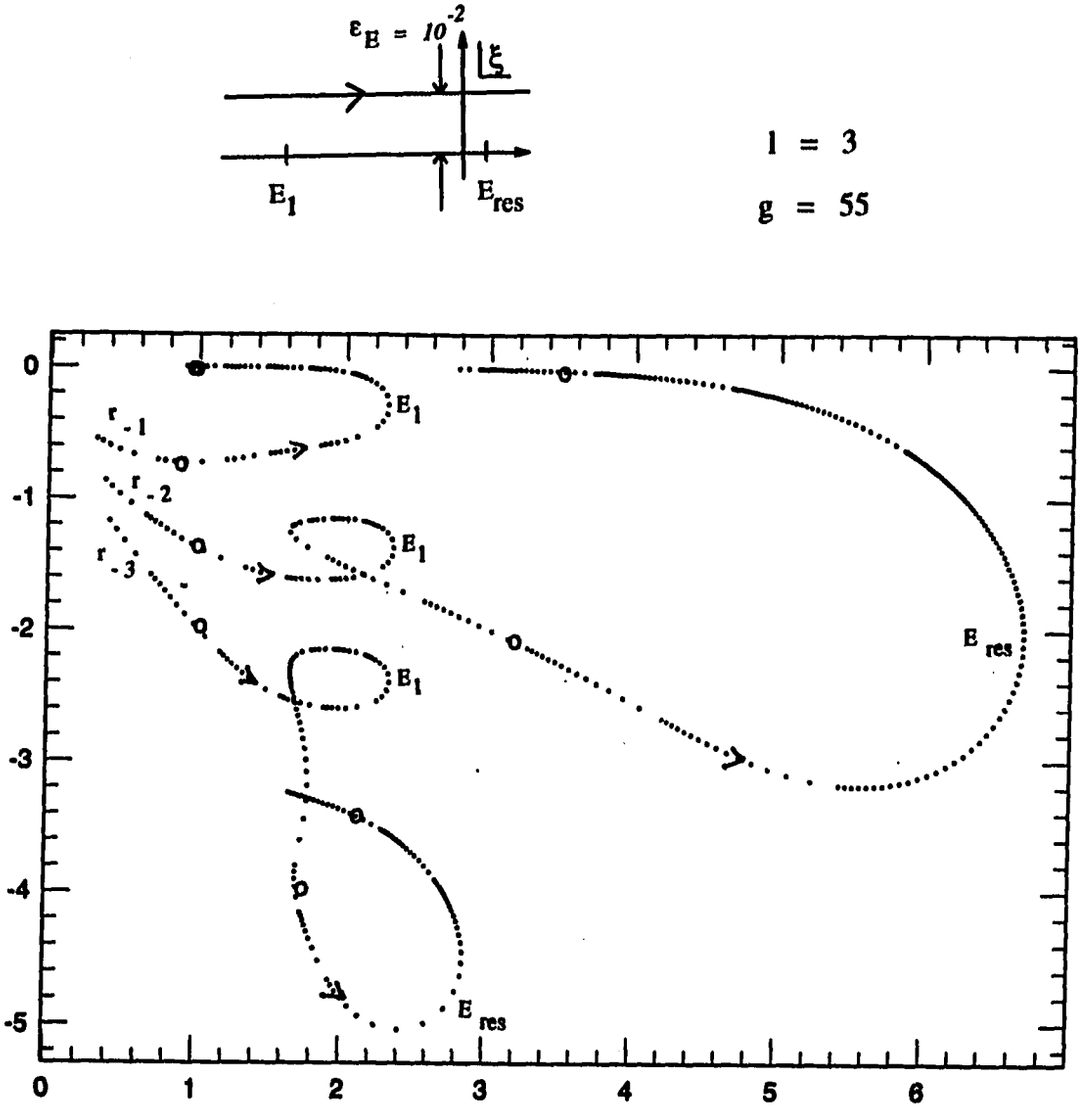

Figure 11.6: First three southern poles of $p_r(r, \mathcal{E}, l)$ for $V_0 < E < V_w$ and $l = 3$, $g = 55$ with one bound state and a resonant state

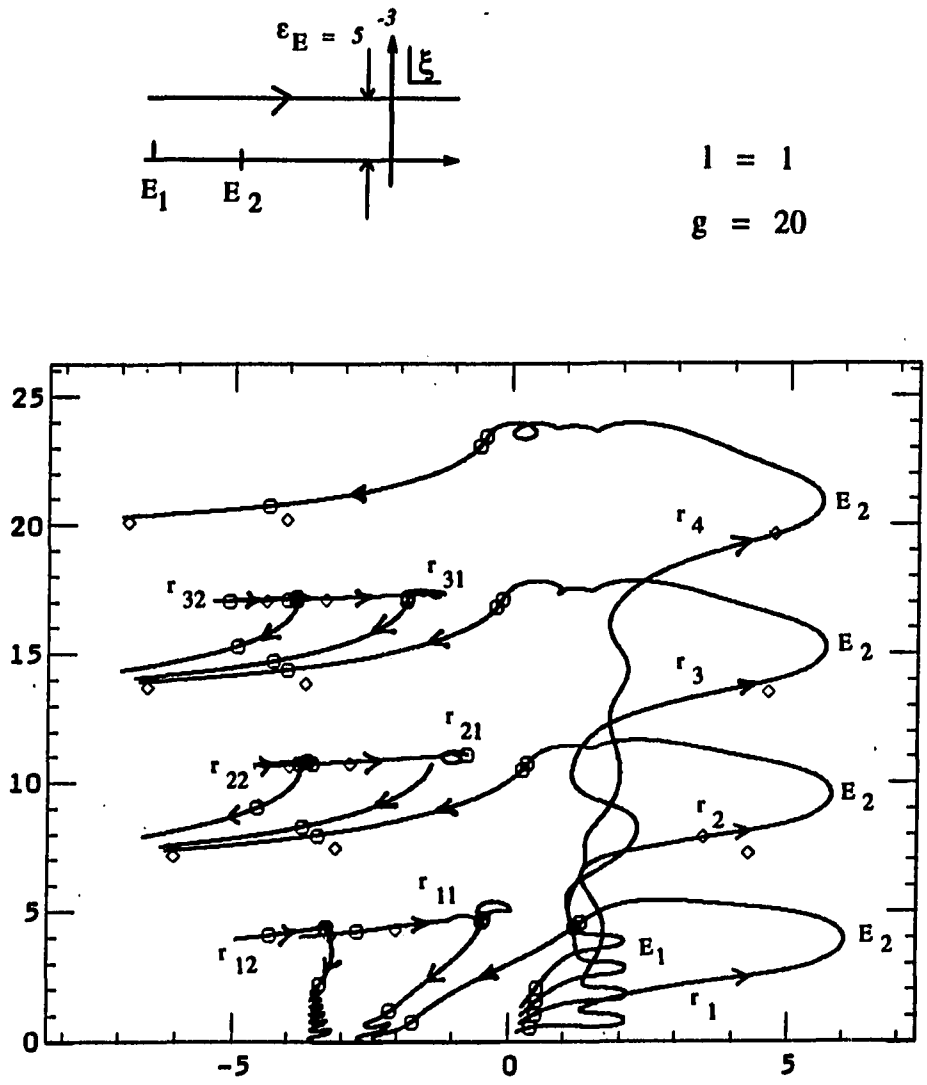

Figure 11.7: Northern and northwestern poles of $p_r(r, \mathcal{E}, l)$ for $V_0 < E < V_w$ and $l = 1, \quad g = 20$ with two bound states

energy approaches an eigenvalue these southern poles move rapidly east and then west as the energy passes by the eigenvalue.

(*ii*) A finite number of the southern poles of rank n and higher move west for positive energy and join the southwestern train of poles.

(*iii*) The remainder of the southern poles move in an arc around $E \approx 0$ and come onto the positive real axis.

(*iv*) The northern poles perform rapid eastward motion for energies near negative energy eigenvalues. A finite number of them come into the unphysical western potential well. The rest of the northern poles join the trains of western poles.

(*v*) The western poles move east with increasing negative energy and move west with increasing positive energy. For energies near $E = 0$ they move down vertically by πR. The first train of northwestern poles fill the unphysical well for $E > V_W$.

The major difference between the set of western poles and the northern-southern poles is the vanishing of the latter into $r = \infty$ for negative energy eigenvalues. This difference will guide our attempt at analytically extending the quantum action variable to scattering states.

CHAPTER 12. QUANTUM ACTION VARIABLE - YUKAWA POTENTIAL

The point $r = \infty$ in the complex r plane has three distinct roles in the context of the quantum motion in the presence of the Yukawa potential. It is the limit point of the set of western turning points. It is the limit point of the northern and southern poles which also vanish into it on energy eigenvalues. It is also the limit point of every western train of poles. The analytic continuation of J_r as a contour integral for energies other than the negative eigenvalues requires that we take away from $r = \infty$ one of the latter two roles. We describe in this Chapter such a definition of J_r. We also demonstrate that this method is sufficiently general to be applicable to potentials that cut off faster than $1/r$.

J_r on negative energy eigenvalues

The Yukawa potential, as seen in Chapter 11, admits of a finite number of energy eigenvalues. For $\mathcal{E} = E_n$, the energy of the nth excited state, there are n poles of p_r in between r_1 and r_2 on the real axis (see figure 12.1). There are no other poles in the plane east of the western turning points. We define J_r for such an energy eigenstate by

$$J_r = \frac{1}{2\pi} \oint_C p_r(r, E_n, l)\, dr, \tag{12.1}$$

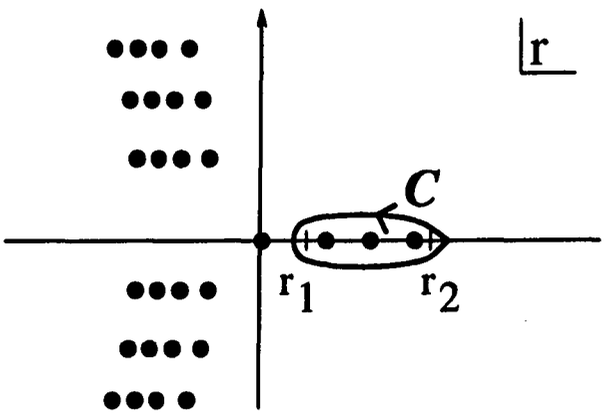

Figure 12.1: Poles of p_r for the energy eigenvalue $E = E_3$

where the counterclockwise contour C encloses the real axis in between r_1 and r_2. The requirement on any analytic extension of J_r is that it reduce to (12.1) for $\mathcal{E} = E_n$. We now provide such a definition of J_r for all energies $\mathcal{E}$.

Modifying the Hamiltonian using ϵ_r

We use the quantum Hamiltonian

$$\widehat{H} = (1 - \epsilon_r \hat{r})^4 \left[\hat{\mathcal{P}}_r^2 + \frac{\hat{L}^2}{\hat{r}^2}\right] + V(\hat{r}) \tag{12.2}$$

corresponding to the classical Hamiltonian (9.36) used in the context of J_{rC}. The correct quantum version of the Hamiltonian must be symmetrized in $\hat{r}$ and $\hat{\mathcal{P}}_r$ to make it Hermitian. We use the unsymmetrized version of it by treating ϵ_r as a small constant; this makes the non-Hermitian part of the Hamiltonian to be of order

ϵ_r. J_r is defined by evaluating a contour integral $\tilde{J}_r(\mathcal{E}, l, \epsilon_r)$ and then taking the limit of $\epsilon_r \rightarrow 0$. We use the coordinate representation. The Schrödinger equation, $\widehat{H}\psi = \mathcal{E}\psi$, with $\widehat{H}$ defined by (12.2), separates in the r, θ and ϕ coordinates as in the case of the usual central force Hamiltonian (4.1). The Schrödinger equation for the radial wave function $\mathcal{U}(r, \mathcal{E}, l, \epsilon_r)$ corresponding to this modified Hamiltonian is

$$\hbar^2 \mathcal{U}'' + \frac{[\mathcal{E} - V_{eff}(r)]}{(1 - \epsilon_r r)^4}\mathcal{U} = 0, \tag{12.3}$$

In the limit of $\epsilon_r \rightarrow 0$ this equation is the usual Schrödinger equation and

$$\mathcal{U}(r, \mathcal{E}, l, \epsilon_r) \rightarrow u(r, \mathcal{E}, l).$$

The classical momentum function $\mathcal{P}_{rc}(r, \mathcal{E}, l, \epsilon_r)$, corresponding to the modified Hamiltonian, is defined by

$$\mathcal{P}_{rc}(r, \mathcal{E}, l, \epsilon_r) = \frac{\sqrt{\mathcal{E} - V_{eff}(r)}}{(1 - \epsilon_r r)^2} = \frac{p_{rc}^2(r, \mathcal{E}, l)}{(1 - \epsilon_r r)^2}, \tag{12.4}$$

with the branch of the square root defined as in the case of p_{rc} in Chapter 10. $\mathcal{P}_{rc}$ has a second order pole at $r = 1/\epsilon_r$. The modification by the introduction of ϵ_r into the Hamiltonian has not introduced any new classical turning points; the turning points of $\mathcal{P}_{rc}(r, \mathcal{E}, l, \epsilon_r)$ are also the the turning points of $p_{rc}(r, \mathcal{E}, l)$ and vice versa. The quantum momentum function equation for $\mathcal{P}(r, \mathcal{E}, l, \epsilon_r)$ corresponding to the Hamiltonian (12.2) is

$$-i\hbar \frac{\partial \mathcal{P}_r(r, \mathcal{E}, l, \epsilon_r)}{\partial r} + \mathcal{P}_r{}^2(r, \mathcal{E}, l, \epsilon_r) = \frac{[E - V(r) - l(l+1)\hbar^2/r^2]}{(1 - \epsilon_r r)^4}. \tag{12.5}$$

We now present an analysis of the locations of the poles of this $\mathcal{P}_r(r, \mathcal{E}, l, \epsilon_r)$ for negative energies in the range $V_0 < E < 0$; the extension to other energies is straightforward.

The point $r = 1/\epsilon_r$ is located in region $2'$ around the turning point r_2. To see how the above modification of $\widehat{H}$, affects the Stokes and anti-Stokes lines pattern, consider a point in the eastern half plane for $Re(r) >> 0$. Here $\sqrt{\mathcal{E} - V_{eff}(r)} \simeq \sqrt{\mathcal{E}} = k$ and $\mathcal{P}_{rc} \simeq k/(1 - \epsilon_r r)^2$. Therefore

$$\mathcal{W}_{rc2}(r) = \int_{r_2}^{r} \mathcal{P}_r(r, \mathcal{E}, l, \epsilon_r)\, dr \simeq c - \frac{1}{\epsilon_r^2} \frac{k}{r - 1/\epsilon_r}, \qquad (12.6)$$

where c is a constant. The terminus of every anti-Stokes line (and therefore of the limit point of the associated set of infinite poles, if any) is a point at which $\mathcal{W}_{rc2} \rightarrow \infty$. From eq. (12.6), which is valid in the eastern half plane, $\mathcal{W}_{rc2} \rightarrow c$ as $r \rightarrow \infty$ and $\rightarrow \infty$ as $r \rightarrow 1/\epsilon_r$. Therefore the point $r = \infty$ does not have the character to be the limit point of the poles of $\mathcal{P}_r$ but the point $r = 1/\epsilon_r$ does. Thus those anti-Stokes lines that were east of the western turning points for the unmodified case treated in Chapter 10 and found their way into $r = \infty$ now go into $r = 1/\epsilon_r$. This is also true of the Stokes lines in the eastern half plane. The picture of Stokes and anti-Stokes lines for the case of this modified Hamiltonian is shown in Figure 12.2. The limit point of the northern and southern zeroes is the terminus of these anti-Stokes lines in the eastern half plane; therefore the limit point of these zeroes is $r = 1/\epsilon_r$ and not $r = \infty$. Furthermore, if the energy of the system is an energy eigenvalue, then, by eq. (6.15), the pole at r_j belonging to the family of northern-southern poles, should have an infinite $\mathcal{W}_{rc2}(r_j)$, i.e., $r_j = 1/\epsilon_r$ for all j. For energy eigenvalues $\mathcal{E} = E_n$, therefore, the northern and southern poles have moved to $r = 1/\epsilon_r$. The modification introduced has little effect in the region west of the western turning points, where the exponential in $\mathcal{P}_{rc}$ overwhelms the r^2 term introduced into the denominator of $\mathcal{P}_{rc}$. Thus the pattern of Stokes and anti-Stokes lines west of the western turning points and the western trains of poles changes little.

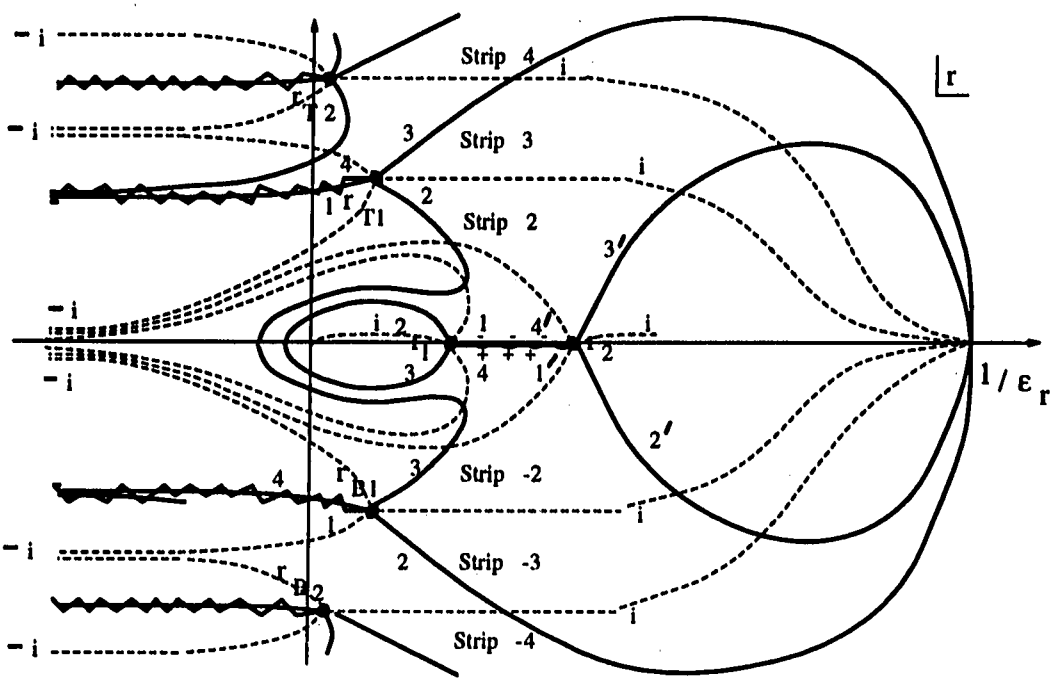

Figure 12.2: Stokes (broken lines) and anti-Stokes lines for $V_0 < E < 0$

In particular the limit point of the western poles continues to be $r = \infty$. The limit points of the two sets of poles, the northern and southern on the one hand and the western on the other, are thus different, which is unlike the cases we have studied without ϵ_r. The locations of the poles of $\mathcal{P}_r(r, \mathcal{E}, l, \epsilon_r)$ in the r and $s = 1/r$ planes for energies in the range $V_0 < E < 0$ are shown in Figure 12.3.

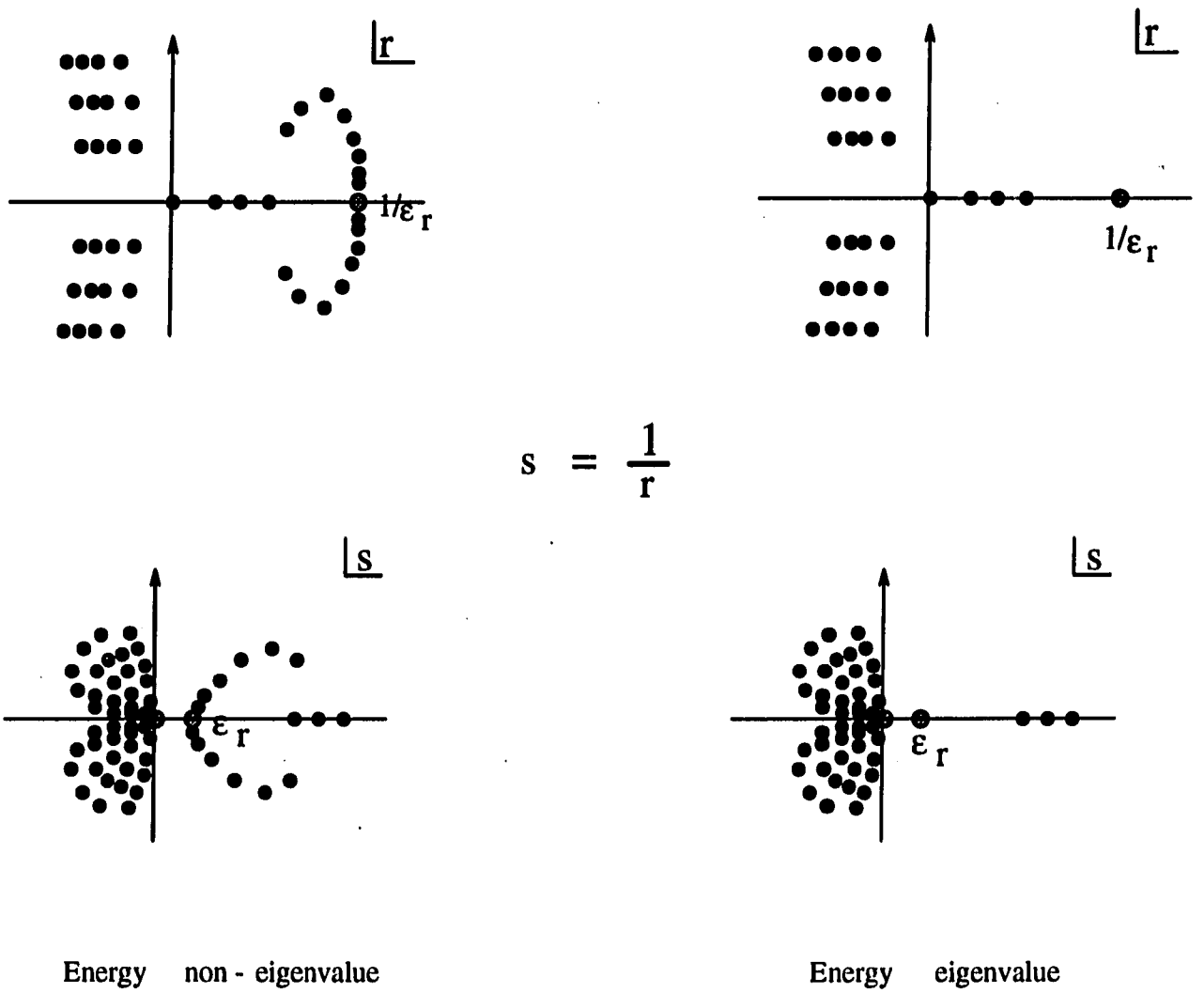

Figure 12.3: Poles of $\mathcal{P}_r(r, \mathcal{E}, l, \epsilon_r)$ for $V_0 < E < 0$

Exploration of the singularity at $r = 1/\epsilon_r$

The point $r = 1/\epsilon_r$ is an irregular singular point of the second order linear differential equation (12.3), as the right hand side has the term $(r - 1/\epsilon_r)^4$ in its denominator. A solution of such a differential equation may have a branch point at an irregular singularity. The presence of a branch cut in $\mathcal{U}(r, \mathcal{E}, l, \epsilon_r)$ may give rise to a branch cut of $\mathcal{P}_r(r, \mathcal{E}, l, \epsilon_r)$. A branch cut would prevent us from using Cauchy's integral theorem in evaluating integrals of $\mathcal{P}_r$ over contours that intersect the cut. We have explored the possible presence of a branch cut of $\mathcal{U}$ originating at the introduced singularity by two methods. The first is by numerically integrating the modified Schrödinger equation (12.3) in the complex r plane around the irregular singularity to a point r_A along paths that are mirror images of each other in the real r axis, shown in Figure 12.4. $\bar{\mathcal{U}}$ and $\bar{\mathcal{U}}'$ are real at $r = 0$, according to the initial conditions (6.10). The line elements and $\mathcal{P}_r^2(r, \mathcal{E}, l, \epsilon_r)$ at corresponding points along the two paths are complex conjugates of each other, thus $\mathcal{U}$ and $\mathcal{U}'$ at r_A obtained by integration along these paths will be complex conjugates of each other; they are equal to each if the imaginary parts of these two functions vanish at r_A. Integration showed the imaginary parts of these functions to be very small in comparison to their real parts; also changing the path of integration resulted in a change in the imaginary parts of $\mathcal{U}$ and $\mathcal{U}'$ while their real parts were stable. The second method is by an approximate local solution of (12.3) . Both methods indicate the absence of such a cut. We describe here the approximate solution.

From eq. (12.3), $\mathcal{U}$ can be approximated by $\bar{\mathcal{U}}(r, \mathcal{E}, l, \epsilon_r)$ for $Re(r) >> r_2$, where

$$\bar{\mathcal{U}}'' + \frac{\mathcal{E}}{\hbar^2 \epsilon_r^4} \frac{\bar{\mathcal{U}}}{(r - 1/\epsilon_r)^4} = 0, \tag{12.7}$$

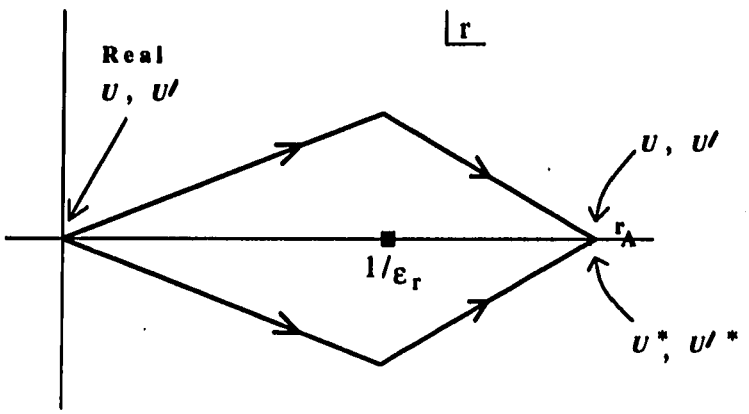

Figure 12.4: Integration paths for the modified Schrödinger equation

ignoring the effective potential in comparison to $\mathcal{E}$. We similarly define $\bar{\mathcal{P}}_r$ as the solution of

$$-i\hbar \frac{\partial \bar{\mathcal{P}}_r(r,\mathcal{E},l,\epsilon_r)}{\partial r} + \bar{\mathcal{P}}_r^2(r,\mathcal{E},l,\epsilon_r) = \bar{\mathcal{P}}_{rc}^2(r,\mathcal{E},L,\epsilon_{rc}), \tag{12.8}$$

$$\text{with} \quad \bar{\mathcal{P}}_{rc}(r,\mathcal{E},l,\epsilon_r) = \frac{\sqrt{\mathcal{E}}}{\hbar^2 \epsilon_r^4}. \tag{12.9}$$

This equation has two independent solutions of the form

$$\begin{aligned} \bar{\mathcal{U}}_1 &= (r - 1/\epsilon_r) \sin\left(\frac{\gamma}{r - 1/\epsilon_r}\right), \\ \bar{\mathcal{U}}_2 &= (r - 1/\epsilon_r) \cos\left(\frac{\gamma}{r - 1/\epsilon_r}\right), \end{aligned} \tag{12.10}$$

where

$$\gamma = \frac{\sqrt{\mathcal{E}}}{\hbar \epsilon_r^2}. \tag{12.11}$$

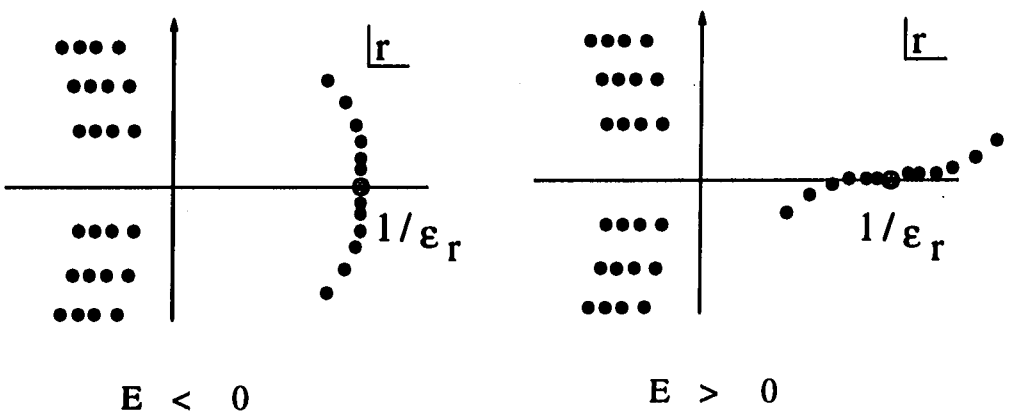

Figure 12.5: Zeroes of $\mathcal{U}(r, \mathcal{E}, l, \epsilon_r)$ in the neighborhood of $1/\epsilon_r$

These solutions have no branch cut at $r = 1/\epsilon_r$ and the accuracy of the approximation of eq. (12.3) by eq. (12.7) increases as one chooses a smaller and smaller ϵ_r. These solutions, and their linear combinations, have an infinite number of zeroes in any neighborhood of $r = 1/\epsilon_r$. It can be shown that these zeroes accumulate around $r = 1/\epsilon_r$ vertically if $E < 0$ and along the real axis for $E > 0$. Figure (12.5) shows the picture of these zeroes for both cases. This structure of the northern and southern poles of $\mathcal{P}_r$ with $r = 1/\epsilon_r$ as their limit point, revealed by $\bar{\mathcal{U}}_1$ and $\bar{\mathcal{U}}_2$ above is the same as the one we obtained in the previous section using the WKB approximations for $\mathcal{U}(r, \mathcal{E}, l, \epsilon_r)$.

An alternate set of linearly independent solutions of eq. (12.7) is

$$\bar{\mathcal{U}}_{1'} = (r - 1/\epsilon_r) \exp\left(\frac{i\gamma}{r - 1/\epsilon_r}\right), \tag{12.12}$$

$$\bar{\mathcal{U}}_{2l} = (r - 1/\epsilon_r) \exp\left(\frac{-i\gamma}{r - 1/\epsilon_r}\right).$$

This set of solutions is illustrative of the character of $\mathcal{U}$ for energy eigenvalues. Since $\gamma = i|\gamma|$ (from eq. (12.11) and the definition of $\sqrt{\mathcal{E}}$), $\bar{\mathcal{U}}_{2l}$, for negative energies, is

$$(r - 1/\epsilon_r) \exp\left(\frac{|\gamma|}{r - 1/\epsilon_r}\right) \rightarrow 0$$

as $r \rightarrow (1/\epsilon_r)_-$. $\bar{\mathcal{U}}_{1l} \rightarrow \infty$, in the same limit and, unlike $\bar{\mathcal{U}}_{2l}$, is not normalizable in the interval $r \in (0, 1/\epsilon_r)$. The energy eigenvalues are therefore those $\mathcal{E}$ for which $\bar{\mathcal{U}}_{1l}$ component is absent in the wave function and the eigenfunctions $\bar{\mathcal{U}}_n$ for $r_2 << r < 1/\epsilon_r$ are

$$\bar{\mathcal{U}}_n = (r - 1/\epsilon_r) \exp\left(\frac{i\gamma_n}{r - 1/\epsilon_r}\right), \tag{12.13}$$

with $\gamma_n = \sqrt{E_n}/\hbar\epsilon_r^2$. These eigenfunctions $\bar{\mathcal{U}}_n$ have no zeroes in the neighborhood of $r = 1/\epsilon_r$, which supports our conclusion in the previous section based on the WKB analysis that the zeroes move into $r = 1/\epsilon_r$ for energy eigenvalues.

The momentum functions $\bar{\mathcal{P}}_r(r, E_n, l, \epsilon_r)$ for the energy eigenvalues (using $\mathcal{P}_r = -i\hbar\mathcal{U}'/\mathcal{U}$) are

$$\bar{\mathcal{P}}_r(r, E_n, \epsilon_r) = \frac{\gamma_n\hbar}{(r - 1/\epsilon_r)^2} - \frac{i\hbar}{r - 1/\epsilon_r}. \tag{12.14}$$

This shows that $\bar{\mathcal{P}}_r$ for energy eigenvalues has a second order pole at $r = 1/\epsilon_r$ just as $\mathcal{P}_{rc}$ does. The residue of $\bar{\mathcal{P}}_r$ at this pole is $-i\hbar$. That this is also the residue of $\mathcal{P}_r$ at $r = 1/\epsilon_r$ can be shown by the expansion of $\mathcal{P}_r$ in a Laurent series centered at $r = 1/\epsilon_r$. $\mathcal{U}_{2l}$, the WKB wave function, for energy eigenvalues, is

$$\mathcal{U}_{2l} \sim \frac{1}{\sqrt{\mathcal{P}_{rc}}} \exp(i\mathcal{W}_{rc2}/\hbar),$$

which is correct up to the first order in $\hbar$. The corresponding momentum function, correct to order $\hbar$, is

$$\mathcal{P}_r^{WKB} = \mathcal{P}_{rc} + \hbar \frac{-iV'_{eff}(r)}{4\mathcal{P}_{rc}^{3/2}}. \tag{12.15}$$

The second term in the above is $\propto \mathcal{P}_{rc}^{-3/2} \sim (r - 1/\epsilon_r)^3$ and is finite at $r = 1/\epsilon_r$. Thus $\mathcal{P}_r$ has the same singularity at $r = 1/\epsilon_r$ as $\mathcal{P}_{rc}$. We now use the Laurent expansion

$$\mathcal{P}_r(r, E_n, l, \epsilon_r) = \frac{a_{-2}}{(r - 1/\epsilon_r)^2} + \frac{a_{-1}}{(r - 1/\epsilon_r)} + \ldots \tag{12.16}$$

in eq. (12.5), with

$$\mathcal{P}_{rc}(r, E_n, l, \epsilon_r) = \frac{A_{-2}}{(r - 1/\epsilon_r)^2} + \frac{A_{-1}}{(r - 1/\epsilon_r)} + \ldots. \tag{12.17}$$

Equating coefficients of every power of $(r - 1/\epsilon_r)$ to zero in this equation we get

$$a_{-2}^2 = A_{-2}^2 \Rightarrow a_{-2} = +A_{-2}, \quad + \text{sign from eq. (12.15)}),$$
$$a_{-1} = \frac{2A_{-2}A_{-1} - 2i\hbar a_{-2}}{2a_{-2}} = A_{-1} - i\hbar. \tag{12.18}$$

To obtain A_{-1} we expand $\sqrt{\mathcal{E} - V_{eff}(r)}$ in eq. (12.4) in a Taylor series around $r = 1/\epsilon_r$:

$$\mathcal{P}_{rc} = \frac{1}{\epsilon_r^2 (r - 1/\epsilon_r)^2} \left[\sqrt{\mathcal{E} - V_{eff}^{(\epsilon)}} - \frac{V_{eff}^{\prime(\epsilon)}}{2\sqrt{\mathcal{E} - V_{eff}^{\epsilon}}} (r - 1/\epsilon_r) + \ldots \right] \tag{12.19}$$

where the superscript ϵ in V and V' refers to the functions evaluated at $r = 1/\epsilon_r$. For any potential that cuts off faster than the Coulomb potential the leading term in $V_{eff}(r)$ is $\propto 1/r^2$ (which could be the angular momentum barrier alone or the

barrier and a part of the potential that is also $\propto 1/r^2$) for $Re(r) >> R$ (or a distance within which the potential is influential). Therefore, for all such potentials including the Yukawa potential, $V'_{eff} \propto 1/r^3$ for large $Re(r)$ and

$$V'^{(\epsilon)}_{eff} = V'_{eff}(r = 1/\epsilon_r) \sim O(\epsilon_r^3).$$

A_{-1}, which is the coefficient of $(r - 1/\epsilon_r)^{-1}$ in eq. (12.19), is $\propto V'^{(\epsilon)}_{eff}/\epsilon_r^2$ and therefore

$$A_{-1} \sim O(\epsilon_r). \tag{12.20}$$

Using (12.20) in (12.18) we get

$$a_{-1} = -i\hbar + O(\epsilon_r). \tag{12.21}$$

We will use this result in the contour integral definition of J_r.

Definition of J_r

The poles of $\mathcal{P}_r$ are shown in Figure 12.6. These poles are also represented in the $s = 1/r$ plane shown in the same figure. We define the contours in the r and s planes and establish the correspondence between them as follows:

(i) The contour C_e in the r plane encloses the poles on the positive real axis and the northern and southern poles for all energies. The corresponding contour in the s plane is C_{es}.

(ii) C_0 encircles the pole at $r = 0$. C_{0s} is the corresponding contour in the s plane.

(iii)C_{ws} is a contour in the s plane that encloses all the western poles. It passes between $s = 0$, which is the limit point of all the western poles, and $s = \epsilon_r$ which is

the limit point of the northern and southern poles. C_w is its image in the r plane.
(iv) C_ϵ encloses the point $r = 1/\epsilon$ in the r plane. $C_{\epsilon s}$ is its image in the s plane. As the limit point of the northern and southern poles is a point in the finite r plane, viz, $1/\epsilon_r$, it is always possible, for all energy, to have the contour C_ϵ enclose the set of northern and southern poles as also the poles on the positive real axis.
(v) C encloses the poles on the real axis for $V_0 < E < 0$. C_s is its image in the s plane.

The poles can be grouped into similar distinct sets for any potential that cuts off for $r \to \infty$ along the real r axis. The characteristic feature of a potential is the number and distribution of poles inside the contour C_{ws} in the s plane. For energy eigenvalues the northern and southern poles disappear into $s = \epsilon_r$.

We first define $\tilde{J}_r(\mathcal{E}, l, \epsilon_r)$ by

$$\tilde{J}_r(\mathcal{E}, l, \epsilon_r) \;=\; \frac{1}{2\pi}\oint_{C_e} \mathcal{P}_r(r, \mathcal{E}, l, \epsilon_r)\, dr \;\; - \;\; \hbar. \tag{12.22}$$

We study its character on energy eigenvalues. For $\mathcal{E} = E_n$, we can distort C_e into C and C_ϵ to evaluate the integral in (12.22). Since $\mathcal{P}_{rc}(r, \mathcal{E}, l, \epsilon_r)$ has no poles at any point in the finite r plane except at $r = 1/\epsilon_r$ and $r = 0$ every pole of $\mathcal{P}_r(r, \mathcal{E}, l, \epsilon_r)$ in the finite r plane excluding $r = 1/\epsilon_r$ and $r = 0$ is a simple pole of residue $-i\hbar$. (see Appendix A). Similarly every pole of $p_r(r, \mathcal{E}, l)$ in the finite r plane excluding $r = 0$ is simple and has residue $-i\hbar$. Thus

$$\frac{1}{2\pi}\oint_C \mathcal{P}_r(r, E_n, l, \epsilon_r)\, dr \;=\; \frac{1}{2\pi}\oint_C p_r(r, E_n, l)\, dr \;=\; n_r\hbar, \tag{12.23}$$

since C encloses the same number of poles, n_r, of both $\mathcal{P}_r(r, E_n, l, \epsilon_r)$ and $p_r(r, E_n, l)$, each of residue $-i\hbar$. Next,

$$\frac{1}{2\pi}\oint_{C_\epsilon} \mathcal{P}_r(r, E_n, l, \epsilon_r)\, dr \;= ia_{-1}, \quad \text{by the residue theorem,}$$

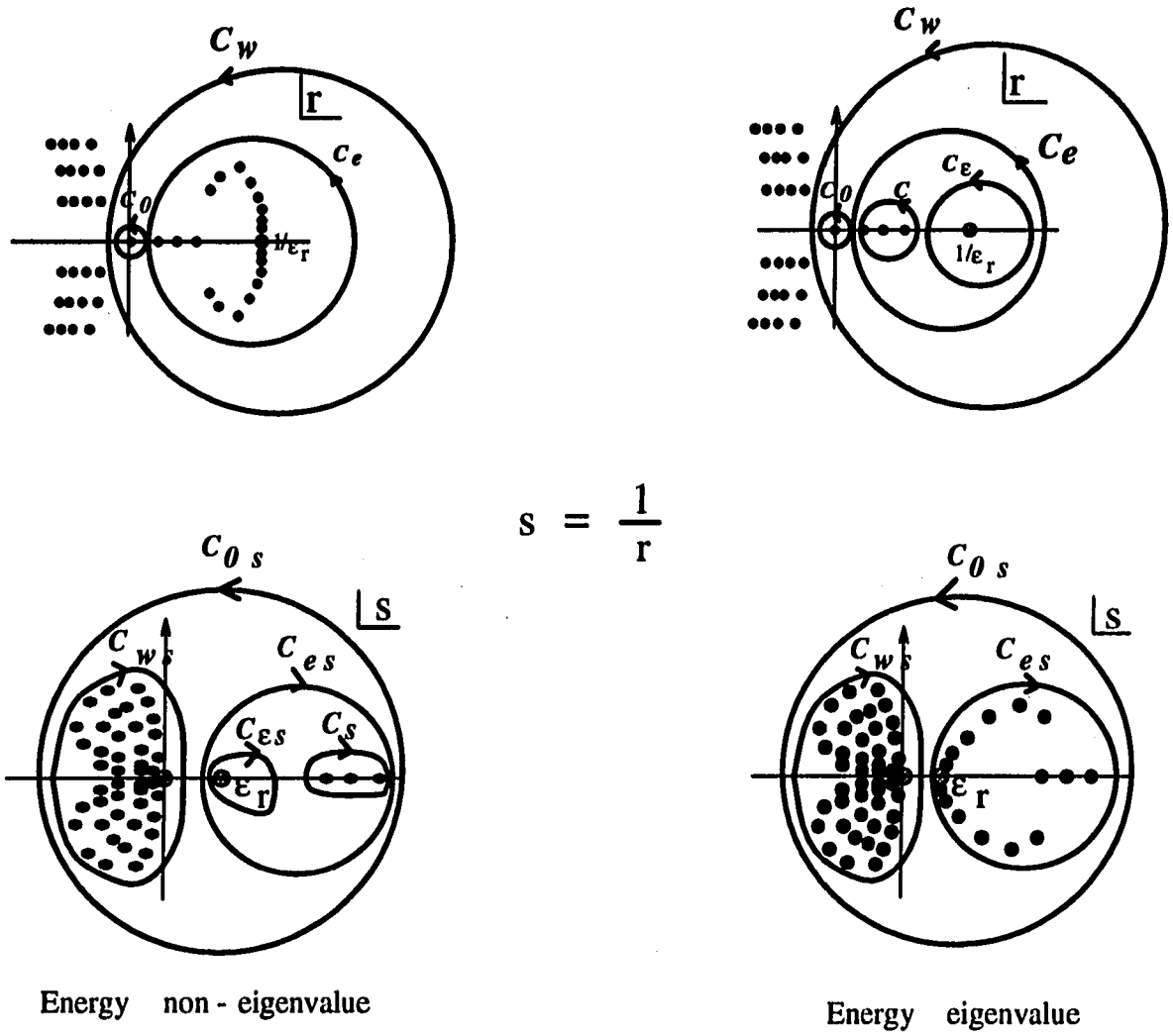

Figure 12.6: Contours used in the definition of $\tilde{J}_r(\mathcal{E}, l, \epsilon_r)$

$$= \quad \hbar + O(\epsilon_r), \tag{12.24}$$

from eq. (12.21), for any central potential that cuts off faster than the Coulomb potential. Using eqs. (12.23) and (12.24) in eq. (12.22) we get

$$\begin{aligned} \tilde{J}_r(E_n, l, \epsilon_r) &= \frac{1}{2\pi}\oint_C \mathcal{P}_r(r, E_n, l)\, dr + \frac{1}{2\pi}\oint_{C_\epsilon} \mathcal{P}_r(r, E_n, l) \; - \; \hbar \\ &= n_r\hbar \; + \; O(\epsilon_r) \end{aligned} \tag{12.25}$$

In the limit of $\epsilon_r \rightarrow 0$, therefore, $\tilde{J}_r(E_n, l, \epsilon_r) \rightarrow J_r(E_n, l)$ for any central potential weaker than the Coulomb potential. Our definition of J_r for any such potential for any energy $\mathcal{E}$ is

$$J_r(\mathcal{E}, l) = \lim_{\epsilon_r \rightarrow 0} \tilde{J}_r(E_n, l, \epsilon_r). \tag{12.26}$$

We now consider the J_r for the Coulomb potential in the context of this definition. The evaluation of $\tilde{J}_r$ for the Yukawa potential can be done by distorting the contour C_{es} into C_{0s} and C_{ws}. One evaluates these two integrals for a non-zero ϵ_r to obtain $\tilde{J}_r(\mathcal{E}, l, \epsilon_r)$. The limit of ϵ_r then yields the action variable J_r for the Yukawa problem. The classical action variable for this potential, as shown in Chapter 9, can be obtained as a perturbative series in inverse powers of the range R. In the limit of infinite range of the potential (the 'Coulomb limit'), only the term independent of the range survives yielding the correct expression for the Coulomb classical radial action variable. A similar result holds in the quantum case. The western poles collapse into $s = 0$ in the limit of infinite R; the perturbative expression for the quantum J_r contains inverse powers of R which, as in the classical case, disappear in the Coulomb limit and we obtain the correct expression (6.6) for the quantum Coulomb J_r.

CHAPTER 13. CONCLUSION

The radial action variable $J_r(E,l)$, extended analytically to both bound and scattering states of a system, provides a link between quantum bound states and resonances. We have demonstrated that the radial action variable can be defined classically and quantum mechanically, for all physically allowed states of a system described by the Yukawa potential. These definitions preserve the algebraic form of the action variable for all energies. Unlike the simpler Coulomb potential, the Yukawa potential has an infinite number of classical turning points in the western half of the complex r plane, with a branch cut of the classical momentum function originating from each of them. The motion of these turning points with energy was examined both analytically and numerically. J_{rc} was defined as a contour integral in the complex r plane with the contour enclosing the two classical turning points r_1 and r_2, which correspond to the limits of the physical bound state motion, and the branch cut between them; this definition is then extended to all energies.

The quantum radial action variable, $J_r(E,l)$, defined as a contour integral in the complex r plane of the quantum momentum function, is quantized in units of $\hbar$ for bound states. The analytic extension of J_r to scattering states required a study of the motion of the poles of the quantum momentum function with energy. The energy dependence of these poles was first studied by a semiclassical method and the

results confirmed by a numerical method. These studies revealed the presence of a train of poles west of each western turning point that do not vanish into $r = \infty$ on energy eigenvalues. They also showed the presence of a second set of infinite poles in the eastern half of the complex r plane that recede to $r = \infty$ on energy eigenvalues. The Yukawa potential thus produces two classes of infinitely many poles of p_r, one that recedes to $r = \infty$ on energy eigenvalues (the 'northern-southern' poles), and the other that is insensitive to energy eigenvalues. Both these sets have the same limit point, viz, $r = \infty$, into which the first set disappears for physical bound state energies.

This study of the Yukawa potential reveals resemblances to the problem of the Coulomb potential with regard to the motion of the poles with energy. The important difference is the presence of the infinite trains of western poles which are insensitive to energy eigenvalues, unlike the northern-southern sequence of poles (which are also present in the Coulomb potential case). Any potential, which results in more than two classical turning points, has, in general, such poles. That these different sets of poles have a common limit point into which the northern-southern poles merge poses a problem to the analytic extension of J_r to scattering states. The analytic extension requires the enclosure of the set of northern-southern poles by a contour in the complex r plane while excluding the set of western trains of poles, so that we obtain, for energy eigenvalues, $J_r = n_r\hbar$. This requires "moving" the limit point of the northern-southern poles from $r = \infty$ to a finite point $r = 1/\epsilon_r$; the northern-southern poles being thus confined to the finite complex r plane can be surrounded by a contour. After the evaluation of J_r as an integral over that contour we make ϵ_r vanishingly small.

The separation of the limit points of the two sets of poles was achieved by considering a modified Yukawa Hamiltonian that describes, in its classical version, a particle whose effective mass increases as it approaches the point $r = 1/\epsilon_T$. The corresponding Schrödinger equation has an irregular singularity at $r = 1/\epsilon_T$ leading to a possible branch point for the wave function. We have examined the nature of the wave function in the neighborhood of the irregular singularity by constructing a local solution and by numerical integration around the singularity. These methods indicate the absence of a branch cut for the wave function, though this result requires further investigation.

The evaluation of $J_{TC}(E, l)$ for the Yukawa potential as a perturbative series in $1/R$, where R is the range of the potential, has been demonstrated. A similar evaluation of J_{TC} and J_T as functions of energy, for a system whose Hamiltonian involves ϵ_T in the manner indicated above requires further study, though we have successfully demonstrated that it provides a means to analytically extend J_T to all energies. We have used the Yukawa potential as a prototype. The method developed here to analytically extend J_T for this potential can be applied to other central potentials that cut off faster than the Coulomb potential. The Coulomb potential, viewed as the long range limit of the Yukawa potential, can also be brought within the fold of this definition of J_T; one first evaluates J_T for the Yukawa potential with a range R and then takes the limit of $R \to \infty$. Particle resonances, understood as composite quantum mechanical states of strongly interacting particles, can be explored by studying the action variable of such states through suitably modeled potentials. One can form families of states of common angular momentum but different action variables, thus providing a new scheme for classifying composite systems.

ACKNOWLEDGEMENTS

I express my gratitude to my adviser Professor Robert A. Leacock for his guidance during this research. I also thank Professors James A. Wilson and Roger K. Alexander of the Department of Mathematics, ISU for useful discussions. I acknowledge my gratitude to the members of my POS committee for their interest in this work. I am indebted to John Lajoie, Karl Kehm and Frank Genalo for aid with numerical computations and Peter Matheos for stimulating discussions. Thanks are also due to Chiho, Mike, Pang and Athan for help during the completion of this work.

I dedicate this dissertation to my parents who have borne stoically the separation of ten thousand miles and many years; without their encouragement and care all through I could not have pursued the path I have. Anju, Dilip, Doctor and Vijaya have provided me a source of comfort and support; words are too inadequate to thank them all. Professor G.A. Nariboli and Dr. Pramoda Nariboli have given me a home away from home; to them, my heartfelt thanks. Professor Leacock was more than my adviser; he was my friend, guide and philosopher. I will always cherish my association with him. Last, but not the least, my grateful thanks to my numerous students and the people of Iowa who made it possible for me to pursue this work.

APPENDIX

Appendix A: Poles of p_r

Let $p_C(x, E)$ be analytic at a point x_0. Assume $p(x, E)$ has a pole of order n at x_0 with $n \geq 1$. Then

$$p_C(x, E) = A_0 + A_1(x - x_0) + \ldots$$

and

$$p(x, E) = \frac{a_{-n}}{(x - x_0)^n} + \frac{a_{-(n-1)}}{(x - x_0)^{(n-1)}} + \ldots.$$

Substituting these expansions for $p_C(x, E)$ and $p(x, E)$ in eq. (3.5) we see that the coefficients of $(x - x_0)^{2n}$ can be matched on both sides only if

$$\begin{aligned} 2n &= n + 1 \quad \Rightarrow \quad n = 1, \\ i\hbar a_{-1} + a_{-1}^2 &= 0 \\ \Rightarrow \; a_{-1} &= -i\hbar \end{aligned}$$

Thus the quantum momentum function, if it is singular at x_0, can only have a simple pole of residue $-i\hbar$ at x_0 where the classical momentum function is analytic.

Appendix B: Perturbative expansion of $p_{rc}(r, \mathcal{E}, L)$

From eqs. (9.25) and (9.26) we have

$$-\frac{L^2}{r_1 r_2}(r-r_1)(r-r_2)\left[1+\sum_{n=1}^{\infty} v_n r^n\right] = Er^2 + gr\exp(-r/R) - L^2.$$

We equate coefficients of r^n on both sides of this equation and obtain v_n.

Case (i): L = 0

Here we have a closed form expression for v_n:

$$v_n = -\frac{\exp(-n\lambda_2)}{r_{2c}^n} \sum_{j=n+1}^{\infty} \frac{(-\lambda_2)^j}{j!},$$

where $\lambda_2 = r_2/R$ and $|\lambda_2| < 1$ for $E < E_h$, from Figure (9.2). Thus $v_n \sim O(\lambda_2^{n+1})$.

Case (ii): $L \neq 0$

We can solve for v_1 and v_2 by equating coefficients of r and r^2; to the leading order in $\lambda_{1,2} = r_{1,2}/R$. We get

$$v_1 \simeq -\frac{r_{2c}+r_{1c}}{r_{2c}-r_{1c}}\left[\frac{\lambda_1^2}{r_{1c}^2}+\frac{\lambda_2^2}{r_{2c}^2}\right].$$

Similarly, $v_2 \sim O(\lambda_{2,3}^3)$. For $n \geq 3$, we get, by equating the coefficient of r^n,

$$v_{n-2} - (r_1+r_2)\, v_{n-1} + r_1 r_2 v_n = -\frac{g r_1 r_{-2}}{L^2}\frac{1}{(n-1)!}\left(\frac{-1}{R}\right)^{n-1}.$$

The asymptotic solution of this difference equation is

$$v_n \approx -\frac{r_1 r_2 g}{L^2}\frac{1}{(n+1)!}\left(\frac{-1}{R}\right)^{n+1} \sim O(\lambda_{1,2})^{n+1}.$$

BIBLIOGRAPHY

[1] R. A. Leacock and M. J. Padgett *Phys. Rev.* **D28**, 2491 (1983).

[2] A. A. Nanayakkara, Ph.D. dissertation, Iowa State University, Ames, Iowa.

[3] H. Goldstein, *Classical Mechanics* (Addison-Wesley, New York, 1980).

[4] R. A. Leacock, *Phys. Lett.* **104A**, 184 (1984).

[5] J. Heading, *An Introduction to Phase-Integral Methods* (John Wiley, New York, 1962).

[6] W. H. Furry, *Phys. Rev. Lett.* **71**, 360 (1947).

[7] Robert A. Leacock (To be published).